Polarized Fluorescence by the Electron Impact Excitation of Atoms

A thesis

submitted to the Faculty of Graduate Studies,

University of Manitoba

In partial fulfillment

of the requirements for the degree

Master of Science

by

Brian John Eves

Winnipeg, Manitoba, Canada

National Library of Canada
Acquisitions and Bibliographic Services
395 Wellington Street
Ottawa ON K1A 0N4
Canada

Bibliothèque nationale du Canada
Acquisitions et services bibliographiques
395, rue Wellington
Ottawa ON K1A 0N4
Canada

Your file Votre référence

Our file Notre référence

0-612-32104-5

Canada

THE UNIVERSITY OF MANITOBA

FACULTY OF GRADUATE STUDIES

*****

COPYRIGHT PERMISSION PAGE

POLARIZED FLUORESCENCE BY THE ELECTRON IMPACT EXCITATION OF ATOMS

BY

BRIAN JOHN EVES

A Thesis/Practicum submitted to the Faculty of Graduate Studies of The University of Manitoba in partial fulfillment of the requirements of the degree of

MASTER OF SCIENCE

Abstract

Polarized radiation emitted by electron impact excited atoms carries information about the anisotropic population of the magnetic sublevels. An overview of the theory necessary to describe the time evolution of an electron impact excited atom, and therefore the emitted radiation, is presented and applied to three cases. The three cases include the $1s4d\text{-}1s2p\text{-}1s^2$ cascade transition in helium, the $3s4d\text{-}3s3p\text{-}3s^2$ cascade transition in magnesium, and the electron impact excitation off of a laser excited P-state to a D-state and subsequent re-emission back to the P-state.

The apparatus required to measure the helium, and magnesium cascade transitions has been built. The apparatus consists of an electron gun aimed at an atom vapour beam. The emitted radiation was detected by two photon detectors, one for each level transition. The equipment is tested by comparing the measured polarization of the 1s4d-1s2p transition in helium to existing published data. The polarization of the 3s4d-3s3p transition in magnesium has also been measured. The coincidence measurements required to complete the determination of the magnetic sublevel populations of the D-state for helium, and magnesium have not yet been made.

Table of Contents

List of Figures

List of Tables

Chapter 1 Introduction

The polarization of light is a common everyday event which occurs, for example, as a result of the scattering processes which make the sky appear blue, or the scattering of light off of the atmosphere, and is also responsible for the ability of polaroid sunglasses to block the glare from the road while driving. In general, any process which is anisotropic will produce polarization of some form. In the case of scattering off of the atmosphere, the anisotropy is supplied by the direction of the incident light, or the position of the sun. By analyzing the polarization we can determine information about the anisotropic process which causes it. In atomic collision experiments the anisotropy is usually supplied by the colliding electron beam. The information obtained from the polarized emission which is due to the de-exciting atoms gives information about the electron excitation of the atom.

The scattering cross section is used to measure the likelihood of an event in a collision. In classical physics the cross section is simply the effective area of the target which is to be hit by a projectile. If the target is a dart board, for example, then it is easy to see that the cross section is highly dependent upon the direction of the projectile. The larger the cross section, the easier the object is to hit. The cross section concept is only valid for large ensembles of targets and projectiles since it is assumed that the projectile is not actually aimed directly at the target, but is instead directed in the general direction of the target. In quantum mechanics the incident projectile is modeled as a plane wave, where the scattered wave is given by

$$\psi_{scat}(\vec{x}) = \frac{1}{(2\pi)^{3/2}}\left(e^{i\vec{p}\cdot\vec{x}} + \frac{e^{ipr}}{r} f(\vec{p}', \vec{p})\right) \text{ (Sakurai1994).} \qquad (1.1)$$

The first term in equation (1.1) is just the original plane wave, while the second term is a spherical wave propagating outward from the collision centre with an amplitude defined by

$$f(\vec{p}',\vec{p}) = -\frac{1}{4\pi}(2\pi)^{3/2}\frac{2m}{\hbar^2}\langle\vec{p}'|V|\psi\rangle. \tag{1.2}$$

Equation (1.2) is called the scattering amplitude and is a measure of the interference between the incident plane wave and the target, in a direction $\vec{p}'$. The differential scattering cross section is defined to be the rate of particles scattered into a unit solid angle divided by the total flux of incident particles or

$$\frac{d\sigma}{d\Omega}d\Omega = \left|f(\vec{p}',\vec{p})\right|^2 d\Omega. \tag{1.3}$$

The quantum mechanical scattering cross section is consistent with the classical equivalent and has units of area. If the scattered particle is not directly measured then the quantity which is usually measured is the integrated scattering cross section, or

$$\begin{aligned}\sigma &= \int \frac{d\sigma}{d\Omega}d\Omega \\ &= \int \left|f(\vec{p}',\vec{p})\right|^2 d\Omega.\end{aligned} \tag{1.4}$$

Only the polarization of the emitted light from electron impact excited atoms will be investigated in this work, and the obtained information will therefore be in terms of the integrated scattering cross sections. The detailed analysis of the polarization from excited atomic systems is required to increase the understanding of the processes which occur in plasmas. The peripheral regions of classical gas-discharge sources exhibit appreciable anisotropy and are key components in maintaining a plasma. The data obtained by

studying the polarized emission from atomic ensembles can help to characterize the principal processes occurring in the peripheral regions (Kazantsev1988).

The first experiments which measured the polarized radiation due to electron impact were carried out in the 1920's. In 1927, shortly after the first measurements, Oppenheimer (Oppenheimer1927) published the first attempt to detail the theory of polarized emission. The theory was later improved upon by Penney in 1932 (Penney1932) when he showed it was necessary to include the effects of the fine and hyperfine structure. The combined Oppenheimer-Penney theory was incomplete however and gave ambiguous results in the limit of small fine and hyperfine structure energies. In 1958, the ambiguities were resolved by Percival and Seaton (Percival1958) and they presented a method for detailing the polarized emission from an excited atom. A more general formalism was introduced in 1973 by Fano and Macek (Fano1973) which included the time modulating effects of internal and external fields. The formalism also explicitly related the scattered electron to the subsequently radiated photon, and therefore enabled the parameters describing excitation to a P-state to be fully determined by electron-photon coincidence experiments. The first electron-photon coincidence measurements were carried out in 1972 by King *et al.*(King1972). A paper by Macek and Hertel (Macek1974) in 1974 detailed how superelastic scattering off of a laser excited state is in fact the time-inverse process of the inelastic electron-photon coincidence measurements. This, along with the advent of the continuous wave dye laser, created the framework for a powerful experimental tool. Superelastic electron scattering has been used extensively ever since to probe the coherence parameters which describe the shape and orientation of the electron excited atomic charge cloud of the P-state. In 1986, Heck and Gauntlett (Heck1986)

presented a method, based upon the work of Blum (Blum1981), for completely determining the parameters necessary to describe the electron excitation of a D-state. The suggested electron-photon-photon coincidence measurement has yet to be realized. In 1995 however, Mikosza *et al.*(Mikosza1995) carried out a photon-photon coincidence experiment for a helium D-P-S cascade transition. Though their measurements did not provide all of the available parameters, a relatively simple experimental setup can be used to determine the scattering cross sections of the magnetic sublevels.

The current work details the theory necessary to follow the time evolution of an excited atomic state, and applies the results to photon-photon coincidence measurements. The two different atoms which are investigated are helium and magnesium. Since magnesium has an isotope with non-zero nuclear spin, the calculations must include the effects of the hyperfine structure. Preliminary experimental work is presented for the 4^1D-2^1P-^1S cascade transition in helium, and for the 4^1P-3^1D-3^1S transition in magnesium.

The recent work by Zetner in 1997(Zetner1997), and work in progress by Johnson, Eves, and Zetner studying inelastic electron scattering off of a laser excited P-state, has also prompted my investigation of the polarized radiation due to the electron impact excitation of a D-state from a laser excited P-state. Not only are the D-P scattering cross sections available, but also some off-diagonal elements are non-zero due to the breaking of axial symmetry by the aligned P-state.

This thesis is organized into six separate chapters. The second chapter develops the theory necessary to describe the time evolution of excited atomic states, while in the third chapter the theory is applied to three separate cases: the photon-photon coincident measurement of helium; the photon-photon coincident measurement of magnesium

including the odd mass isotope; the polarized radiation from a D-state excited by electron impact from a laser induced P-state. The fourth chapter describes the apparatus designed and constructed to carry out a photon-photon coincidence measurement, while chapter five gives the preliminary results for the D-P transitions and some diagnostic tests of the photon-photon coincidence apparatus. The last chapter provides an overall summary of the work.

Chapter 2 Theory

2.1 Introduction

The excitation of an atom by an electron is a complex process, and not very well understood. Once excited however, the behaviour of the atom can be followed through its evolution until it ultimately decays to the ground state. The information which defines the state of the evolving atom is given by the polarized photons which are emitted after each energy level transition. If the scattered electron and all of the emitted photons are detected, the initial excited state of the atom can be reconstructed, and information can be obtained about the initial electron induced excitation. This chapter provides the necessary tools to describe the time evolution of an ensemble of excited atoms which have been excited to a D-state. The procedure is general enough, however, to be applied to the time evolution of other atomic systems. The theory contained in this chapter is an expansion of the work by Blum (Blum1981) who describes the evolution of the density matrix and applies the theory to a single cascade transition. The analysis of multiple cascades has already been presented by Heck and Gauntlett, Mikosza *et al.*, and Wang *et al.* (Heck1986,Mikosza1996,Wang1995).

2.2 Density Matrix Theory

Density matrices are useful when describing a mixed ensemble of states. The density operator for a system is defined as

$$\rho \equiv \sum_i w_i \left|\alpha_i\right\rangle\left\langle\alpha_i\right|, \tag{2.2.1}$$

where the weighting factors must satisfy

$$\sum_i w_i = 1. \tag{2.2.2}$$

Equation (2.2.1) describes a system in which a fraction of the ensemble, w_i, is in the state $|\alpha_i\rangle$. The density matrix for a general two state system is

$$\langle\beta_i|\rho|\beta_j\rangle = \begin{pmatrix} w_1|\langle\beta_1|\alpha_1\rangle|^2 + w_2|\langle\beta_1|\alpha_2\rangle|^2 & w_1\langle\beta_1|\alpha_1\rangle\langle\alpha_1|\beta_2\rangle + w_2\langle\beta_1|\alpha_2\rangle\langle\alpha_2|\beta_2\rangle \\ w_1\langle\beta_2|\alpha_1\rangle\langle\alpha_1|\beta_1\rangle + w_2\langle\beta_2|\alpha_2\rangle\langle\alpha_2|\beta_1\rangle & w_1|\langle\beta_2|\alpha_1\rangle|^2 + w_2|\langle\beta_2|\alpha_2\rangle|^2 \end{pmatrix}. \tag{2.2.3}$$

The diagonal elements of equation (2.2.3) give the total probability that the system is in an arbitrary state $|\beta_i\rangle$, and are necessarily real. The off-diagonal elements represent the excitation of the system into a coherent superposition of basis states. If only the diagonal elements are non-zero then the density matrix is said to be incoherent, since no phase relation is defined between the states. A density matrix is coherent if at least one off-diagonal element is non-zero. Since the total probability of a system must add to one, the trace of the density matrix must also equal one.

The ensemble average of an observable is found by summing the weighted expectation value for each state or

$$\begin{aligned} \langle A\rangle &= \sum_i w_i \langle\alpha_i|A|\alpha_i\rangle \\ &= \sum_{jj'i} w_i \langle\alpha_i|\beta_{j'}\rangle\langle\beta_{j'}|A|\beta_j\rangle\langle\beta_j|\alpha_i\rangle \\ &= \sum_{jj'} \langle\beta_j|\rho|\beta_{j'}\rangle\langle\beta_{j'}|A|\beta_j\rangle \\ &= \text{trace}[\rho A]. \end{aligned} \tag{2.2.4}$$

The above result is general, and therefore proves that the density matrix contains all the information inherent in a system. If the operator only acts on a portion of the system,

$$\langle \alpha_{i'}\beta_{j'}|A(\alpha)|\alpha_i\beta_j\rangle = \langle \alpha_{i'}|A(\alpha)|\alpha_i\rangle \delta_{j,j'}, \tag{2.2.5}$$

then the ensemble average is

$$\begin{aligned}\langle A(\alpha)\rangle &= trace[\rho\, A(\alpha)] \\ &= \sum_{ii'jj'} \langle \alpha_{i'}\beta_{j'}|\rho|\alpha_i\beta_j\rangle\langle \alpha_{i'}\beta_{j'}|A(\alpha)|\alpha_i\beta_j\rangle \\ &= \sum_{ii'j} \langle \alpha_{i'}\beta_j|\rho|\alpha_i\beta_j\rangle\langle \alpha_{i'}|A(\alpha)|\alpha_i\rangle \\ &= \sum_{ii'} \langle \alpha_{i'}|\rho(\alpha)|\alpha_i\rangle\langle \alpha_{i'}|A(\alpha)|\alpha_i\rangle \\ &= trace[\rho(\alpha)\, A(\alpha)],\end{aligned} \tag{2.2.6}$$

where the reduced density matrix is defined by

$$\langle \alpha_{i'}|\rho(\alpha)|\alpha_i\rangle = \sum_j \langle \alpha_{i'}\beta_{j'}|\rho|\alpha_i\beta_j\rangle \text{ (Blum1981).} \tag{2.2.7}$$

The reduced density matrix only contains information on the α system.

2.2.1 The Photon density matrix

An ensemble of photons can be efficiently described by the definition of a photon density matrix. A convenient basis for the density matrix is the helicity states of a photon. The quantization axis for a helicity state is the direction of propagation of the photon, while helicity is defined as the component of angular momentum along the quantization axis, and has two values, $\lambda = \pm 1$. The density matrix for the two state system is simply

$$\rho = \begin{pmatrix} \rho_{+1,+1} & \rho_{+1,-1} \\ \rho_{-1,+1} & \rho_{-1.-1} \end{pmatrix}. \tag{2.2.8}$$

What makes the helicity representation useful is that the helicity states can be shown to be synonymous with right and left hand polarized light, for example see Blum (1981). The expansion of the helicity states into a Cartesian basis is then

$$|\pm 1\rangle = \mp\frac{1}{\sqrt{2}}\left(\left|\mathbf{e}_x\right\rangle \pm i\left|\mathbf{e}_y\right\rangle\right), \tag{2.2.9}$$

or

$$\left|\mathbf{e}_x\right\rangle = -\frac{1}{\sqrt{2}}(|1\rangle - |-1\rangle), \tag{2.2.10}$$

and

$$\left|\mathbf{e}_y\right\rangle = \frac{i}{\sqrt{2}}(|1\rangle + |-1\rangle). \tag{2.2.11}$$

The helicity representation is beneficial as a mathematical description of the photon ensemble, however, the Stokes parameters are more useful from an experimental view point. The Stokes parameters are defined in terms of measurable quantities as

- the total beam intensity, I
- the degree of linear polarization with respect to two orthogonal axes oriented at 45° to the x axis

$$\eta_1 = \frac{\mathrm{I}(\pi/4) - \mathrm{I}(3\pi/4)}{\mathrm{I}} \tag{2.2.12a}$$

- the degree of circular polarization

$$\eta_2 = \frac{\mathrm{I}_{+1} - \mathrm{I}_{-1}}{\mathrm{I}} \tag{2.2.12b}$$

- the degree of linear polarization with respect to the x and y axes

$$\eta_3 = \frac{\mathrm{I}(0) - \mathrm{I}(\pi/2)}{\mathrm{I}} \tag{2.2.12c}$$

The photon density matrix can be expressed in these quantities by first ensuring that the trace of the matrix is equal to the total intensity of the ensemble of photons, and by then finding the specific intensities as noted above. For example,

$$I(0) = \langle \mathbf{e}_x | \rho | \mathbf{e}_x \rangle \ ,$$

and

$$I(\pi/2) = \langle \mathbf{e}_y | \rho | \mathbf{e}_y \rangle \ .$$

The density matrix written it terms of the Stokes parameters is therefore

$$\rho = \frac{\mathrm{I}}{2} \begin{pmatrix} 1+\eta_2 & -\eta_3 + i\eta_1 \\ -\eta_3 - i\eta_1 & 1-\eta_2 \end{pmatrix}, \tag{2.2.13}$$

where

$$I = \rho_{1,1} + \rho_{-1.-1} \tag{2.2.14a}$$

$$I \cdot \eta_1 = -i\left(\rho_{1,-1} - \rho_{-1,1}\right) \tag{2.2.14b}$$

$$I \cdot \eta_2 = \rho_{1,1} - \rho_{-1.-1} \tag{2.2.14c}$$

$$I \cdot \eta_3 = -\left(\rho_{1,-1} + \rho_{-1,1}\right). \tag{2.2.14d}$$

Often it is necessary to prepare a specific photon density matrix. A purely polarized state can be written as

$$|\mathbf{e}\rangle = \cos\beta \left|\mathbf{e}_x\right\rangle + e^{i\delta} \sin\beta \left|\mathbf{e}_y\right\rangle \ , \tag{2.2.15}$$

where β is the angle of a polarizer with respect to the x-axis and δ is the phase shift between the two axes. The photon density matrix is then given by

$$\rho = I|\mathbf{e}\rangle\langle\mathbf{e}| = \frac{I}{2} \begin{pmatrix} 1+\sin 2\beta \sin\delta & -\cos 2\beta + \mathrm{i} \sin 2\beta \cos\delta \\ -\cos 2\beta - \mathrm{i} \sin 2\beta \cos\delta & 1-\sin 2\beta \sin\delta \end{pmatrix}, \tag{2.2.16}$$

and can represent any purely polarized photon state.

2.3 Scattering Theory

The state vector for a projectile electron with momentum, $\vec{p}$, and spin, m, is $|\vec{p}\,m\rangle$. The target atom of total angular momentum, J, and magnetic quantum number, M, can be written as $|\alpha JM\rangle$, where α represents all the other quantum numbers needed to completely define the atom. The quantization axis for the atomic system is along the direction of motion of the incident electron, $\hat{p}$, and is shown in Figure 2.1 along with the relevant quantum numbers.

If a collision occurs between the electron and the atom, then the states are no longer independent and must be written as the single state vector $|\alpha JM;\vec{p}m\rangle$. The excited state can be related to the initial state via a transformation operator defined by

$$\left|\alpha J_f M_f;\vec{p}_f m_f\right\rangle = \hat{S}\left|\alpha J_i M_i;\vec{p}_i m_i\right\rangle. \tag{2.3.1}$$

The density matrix of the initial state,

$$\rho_{in} = \sum_i w_i \left|\alpha J_i M_i;\vec{p}_i m_i\right\rangle\left\langle\alpha J_i M_i;\vec{p}_i m_i\right|, \tag{2.3.2}$$

is then related to that of the final state by

$$\rho_0 = \hat{S}\rho_{in}\hat{S}^{+}. \tag{2.3.3}$$

The above density matrix contains all the information about the collision process, including the trivial case where the initial state is the same as the final state. To concentrate upon transitions between differing states, the transition operator, $\hat{T}$, is defined as

$$\hat{T} = \hat{S} - 1, \tag{2.3.4}$$

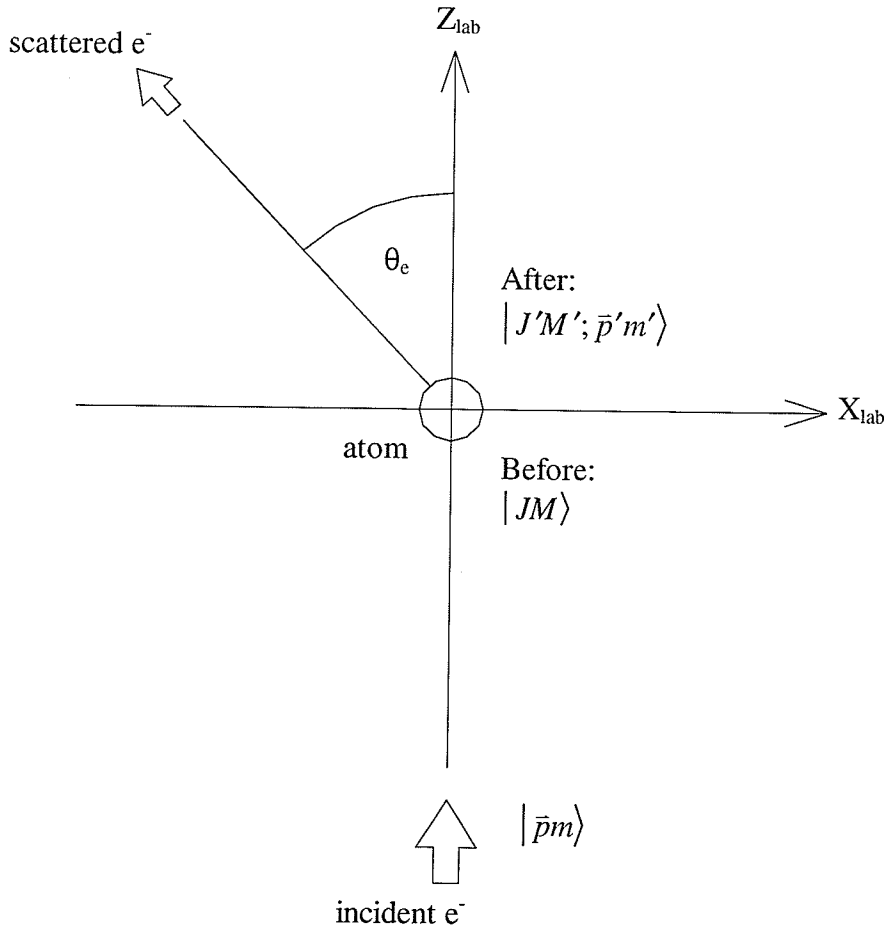

Figure 2.1: Initial scattering geometry showing the relevant quantum numbers. The incident electron and atom wave functions are initially separate. After the collision, the electron scatters off at an able θ_e and the wave functions are no longer independent.

where it is understood that the subtraction is by a unit matrix. The density matrix which describes the excited ensemble of atoms is

$$\rho_{out} = \hat{T}\rho_{in}\hat{T}^{+}. \tag{2.3.5}$$

The initial density matrix characterizes an ensemble of atoms which are all commonly in their ground state. Electron scattering off of excited atoms is discussed in section 3.4. If no attempt is made to prepare the initial spin states of the incident electrons, and the atomic electrons, then each spin dependent state is populated with equal probability and

$$\rho_{in} = \frac{1}{2(2S+1)}\sum_{M_i m_i} |\alpha S M_i; \vec{p} m_i\rangle\langle \alpha S M_i; \vec{p} m_i|, \tag{2.3.6}$$

where the total angular momentum of the atom reduces to the atomic spin, S, for the ground state. Writing only the essential quantum numbers, the excited ensemble of atoms is now represented by

$$\begin{aligned}\rho_{out} &= \hat{T}\rho_{in}\hat{T}^{+} \\ &= \frac{1}{2(2S_0+1)}\sum_{M_i m_i} \hat{T}|M_i m_i\rangle\langle M_i m_i|\hat{T}^{+},\end{aligned} \tag{2.3.7}$$

which has matrix elements

$$\begin{aligned}\langle M_f' m_f'|\rho_{out}|M_f m_f\rangle &= \frac{1}{2(2S_0+1)}\sum_{M_i m_i}\langle M_f' m_f'|\hat{T}|M_i m_i\rangle\langle M_i m_i|\hat{T}^{+}|M_f m_f\rangle \\ &= \frac{1}{2(2S_0+1)}\sum_{M_i m_i} f(M_f' m_f'; M_i m_i) f(M_f m_f; M_i m_i)^{*}.\end{aligned} \tag{2.3.8}$$

The bra-ket of the transition operator is called the scattering amplitude $f(M_f m_f; M_i m_i)$ and is usually normalized to the differential scattering cross section by

$$|f(M_f m_f; M_i m_i)|^2 = \frac{d\sigma}{d\Omega}(M_f m_f; M_i m_i). \tag{2.3.9}$$

If the spins of the electrons, atomic or scattered, are left unobserved then the density matrix must be summed over all the spin states, with the resulting reduced density matrix being only dependent upon the orbital angular momentum, or

$$\begin{aligned}\left\langle M_f' \left| \rho_{out} \right| M_f \right\rangle &= \sum_{m_f' m_f} \left\langle M_f' m_f' \left| \rho_{out} \right| M_f m_f \right\rangle \\ &= \frac{1}{2(2S_0+1)} \sum_{m_f' m_f} \sum_{M_i m_i} f\left(M_f' m_f'; M_i m_i\right) f\left(M_f m_f; M_i m_i\right)^* \\ &= \left\langle f\left(M_f'\right) f\left(M_f\right)^* \right\rangle, \end{aligned} \tag{2.3.10}$$

where the angle brackets indicate an average over all spins.

2.4 Expansion of the Density Matrix into State Multipoles

In order to calculate the evolution of the excited density matrix, careful consideration of the appropriate quantization axis to use is required. In analyzing the electron-atom collision, it is advantageous to use the electron beam direction as the z-axis, while for the calculation of the electric dipole operator elements, it is more convenient to use the photon direction as the quantization axis. By expanding the density matrix into irreducible spherical tensors it becomes a simple matter to express the density matrix in any rotated basis.

A convenient expression for the spherical tensors, as proposed by Blum (Blum1981), is

$$T_Q^K(J'J) = \sum_{M'M} (-1)^{J'-M'} (2K+1)^{1/2} \begin{pmatrix} J' & J & K \\ M' & -M & -Q \end{pmatrix} \left| J'M' \right\rangle \left\langle JM \right|, \tag{2.4.1}$$

where its matrix elements are simply

$$\left\langle J'M'\left|T_Q^K(J'J)\right|JM\right\rangle = (-1)^{J'-M'}(2K+1)^{1/2}\begin{pmatrix} J' & J & K \\ M' & -M & -Q \end{pmatrix}, \tag{2.4.2}$$

and the inverse relation is given by

$$|J'M'\rangle\langle JM| = \sum_{KQ}(-1)^{J'-M'}(2K+1)^{1/2}\begin{pmatrix} J' & J & K \\ M' & -M & -Q \end{pmatrix}T_Q^K(J'J). \tag{2.4.3}$$

The definition of an irreducible spherical tensor can be given in terms of how it transforms under a rotation, specifically

$$T_Q^K(J'J) = \sum_q T_q^K(J'J)D_{qQ}^K(R) \tag{2.4.4}$$

where $D_{qQ}^K(R)$ is the rotation matrix for the Euler angles, $R = \{\gamma,\beta,\alpha\}$, defined by

$$\begin{aligned} D_{M'M}^J(R) &= e^{-i(M'\gamma+M\alpha)}\left\langle JM'\left|e^{-iJ_y\beta/\hbar}\right|JM\right\rangle \\ &= e^{-i(M'\gamma+M\alpha)}d_{M'M}^J(\beta). \end{aligned} \tag{2.4.5}$$

The rotation of a coordinate system by the Euler angles is illustrated in Figure 2.2. Equation (2.4.4) says that an irreducible spherical tensor can be rewritten as a sum of irreducible spherical tensors defined according to a rotated basis, where the coefficients are simply the rotation matrix elements. The usefulness of expanding a density matrix into irreducible spherical tensors is a direct consequence of the above property, since a system can be analyzed in the most convenient basis, and then, when appropriate, rotated onto a different basis to aid in subsequent analysis. The tensors, defined by equation (2.4.1), do indeed satisfy equation (2.4.4) upon substitution.

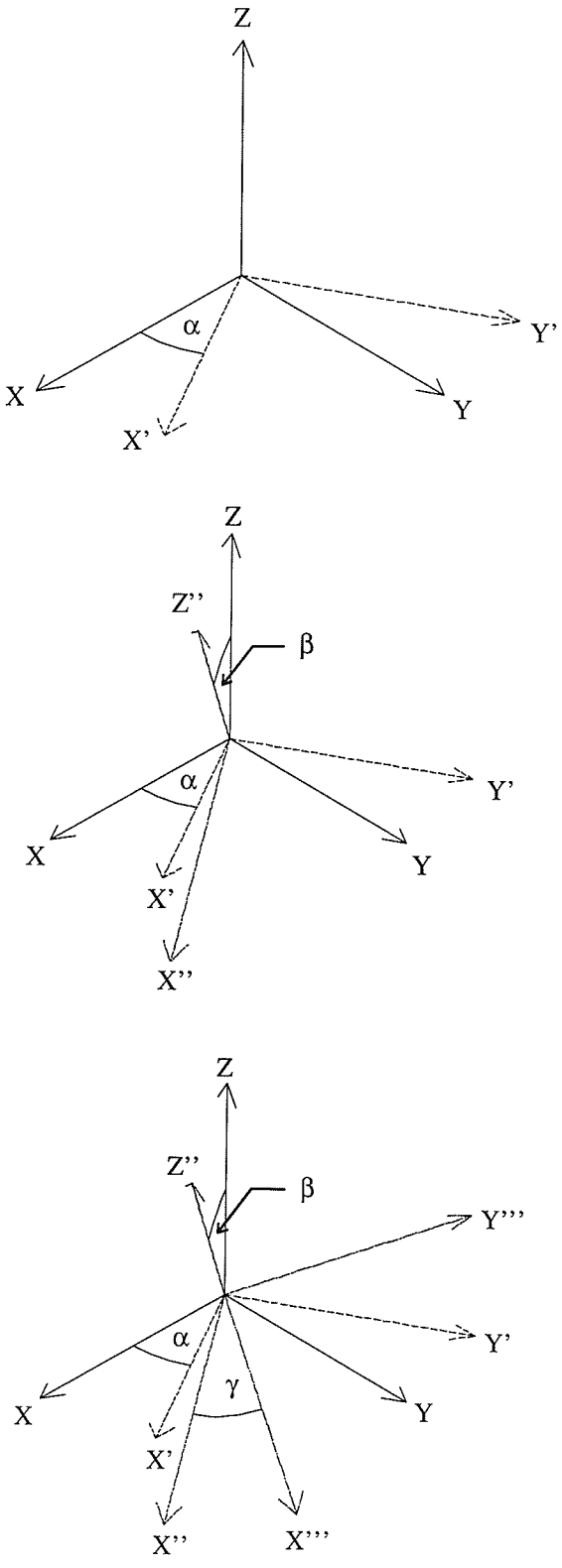

Figure 2.2: Rotation of a coordinate system due to a rotation defined by the Euler angles

Having defined the irreducible spherical tensors, the density matrix is expanded into a sum of such tensors according to

$$\begin{aligned}\rho &= \sum_{J'M'JM} \langle J'M'|\rho|JM\rangle |J'M'\rangle\langle JM| \\ &= \sum_{J'JKQ}\left[\sum_{M'M}\langle J'M'|\rho|JM\rangle(-1)^{J'-M'}\begin{pmatrix} J' & J & K \\ M' & -M & -Q\end{pmatrix}(2K+1)^{1/2}\right]T_Q^K(J'J) \\ &= \sum_{J'JKQ}\langle T_Q^K(J'J)^+\rangle T_Q^K(J'J), \end{aligned} \tag{2.4.6}$$

where the state multipoles, the coefficients of the above expansion, are defined as

$$\begin{aligned}\langle T_Q^K(J'J)^+\rangle &= \sum_{M'M}\langle J'M'|\rho|JM\rangle(-1)^{J'-M'}\begin{pmatrix} J' & J & K \\ M' & -M & -Q\end{pmatrix}(2K+1)^{1/2} \\ &= \mathrm{Tr}\{\rho \mathrm{T}_{\mathrm{Q}}^{\mathrm{K}}(J'J)^+\}. \end{aligned} \tag{2.4.7}$$

The above two equations provide a mechanism for finding the state multipoles of a given density matrix, and conversely, for finding the density matrix, having been given a set of state multipoles. The usefulness of this is apparent when a given density matrix must be acted upon by a state or operator defined according to a different basis. Using equation (2.4.7) the density matrix can be rewritten in terms of state multipoles in the correct basis, and the required density matrix elements are simply found by the action of the states upon the spherical tensor. Often it is more convenient to manipulate the state multipoles rather than the tensor operators. The analogous form of equation (2.4.4), the expansion of a tensor into a set of tensors with a different frame of reference, is given below for the state multipoles as

$$\langle T_Q^K(J'J)^+\rangle = \sum_q \langle T_q^K(J'J)^+\rangle D_{Qq}^K(R), \tag{2.4.8}$$

where the inverse relation is

$$\left\langle T_q^K(J'J)^+ \right\rangle = \sum_Q \left\langle T_Q^K(J'J)^+ \right\rangle D_{Qq}^K(R)^* , \tag{2.4.9}$$

and the superscripts over the state multipoles explicitly define the quantization axis.

2.5 Symmetry Considerations

If the scattering process shows a high degree of symmetry then the amount of information that can be extracted from the experiment will be less than for a more general system. For scattering illustrated in Figure 2.1 there are two main symmetries. The first is due to the invariance of the transition operator $\hat{T}$ with respect to parity and rotation (defined by an electromagnetic interaction Hamiltonian). This requires that there be reflection invariance within the scattering plane, or the density matrix be invariant under a rotation of π about the y-axis and an inversion of parity. The symmetry condition can be applied to the density matrix when it is written as a function of the scattering amplitudes, equation (2.5.8) or when it has been expanded into a linear superposition of irreducible spherical tensors, equation (2.4.6). Both approaches are identical.

The rotation about the y-axis is achieved by the rotation operator $D(0,\pi,0)$ acting upon a state ket, or

$$D(0,\pi,0)\left| JM;\vec{p}m \right\rangle = (-1)^{J+1/2-M-m_\varepsilon}\left| J-M;-\vec{p}-m \right\rangle . \tag{2.5.1}$$

The action of the parity operator on a similar state ket is

$$\mathrm{P}\left| JM;\vec{p}m \right\rangle = \pi\left| JM;-\vec{p}m \right\rangle , \tag{2.5.2}$$

where π is the parity eigen value with possible values of ± 1, and the combined effect of $M = \mathrm{P}\,D(0,\pi,0)$ is therefore

$$M\left|JM;\vec{p}m\right\rangle = \pi(-1)^{J+1/2-M-m}\left|J-M;\vec{p}-m\right\rangle. \tag{2.5.3}$$

If an arbitrary density matrix representing an electron excited ensemble of atoms,

$$\rho = w_i \sum_i \hat{T}\left|M_i m_i\right\rangle\left\langle M_i m_i\right|\hat{T}^+, \tag{2.5.4}$$

is to remain invariant under the effect of the combined symmetry operators then

$$\begin{aligned}\left\langle M_f' m_f'\left|\rho\right|M_f m_f\right\rangle &= \left\langle M_f' m_f'\left|M^+ M\rho M^+ M\right|M_f m_f\right\rangle \\ &= (-1)^{\alpha} w_i \sum_i \left\langle -M_f' - m_f'\left|\hat{T}\right|-M_i - m_i\right\rangle\left\langle -M_i - m_i\left|\hat{T}^+\right|-M_f - m_f\right\rangle \\ &= (-1)^{\alpha} w_i \sum_i f\left(-M_f' - m_f'; -M_i - m_i\right) f\left(-M_f - m_f; -M_i - m_i\right)^*,\end{aligned} \tag{2.5.5}$$

where

$$\alpha = 2J_f + 2J_i + 4(1/2) - M_f' - M_f - m_f' - m_f - 2M_i - 2m_i. \tag{2.5.6}$$

If the initial state is the ground state with zero spin and the incident and scattered electron spins are unresolved then

$$\begin{aligned}\left\langle M_f'\left|\rho\right|M_f\right\rangle &= \sum_{m_f m_f'}\left\langle M_f' m_f'\left|\rho\right|M_f m_f\right\rangle \\ &= (-1)^{M_f' + M_f}\frac{1}{2}\sum_{m_i m_f m_f'}(-1)^{m_f' + m_f + 2m_i} f\left(-M_f' - m_f'; 0 - m_i\right) f\left(-M_f - m_f; 0 - m_i\right)^* \\ &= (-1)^{M_f' + M_f}\left\langle f\left(-M_f'\right) f\left(-M_f\right)^*\right\rangle.\end{aligned} \tag{2.5.7}$$

The above relation implies that

$$\frac{d\sigma}{d\Omega}(\pm M) = \frac{d\sigma}{d\Omega}(M),$$

where $d\sigma(M)/d\Omega$ refers to the differential scattering cross section for excitation of the M^{th} magnetic sublevel.

Applying the reflection invariance symmetry operators to the density matrix expanded into a superposition of irreducible spherical tensors gives

$$
\begin{aligned}
M^{+}(R)\rho M &= \sum_{J'JKQ}\left\langle T_Q^K(J'J)^{+}\right\rangle D^{+}(0,\pi,0)T_Q^K(J'J)D(0,\pi,0) \\
&= \sum_{J'JKQ}\left\langle T_Q^K(J'J)^{+}\right\rangle \sum_q d_{Qq}^K(\pi)^{*}T_q^K(J'J) \\
&= \sum_{J'JKQ}\left\langle T_Q^K(J'J)^{+}\right\rangle \sum_q (-1)^{K+q}\delta_{Q,q}T_q^K(J'J) \\
&= \sum_{J'JKQ}(-1)^{K+Q}\left\langle T_Q^K(J'J)^{+}\right\rangle T_Q^K(J'J), \qquad (2.5.8)
\end{aligned}
$$

and therefore, $K+Q$ must be an even integer for the density matrix to remain invariant.

The second applicable symmetry is a direct consequence of not detecting the scattered electrons. Without their detection the scattering plane is not defined and the density matrix must be invariant for any rotation about the electrons' initial direction of propagation. An arbitrary rotation applied about the z-axis,

$$
D(0,0,\varphi)\left|JM;\vec{p}m\right\rangle = e^{iM\varphi}\left|JM;\vec{p}m\right\rangle, \qquad (2.5.9)
$$

to the density matrix defined by (2.5.4) yields

$$
\begin{aligned}
\left\langle M_f'm_f'\left|\rho\right|M_fm_f\right\rangle &= \left\langle M_f'm_f'\left|D^{+}(0,0,\pi)D(0,0,\pi)\rho D^{+}(0,0,\pi)D(0,0,\pi)\right|M_fm_f\right\rangle \\
&= e^{i(M_f-M_f')\varphi}w_i\sum_i\left\langle M_f'm_f'\left|\hat{T}\right|M_im_i\right\rangle\left\langle M_im_i\left|\hat{T}^{+}\right|M_fm_f\right\rangle \\
&= e^{i(M_f-M_f')\varphi}\left\langle M_f'm_f'\left|\rho\right|M_fm_f\right\rangle. \qquad (2.5.10)
\end{aligned}
$$

The only way in which equation (2.5.10) can be satisfied for an arbitrary rotation is if $M_f' = M_f$, and all off-diagonal elements are zero. If the scattered electrons are not measured then electron induced excitation to a singlet D-state is described by the three independent parameters $\sigma(M)$ for M=0,1,2 where $\sigma(M)$ is the integrated scattering cross section for excitation of the M^{th} magnetic sublevel. The relation between integrated and differential scattering cross sections is given in equation (1.4). An axially symmetric system is therefore incoherent.

Axial symmetry applied to the density matrix expanded into irreducible spherical tensors requires that

$$\begin{aligned} D^{+}(0,0,\varphi)\rho D(0,0,\varphi) &= \sum_{J'JKQ} \left\langle T_Q^K (J'J)^{+} \right\rangle D^{+}(0,0,\varphi) T_Q^K (J'J) D(0,0,\varphi) \\ &= \sum_{J'JKQ} \left\langle T_Q^K (J'J)^{+} \right\rangle \sum_q e^{iq\varphi} \delta_{Q,q} T_q^K (J'J) \\ &= \sum_{J'JKQ} (-1)^{iQ\varphi} \left\langle T_Q^K (J'J)^{+} \right\rangle T_Q^K (J'J). \end{aligned} \tag{2.5.11}$$

If the density matrix is to be invariant then the above equation should hold for all φ. This implies that Q must equal zero, or

$$\rho = \sum_{J'JK} \left\langle T_0^K (J'J)^{+} \right\rangle T_0^K (J'J), \tag{2.5.12}$$

and from equation (2.5.8), K must be an even integer and, hence only even state multipoles contribute. According to the previous results for an axially symmetric system, the density matrix for a D-state can be expressed as

$$\rho = \sum_{J'J} \left\langle T_0^0 (J'J)^{+} \right\rangle T_0^0 (J'J) + \left\langle T_0^2 (J'J)^{+} \right\rangle T_0^2 (J'J) + \left\langle T_0^4 (J'J)^{+} \right\rangle T_0^4 (J'J). \tag{2.5.13}$$

2.6 The Time Evolution Operator for an Excited Atomic System

Once excited by electron impact, the atom will reside in the excited state until a time t, at which point it will decay down to a lower energy state. If no electric or magnetic fields were present, and if the effects due to the fine or hyperfine coupling were minimal, then upon de-excitation the state of the atom will not have changed. The emitted photon, which carries information about the excited state, can then be used to probe the physical properties of the excitation process. To determine how the photon is related to the excited state, the Hamiltonian of the system must first be defined and then used to

describe the time evolution of the excited atom density matrix.

The time development of an atomic system is governed by the wave equation

$$\hat{H}\Psi(t) = i\hbar\frac{d\Psi}{dt}\ , \tag{2.6.1}$$

where the Hamiltonian for the system includes contributions from the canonical momentum and the scalar potential field due to the point charges. In the non-relativistic limit, the components of the canonical momentum reduce to the momentum of the particle and the time dependent vector potential. The Hamiltonian can then be written as

$$\hat{H}=\frac{1}{2\mu_N}\left[\hat{p}_N - Ze\hat{A}(\vec{r}_N,t)\right]^2 + Ze\phi(\vec{r}_N)+\frac{1}{2\mu}\sum_l\left[\hat{p}_l + e\hat{A}(\vec{r}_l,t)\right]^2 - e\phi(\vec{r}_l), \tag{2.6.2}$$

where $\hat{p}_N$ and $\hat{r}_N$ are the momentum and position operators for the nucleons, and $\hat{p}_l$ and $\hat{r}_l$ are the momentum and position operators for the electrons. If we study only those cases where a single valence electron makes a transition, and assume that the atomic constituents remain unaffected during the process, then the constant terms can be ignored and

$$\begin{aligned}\hat{H} &= \frac{1}{2\mu}\left[\hat{p} + e\hat{A}(\vec{r},t)\right]^2 - e\phi(\vec{r}) \\ &= \hat{H}_a + \hat{H}_i(t)\ ,\end{aligned} \tag{2.6.3}$$

where

$$\hat{H}_a = \frac{1}{2\mu}\hat{p}^2 - e\phi(\vec{r})\text{, and} \tag{2.6.4}$$

$$\hat{H}_i = \frac{e}{\mu}\hat{A}(\vec{r},t)\cdot\hat{p} + \frac{e^2}{2\mu}\hat{A}^2(\vec{r},t). \tag{2.6.5}$$

The term $\hat{H}_a$ is called the atomic Hamiltonian and generates the time independent energy eigenstates of the atom, or in our case those of the excited electron. The second term, $\hat{H}_i$, mediates the interaction between the atom and the radiation field, and therefore earns itself the title 'the interaction Hamiltonian'. The main component of the interaction Hamiltonian is the vector field operator, $\hat{A}$, which, according to the rules of second quantization, can be expanded in terms of the photon creation and annihilation operators, $\hat{a}_k^+$ and $\hat{a}_k$, as

$$\hat{A} = \sum_k \left(\frac{2\pi\hbar}{\omega_k} \right) \left\{ \hat{a}_k e^{-i\omega_k t + i\vec{k}\cdot\vec{r}} + \hat{a}_k^+ e^{i\omega_k t - i\vec{k}\cdot\vec{r}} \right\} \vec{\varepsilon}_k \,. \tag{2.6.6}$$

The sum is over all photon modes in a cavity which have direction $\vec{k}$, energy $\hbar\omega_k$, and polarization $\vec{\varepsilon}_k$. The action of the photon creation and annihilation operators on a photon eigenstate $|n_k\rangle$ is defined as

$$\hat{a}_k^+ |n_k\rangle = (n_k + 1)^{1/2} |n_k + 1\rangle, \tag{2.6.7}$$

and

$$\hat{a}_k |n_k\rangle = n_k^{1/2} |n_k - 1\rangle. \tag{2.6.8}$$

From the above definitions it is apparent that these operators are responsible for the emission and absorption of photons which correlate directly with de-excitation and excitation processes of an atom. For more details see Loudon (Loudon1983).

Having defined the Hamiltonian, it must still be shown how the system evolves with time. Since the interaction Hamiltonian is itself dependent upon time, we cannot write down a simple time evolution operator. To overcome this difficulty the base eigenstates are transformed according to

$$\Psi_s(t) = e^{\frac{-i\hat{H}_r t}{\hbar}}\Psi(t), \tag{2.6.9}$$

where $\hat{H}_r$ is the radiation field Hamiltonian and is defined in terms of the number operator $\hat{n}_k = \hat{a}_k^+ \hat{a}_k$ as

$$\hat{H}_r = \sum_k \hbar\omega_k \hat{n}_k , \tag{2.6.10}$$

and satisfies the time independent energy eigen value relation

$$\hat{H}_r \left| n_k \right\rangle = \hbar\omega_k n_k \left| n_k \right\rangle . \tag{2.6.11}$$

By applying the above transformation to the wave functions of equation (2.6.1) one finds that (Loudon1983)

$$\begin{aligned}\left\{\hat{H}_a + \hat{H}_i(t)\right\} e^{\frac{i\hat{H}_r t}{\hbar}}\Psi_s(t) &= i\hbar\frac{d}{dt}\left\{e^{\frac{i\hat{H}_r t}{\hbar}}\Psi_s(t)\right\} \\ &= i\hbar\left\{\frac{i\hat{H}_r}{\hbar}e^{\frac{i\hat{H}_r t}{\hbar}}\Psi_s(t) + e^{\frac{i\hat{H}_r t}{\hbar}}\frac{d\Psi_s(t)}{dt}\right\}.\end{aligned} \tag{2.6.12}$$

Multiplying both sides by $e^{-i\hat{H}_r t/\hbar}$ and noting that $\hat{H}_r$ and $\hat{H}_i$ do not commute yields

$$\left\{\hat{H}_a + \hat{H}_r + e^{\frac{-i\hat{H}_r t}{\hbar}}\hat{H}_i e^{\frac{i\hat{H}_r t}{\hbar}}\right\}\Psi_s(t) = i\hbar\frac{d\Psi_s(t)}{dt}, \tag{2.6.13}$$

where the application of the proper commutation relations gives

$$\left\{\hat{H}_a + \hat{H}_r + \hat{H}_i(t=0)\right\}\Psi_s(t) = i\hbar\frac{d\Psi_s(t)}{dt}. \tag{2.6.14}$$

The Hamiltonian on the left hand side is now time independent and the evolution of the wave function, $\Psi_s(t)$, can be described by the comparatively simple time evolution operator

$$U_s(t) = e^{\frac{-i\hat{H}_s t}{\hbar}}, \tag{2.6.15}$$

where

$$\hat{H}_s = \hat{H}_a + \hat{H}_r + \hat{H}_i = \hat{H}_o + \hat{H}_i. \tag{2.6.16}$$

Unfortunately, the Schrodinger equation cannot be solved in closed form for the above Hamiltonian due to the presence of the interaction Hamiltonian. In order to solve the Schrodinger equation, time-dependent perturbation theory must be applied. Of course, finding the eigen value solutions to the atomic Hamiltonian is in itself a daunting task for atoms other than hydrogen, but in principle it is possible. The radiation field Hamiltonian can also be solved in closed form, and the appropriate eigen value/eigen function solutions to both of the previous Hamiltonians are

$$\hat{H}_a|n_a\rangle = E_a|n_a\rangle, \tag{2.6.17}$$

and

$$\hat{H}_r|n_r\rangle = E_r|n_r\rangle. \tag{2.6.18}$$

The time evolution operator for a system composed of the above Hamiltonians is

$$\hat{U}_o(t) = e^{\frac{-i\hat{H}_o t}{\hbar}}. \tag{2.6.19}$$

A useful transformation of the atomic time evolution operator, given by equation (2.6.15), results if the complex conjugate of the previous time evolution operator is applied to it. The time evolution of the new operator is

$$i\hbar\frac{d}{dt}\left\{\hat{U}_o^+(t)\hat{U}_s(t)\right\} = i\hbar\left\{\frac{i\hat{H}_o}{\hbar}e^{\frac{i\hat{H}_o t}{\hbar}}\hat{U}_s(t) + e^{\frac{i\hat{H}_o t}{\hbar}}\frac{d}{dt}\hat{U}_s(t)\right\}$$

$$= i\hbar\left\{\frac{i\hat{H}_o}{\hbar}\hat{U}_o^+(t)\hat{U}_s(t) + \hat{U}_o^+(t)\frac{\hat{H}_s\hat{U}_s(t)}{i\hbar}\right\}$$

$$= \hat{U}_o^+(t)\hat{H}_i\hat{U}_o(t)\hat{U}_o^+(t)\hat{U}_s(t)$$

$$i\hbar\frac{d}{dt}\hat{U}'(t) = \hat{H}_i'\hat{U}'(t) \tag{2.6.20}$$

where

$$\hat{U}'(t) = \hat{U}_o^+(t)\hat{U}(t), \tag{2.6.21}$$

and

$$\hat{H}_i'(t) = \hat{U}_o^+(t)\hat{H}_i\hat{U}_o(t). \tag{2.6.22}$$

The benefit of the above transform arises when both sides of equation (2.6.20) are integrated with respect to time, giving

$$\hat{U}'(t) = 1 - \frac{i}{\hbar}\int_0^t \hat{H}_i'(\tau)\hat{U}'(\tau)d\tau,$$

where the above recursive formula, in its expanded form, is called the Dyson series. This is useful since the time evolution operator, $\hat{U}_s(t)$, has been expanded in a power series of $\hat{H}_i'(t)$, and can be calculated to any degree of accuracy depending on the number of terms included. To the first order,

$$\hat{U}_s(t) = \hat{U}_o(t)\left\{1 - \frac{i}{\hbar}\int_0^t \hat{U}_o^+(\tau)\hat{H}_i\hat{U}_o(\tau)d\tau\right\}. \tag{2.6.23}$$

2.7 The Time Evolution of the Density Matrix

The density matrix of the excited atoms directly after the collision is $\rho(t=0)$, which evolves in time according to the time evolution operator as

$$\rho(t) = \hat{U}_s(t)\rho(0)\hat{U}_s^+(t). \qquad (2.7.1)$$

This matrix contains all the observable information about the state of the atom immediately after the collision. To filter this information out of the time evolving density matrix, the photons emitted during de-excitation can be observed and the resulting information can be directly related to the reduced density matrix of the photon. Such a matrix completely defines the photon, and is only a function of the initial state.

The notation which will be used in the following sections is summarized by the energy scheme in Figure 2.3. The different coordinate axes which will be used to simplify the analysis are shown for each part of the cascade: the initial electron excitation to the D-state in Figure 2.4; the decay to the P-state in Figure 2.5; the final decay to the ground state in Figure 2.6.

The state ket of an atom with orbital angular momentum L_i, and z-component M_i is, in general, defined by the complete set of quantum numbers $|\alpha L_i M_i\rangle$, where α represents all the other quantum numbers required to define the state completely. We can represent such a state in the more concise form, $|L_i M_i\rangle$, or even just $|i\rangle$ so long as no confusion is possible. A photon is completely described by the ket $|\omega_k \hat{k} \lambda_k\rangle$, which specifies the energy $\hbar\omega_k$, the direction of propagation $\hat{k}$, and the helicity λ_k. To make subsequent calculations easier the quantization axis will be defined to be the direction of propagation of the emitted photon. This axis will obviously change as the atom emits the second photon in the cascade. The density matrix for a specific energy level, i, with

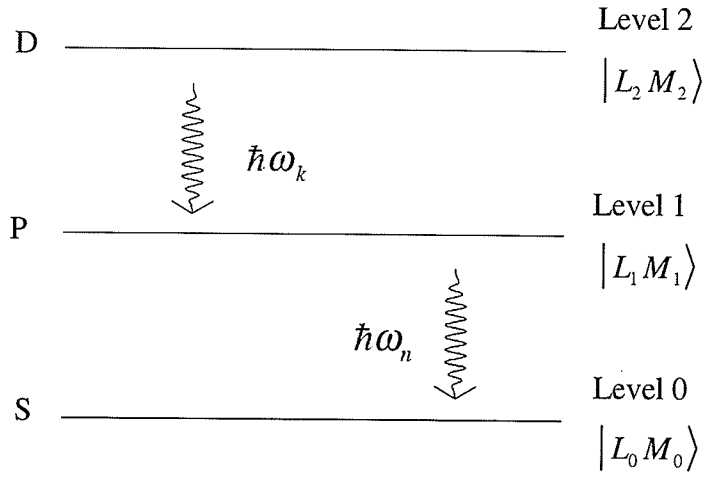

Figure 2.3: The energy level scheme for the D-P-S cascade transition illustrating the general notation which will be used in the following sections.

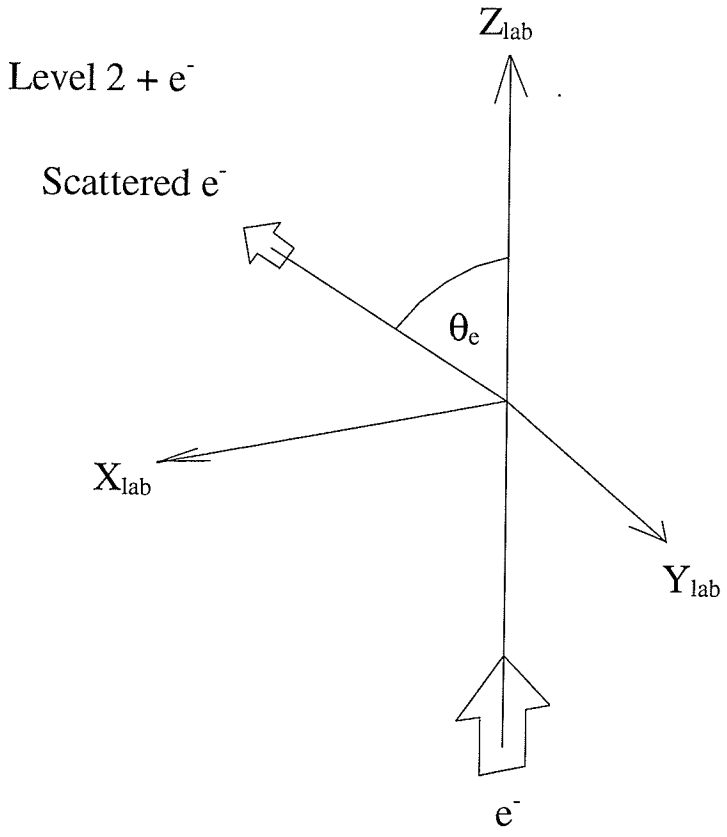

Figure 2.4: The initial electron excitation of the atom. The scattering plane is defined by the Z-axis and X-axis. This coordinate system is called the lab frame, where the Z-axis is along the direction of propagation of the incident electrons.

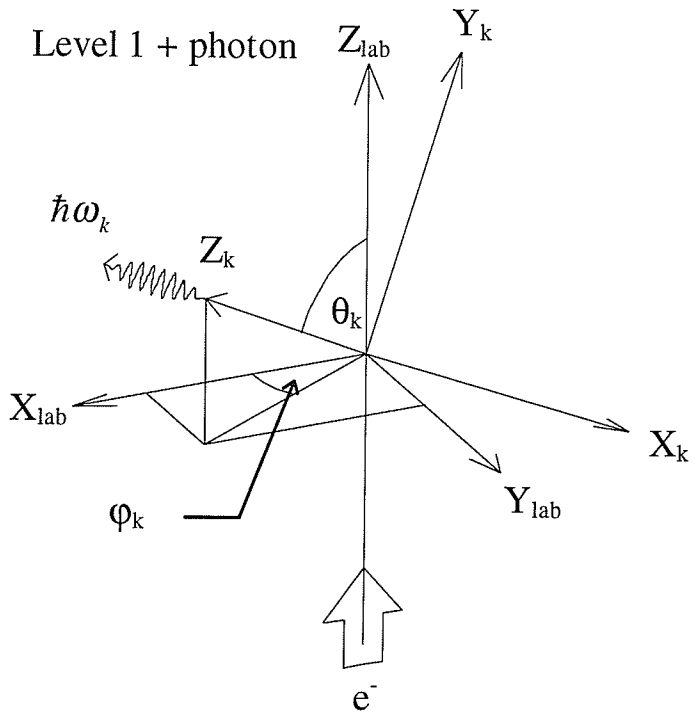

Figure 2.5: The atom after de-exciting to the P-state. To aid in the analysis of the dipole operators the quantization axis is defined by the Z_k-axis. The two sets of axes, the lab frame and the current photon frame, are related by the angles θ_k,φ_k.

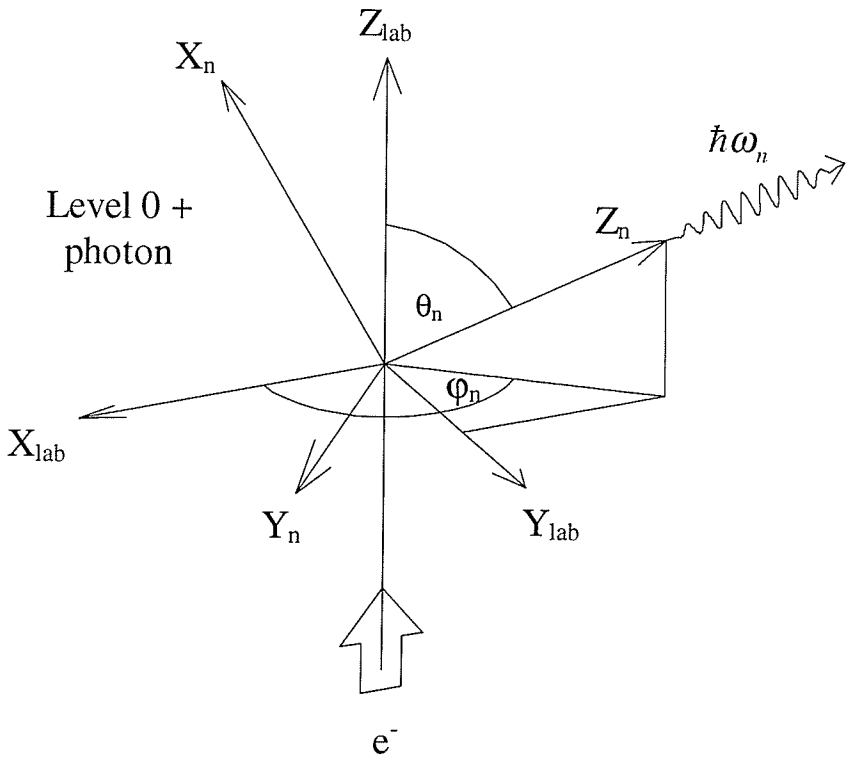

Figure 2.6: The atom after de-exciting to the ground state. To aid in the analysis of the dipole operators, the quantization axis is now defined by the Z_n-axis. The two sets of axes, the lab frame and the current photon frame, are related by the angles θ_n,φ_n.

quantum numbers defined by a z-axis in direction $\hat{k}$ will be characterized by $\rho_i^{\hat{k}}(t)$, and a density matrix which also defines a specific photon will be characterized by $\rho_{i,kk'}^{\hat{k}}(t)$.

Using the above notation, the density matrix for the initially excited state is

$$\rho_2^{\hat{k}}(t) = \hat{U}_s(t)\rho_2^{\hat{k}}(0)\hat{U}_s^+(t). \tag{2.7.2}$$

If, at a time t_1, the atom de-excites via photon emission to energy level 1, then the corresponding density matrix elements are given by

$$\left\langle 1;\hat{k}\left|\rho_2^{\hat{k}}(t_1)\right|1';\hat{k}'\right\rangle = \left\langle 1;\hat{k}\left|\hat{U}_s(t_1)\rho_2^{\hat{k}}(0)\hat{U}_s^+(t_1)\right|1';\hat{k}'\right\rangle. \tag{2.7.3}$$

The above equation is a function of both the emitted photon and the subsequent atomic state. Since it is the photon which will be measured, the reduced density matrix is formed by summing over the atomic states

$$\rho_{1,kk'}^{\hat{k}}(t_1) = \sum_{J_1 M_1}\left\langle 1;\hat{k}\left|\hat{U}_s(t_1)\rho_2^{\hat{k}}(0)\hat{U}_s^+(t_1)\right|1;\hat{k}'\right\rangle \tag{2.7.4}$$

giving a photon density matrix which only describes the emitted photon.

To continue characterizing the time evolution of the atom, the density matrix describing the first energy level, $\rho_1^{\hat{k}}(t;t_1)$, must also be subjected to the time evolution operators as in equation (2.7.2). A difficulty arises due to the definition of the quantization axis, which requires that all quantum numbers be related to the direction of propagation of the emitted photon. When a second photon is emitted, the time evolution operators and the states of the system are quantized according to it, however, the actual density matrix , $\rho_1^{\hat{k}}(t;t_1)$, is defined according to the direction of propagation of the first photon. This can be resolved by expanding $\rho_1^{\hat{k}}(t;t_1)$ into its state multipoles and then expanding them into a set of multipoles whose quantization axis is that of the second

photon. The resulting density matrix will be defined by $\rho^{\hat{n}}_{1,kk'}$, and its evolution characterized by

$$\rho^{\hat{n}}_{1,kk'}(t;t_1) = \hat{U}_s(t;t_1)\rho^{\hat{n}}_{1,kk'}(t_1)\hat{U}^+_s(t;t_1). \tag{2.7.5}$$

After the emission of the second photon in direction $\hat{n}$, and at a time t_2, the density matrix elements are

$$\langle 0;\hat{n}|\rho^{\hat{n}}_{1,kk'}(t_2;t_1)|0';\hat{n}'\rangle = \langle 0;\hat{n}|\hat{U}_s(t_2;t_1)\rho^{\hat{n}}_{1,kk'}(t_1)\hat{U}^+_s(t_2;t_1)|0;\hat{n}'\rangle. \tag{2.7.6}$$

Since the ground state is non-degenerate, the atomic density matrix and the photon density matrix are both given by the single element shown above.

A two level cascade process for an axially symmetric system is almost completely described by the previous density matrices. To pull out the information describing the initial collision-excited state, all that is required is the calculation and then measurement of both the photon polarization density matrices. As mentioned beforehand, for the excitation of an atomic D state there are only 3 unknowns available for measurement if the collision process is axially symmetric.

2.7.1 Evaluation of the Density Matrix Elements

The term $\langle 1;\hat{k}|\rho^{\hat{k}}_2(t_1)|1';\hat{k}'\rangle$, and the corresponding terms for the different energy level transitions are common elements of the photon density matrix. To analyze them, the time evolution operators are explicitly included and completeness is applied using the excited state eigenkets, or

$$\left\langle 1;\hat{k}\left|\rho_2^{\hat{k}}(t_1)\right|1';\hat{k}'\right\rangle = \left\langle 1;\hat{k}\left|\hat{U}_s(t_1)\rho_2^{\hat{k}}(0)\hat{U}_s^{+}(t_1)\right|1';\hat{k}'\right\rangle$$
$$= \sum_{J_2'M_2'}\sum_{J_2M_2}\left\langle 1;\hat{k}\left|\hat{U}_s(t_1)\right|2'\right\rangle\left\langle 2'\left|\rho_2^{\hat{k}}(0)\right|2\right\rangle\left\langle 2\left|\hat{U}_s^{+}(t_1)\right|1';\hat{k}'\right\rangle. \qquad (2.7.7)$$

Since

$$\left\langle 2\left|\hat{U}_s^{+}(t_1)\right|1';\hat{k}'\right\rangle = \left\langle 1';\hat{k}'\left|\hat{U}_s(t_1)\right|2\right\rangle^{*}, \qquad (2.7.8)$$

we need to explicitly evaluate only two distinct matrix elements. The first to be considered, the matrix element of the time evolution operator, is evaluated by applying first order perturbation theory to the evolution operator, or from equation (2.6.23)

$$\left\langle 1;\hat{k}\left|\hat{U}_s(t_1)\right|2'\right\rangle = \left\langle 1;\hat{k}\left|\hat{U}_o(t_1)\right\{1-\frac{i}{\hbar}\int_0^{t_1}\hat{U}_o^{+}(\tau)\hat{H}_i\hat{U}_o(\tau)d\tau\right\}\right|2'\rangle. \qquad (2.7.9)$$

The action of the time evolution operator $\hat{U}_o(t_1)$ on the different basis states is

$$\hat{U}_o(t_1)\left|1;\hat{k}\right\rangle = e^{\frac{-i\hat{H}_o t_1}{\hbar}}\left|1;\hat{k}\right\rangle = e^{\frac{-iE_1 t_1}{\hbar}}e^{-i\omega_k t_1}\left|1;\hat{k}\right\rangle, \text{ and} \qquad (2.7.10)$$

$$\hat{U}_o(t_1)\left|2'\right\rangle = e^{\frac{-i\hat{H}_o t_1}{\hbar}}\left|2'\right\rangle = e^{\frac{-iE_{2'}t_1}{\hbar}}e^{\frac{-\gamma_{2'}t_1}{2}}\left|2'\right\rangle. \qquad (2.7.11)$$

An extra factor has been included for the time evolution of the excited state which accounts for the radiation of the moving electron before the state de-excites. The factor is an inherent component of the de-excitation process and specifies the minimum linewidth that can be achieved for the transition. The term γ_2 is therefore called the natural linewidth of the transition. Application of the above results to equation (2.7.9) yields

$$\left\langle 1;\hat{k}\left|\hat{U}_s(t_1)\right|2'\right\rangle = -\frac{i}{\hbar}e^{\frac{-iE_1t_1}{\hbar}}e^{-i\omega_k t_1}\int_0^{t_1}\left\langle 1;\hat{k}\left|\hat{U}_o^+(\tau)\hat{H}_i\hat{U}_o(\tau)\right|2'\right\rangle d\tau$$

$$= -\frac{i}{\hbar}e^{\frac{-iE_1t_1}{\hbar}}e^{-i\omega_k t_1}\left\langle 1;\hat{k}\left|\hat{H}_i\right|2'\right\rangle\int_0^{t_1}e^{\frac{iE_1\tau}{\hbar}}e^{i\omega_k\tau}e^{\frac{-iE_{2'}\tau}{\hbar}}e^{\frac{-\gamma_2'}{2}}d\tau$$

$$= \frac{i}{\hbar}\left\langle 1;\hat{k}\left|\hat{H}_i\right|2'\right\rangle e^{\frac{-iE_1t_1}{\hbar}}e^{-i\omega_k t_1}\frac{1-e^{-i(\omega_{2'1}-\omega_k)t_1}e^{\frac{-\gamma_{2'}}{2}}}{i(\omega_{2'1}-\omega_k)+\gamma_{2'}/2}, \qquad (2.7.12)$$

where

$$\omega_{2'1} = \frac{E_{2'} - E_1}{\hbar}. \qquad (2.7.13)$$

The next step requires finding the matrix elements of the perturbing interaction Hamiltonian. To evaluate $\left\langle 1;\hat{k}\left|\hat{H}_i\right|2'\right\rangle$ recall that

$$\hat{H}_i = \frac{e}{\mu}\hat{A}(\vec{r})\cdot\hat{p} + \frac{e^2}{2\mu}\hat{A}^2(\vec{r}),$$

and

$$\hat{A}(\vec{r}) = \sum_k\left(\frac{2\pi\hbar}{\omega_k}\right)^{1/2}\left\{\hat{a}_k e^{i\vec{k}\cdot\vec{r}} + \hat{a}_k^+ e^{-i\vec{k}\cdot\vec{r}}\right\}\vec{\varepsilon}_k .$$

The squared vector potential term mediates a transition with the emission, or absorption of two photons. There is a very small probability of such a process occurring, as demonstrated by Mizushima (Mizushima1970) , and will not be considered here. Using the above equations the interaction Hamiltonian matrix elements become

$$\begin{aligned}\left\langle 1;\hat{k}\left|\hat{H}_i\right|2'\right\rangle &= \frac{e}{\mu}\left\langle 1;\hat{k}\left|\hat{A}(\vec{r})\cdot\hat{p}\right|2'\right\rangle \\ &= \frac{e}{\mu}\sum_{k'}\left(\frac{2\pi\hbar}{\omega_{k'}}\right)^{1/2}\left\{\left\langle 1;\hat{k}\left|\hat{a}_{k'}e^{i\vec{k}'\cdot\vec{r}}\,\vec{\varepsilon}_{k'}\cdot\hat{p}\right|2'\right\rangle+\left\langle 1;\hat{k}\left|\hat{a}_{k'}^{+}e^{-i\vec{k}'\cdot\vec{r}}\,\vec{\varepsilon}_{k'}\cdot\hat{p}\right|2'\right\rangle\right\} \\ &= \frac{e}{\mu}\left(\frac{2\pi\hbar}{\omega_k}\right)^{1/2}\langle 1|e^{i\vec{k}\cdot\vec{r}}\,\vec{\varepsilon}_k\cdot\hat{p}|2'\rangle. \end{aligned} \tag{2.7.14}$$

The electric dipole approximation is now made, in which the size of the atom is assumed to be small as compared to the wavelength of the radiation field. The exponential, approximated to the first order, is therefore one. The resulting expression is usually written in terms of $\hat{r}$ by making use of the commutation relation between it and the atomic Hamiltonian, or

$$\left[\hat{r},\hat{H}_o\right]=\frac{i\hbar\hat{p}}{\mu}.$$

The resulting expression for the matrix elements of the interaction Hamiltonian is

$$\left\langle 1;\hat{k}\left|\hat{H}_i\right|2'\right\rangle=-ie\left(\frac{2\pi\hbar}{\omega_k}\right)^{1/2}\omega_{2'1}\langle 1|\vec{\varepsilon}_k\cdot\hat{r}|2'\rangle, \tag{2.7.15}$$

and the time evolution operator becomes

$$\begin{aligned}\left\langle 1;\hat{k}\left|\hat{U}_s(t_1)\right|2'\right\rangle &= \frac{i}{\hbar}\left\langle 1;\hat{k}\left|\hat{H}_i\right|2'\right\rangle e^{\frac{-iE_1t_1}{\hbar}}e^{-i\omega_k t_1}\frac{1-e^{-i(\omega_{2'1}-\omega_k)t_1}e^{\frac{-\gamma_{2'}}{2}}}{i(\omega_{2'1}-\omega_k)+\gamma_{2'}/2} \\ &= \frac{e}{\hbar}\left(\frac{2\pi\hbar}{\omega_k}\right)^{1/2}\omega_{2'1}\langle 1|\vec{\varepsilon}_k\cdot\hat{r}|2'\rangle e^{\frac{-iE_1t_1}{\hbar}}e^{-i\omega_k t_1}\frac{1-e^{-i(\omega_{2'1}-\omega_k)t_1}e^{\frac{-\gamma_{2'}}{2}}}{i(\omega_{2'1}-\omega_k)+\gamma_{2'}/2}. \end{aligned} \tag{2.7.16}$$

The position operator, $\hat{r}$, is a vector operator, or tensor of rank one. The matrix element of $\vec{\varepsilon}_k\cdot\hat{r}$ can be evaluated using the Wigner-Eckart Theorem, which separates the physical orientation of the system with respect to the quantization axis from the physics of the

interaction. For a tensor of rank K, and magnetic quantum number Q the Wigner-Eckart Theorem states that

$$\langle L_1 M_1 | V_Q^K | L_2 M_2 \rangle = (-1)^{L_1 - M_1} \begin{pmatrix} L_1 & K & L_2 \\ -M_1 & Q & M_2 \end{pmatrix} \langle L_1 \| V^K \| L_2 \rangle, \tag{2.7.17}$$

where the Wigner 3j symbol has been used, and the physics of the interaction is given solely by the reduced matrix element $\langle L_1 \| V^K \| L_2 \rangle$. Writing the components of the position operator in the helicity basis of the photon k,

$$\hat{r} = r_{-1}\vec{\varepsilon}_{k,-1} + r_0\vec{\varepsilon}_{k,0} + r_1\vec{\varepsilon}_{k,1}, \tag{2.7.18}$$

and applying the Wigner-Eckart Theorem gives

$$\langle 1; \hat{k} | \hat{U}_s(t_1) \| 2' \rangle = \frac{e}{\hbar}\left(\frac{2\pi\hbar}{\omega_k}\right)^{1/2} \omega_{2'1} W_{2'1}(t_1) (-1)^{L_1 - M_1} \begin{pmatrix} L_1 & 1 & L_{2'} \\ -M_1 & \lambda_k & M_{2'} \end{pmatrix} \langle 1 \| r_\lambda \| 2' \rangle, \tag{2.7.19}$$

where

$$W_{2'1}(t_1) = \frac{e^{\frac{-iE_1 t_1}{\hbar}} e^{-i\omega_k t_1}\left(1 - e^{-i(\omega_{2'1} - \omega_k)t_1} e^{\frac{-\gamma_{2'}}{2}}\right)}{i(\omega_{2'1} - \omega_k) + \gamma_{2'}/2}. \tag{2.7.20}$$

The above is the first of two matrix elements required to describe the time evolution of the excited state density matrix.

The second, according to equation (2.7.7), is the density matrix element of state 2 at the time of excitation. A general approach, independent of the excitation method, is to write the density matrix as a superposition of spherical irreducible tensors, or

$$\rho_2^{\hat{k}}(0) = \sum_{L_{2'} L_2 K Q} \left\langle T_Q^K (L_{2'} L_2)^+ \right\rangle^{\hat{k}} T_Q^K (L_{2'} L_2). \tag{2.7.21}$$

Recalling that the matrix elements of the tensor operator are

$$\left\langle L_{2'} M_{2'} \left| T_Q^K \left(L_{2'} L_2 \right) \right| L_2 M_2 \right\rangle = (-1)^{L_{2'} - M_{2'}} (2K+1)^{1/2} \begin{pmatrix} L_{2'} & L_2 & K \\ M_{2'} & -M_2 & -Q \end{pmatrix}, \tag{2.7.22}$$

then the components of the density matrix are

$$\left\langle L_{2'} M_{2'} \left| \rho_2^{\hat{k}}(0) \right| L_2 M_2 \right\rangle = \sum_{KQ} (-1)^{L_{2'} - M_{2'}} (2K+1)^{1/2} \begin{pmatrix} L_{2'} & L_2 & K \\ M_{2'} & -M_2 & -Q \end{pmatrix} \left\langle T_Q^K \left(L_{2'} L_2 \right)^+ \right\rangle^{\hat{k}}. \tag{2.7.23}$$

As mentioned previously, the state multipoles contain the 'physics' of the state and for excitation by electron collision they can be written in terms of the scattering amplitudes. In the case of excitation by decay from a higher lying atomic state, the state multipoles can be found from the time-evolved density matrix of the higher lying state by the procedure we now describe.

Applying the results of the previous analysis, equations (2.7.19) and (2.7.23), to equation (2.7.7) gives the time evolution of the density matrix as

$$\begin{aligned} \left\langle 1; \hat{k} \left| \rho_2^{\hat{k}}(t_1) \right| 1'; \hat{k}' \right\rangle &= \left\langle 1; \hat{k} \left| \hat{U}_s(t_1) \rho_2^{\hat{k}}(0) \hat{U}_s^+(t_1) \right| 1'; \hat{k}' \right\rangle \\ &= \sum_{L_2 M_2' L_2 M_2} \left\langle 1; \hat{k} \left| \hat{U}_s(t_1) \right| 2' \right\rangle \left\langle 2' \left| \rho_2^{\hat{k}}(0) \right| 2 \right\rangle \left\langle 2 \left| \hat{U}_s^+(t_1) \right| 1'; \hat{k}' \right\rangle \\ &= \sum_{L_2 M_2' L_2 M_2} \sum_{KQ} C_{21,k}(t_1) (-1)^{L_1 - M_1 + L_{1'} - M_{1'} + L_{2'} - M_{2'}} (2K+1)^{1/2} \\ &\quad \begin{pmatrix} L_1 & 1 & L_{2'} \\ -M_1 & \lambda_k & M_{2'} \end{pmatrix} \begin{pmatrix} L_{2'} & L_2 & K \\ M_{2'} & -M_2 & -Q \end{pmatrix} \begin{pmatrix} L_{1'} & 1 & L_2 \\ -M_{1'} & \lambda_{k'} & M_2 \end{pmatrix} \\ &\quad \left\langle 1 \left\| r_{\lambda'} \right\| 2' \right\rangle \left\langle T_Q^K \left(L_{2'} L_2 \right)^+ \right\rangle^{\hat{k}} \left\langle 1' \left\| r_{\lambda} \right\| 2 \right\rangle^* \end{aligned} \tag{2.7.24}$$

where

$$C_{21,k}(t_1) = \frac{2\pi e^2}{\hbar \omega_k} \omega_{21}^2 W_{2'1}(t_1) W_{21'}(t_1)^*, \tag{2.7.25}$$

and the approximations $\omega_k \cong \omega_{k'}$ and $\omega_{2'1} \cong \omega_{21'} = \omega_{21}$ have been made. The above term is dependent upon two differing frequencies: the frequency of the radiation field, which interacts with the atom, and the energy difference between the transition states. To collapse the expression into only a function of the transition frequency, it is multiplied by the density of states of ω_k and integrated over all positive real numbers. However, since the trace of the photon density matrix has been defined to be in units of intensity, the expression must first be multiplied by the energy of each photon. The required integration is

$$\int_0^\infty \hbar\omega_k C_{21,k}(t_1)\rho_{\omega_k} d\omega_k d\Omega = 2\pi e^2 \frac{d\Omega}{2\pi^2 c^3}\omega_{21}^2 \int_0^\infty \omega_k^2 W_{2'1}(t_1) W_{21'}(t_1)^* d\omega_k$$
$$= \frac{e^2 d\Omega}{\pi c^3}\omega_{21}^2 \int_0^\infty \omega_k^2 W_{2'1}(t_1) W_{21'}(t_1)^* d\omega_k ,$$

which can be evaluated with the help of the integral (Heitler1944)

$$\int_0^\infty f(\omega)\frac{1-e^{i(\omega-\omega_0)t-\gamma t/2}}{\omega_0-\omega-i\gamma/2}d\omega = i\pi f(\omega_0 - i\gamma/2), \tag{2.7.26}$$

and therefore

$$C_{21}(t_1) = \int_0^\infty h\omega_k C_{21,k}(t_1)\rho_{\omega_k} d\omega_k d\Omega$$
$$= \frac{e^2\omega_{21}^4}{c^3}\frac{1-e^{-i\omega_{22'}t_1}e^{-\gamma_{22'}t_1}}{i\omega_{22'}+\gamma_{22'}}d\Omega, \tag{2.7.27}$$

where

$$\omega_{22'} = \omega_{21'} - \omega_{2'1} \text{ and } \gamma_{22'} = \frac{\gamma_2 + \gamma_{2'}}{2}. \tag{2.7.28}$$

The effects of a finite detector area have also been included by the addition of the solid angle. Equation (2.7.23) can now be written as

$$\begin{aligned}\left\langle 1;\hat{k}\left|\rho_2^{\hat{k}}(t_1)\right|1';\hat{k}'\right\rangle &= \left\langle 1;\hat{k}\left|\hat{U}_s(t_1)\rho_2^{\hat{k}}(0)\hat{U}_s^{+}(t_1)\right|1';\hat{k}'\right\rangle \\ &= \sum_{L_2M_2'}\sum_{L_2M_2}\left\langle 1;\hat{k}\left|\hat{U}_s(t_1)\right|2'\right\rangle\left\langle 2'\left|\rho_2^{\hat{k}}(0)\right|2\right\rangle\left\langle 2\left|\hat{U}_s^{+}(t_1)\right|1';\hat{k}'\right\rangle \\ &= \sum_{L_2M_2'}\sum_{L_2M_2}C_{21,k}(t_1)\left\langle L_1M_1\left|\vec{\varepsilon}_k\cdot\hat{r}\right|L_{2'}M_{2'}\right\rangle\left\langle L_{2'}M_{2'}\left|\rho_2^{\hat{k}}(0)\right|L_2M_2\right\rangle \\ &\qquad \left\langle L_2M_2\left|\vec{\varepsilon}_{k'}^{*}\cdot\hat{r}\right|L_{1'}M_{1'}\right\rangle\end{aligned} \tag{2.7.28}$$

where the contributions from the dipole operator terms are clearly visible.

If the electron source, which is exciting the atoms, is a continuous beam then there is no way to keep track of the amount of time elapsed before the atom decays. In fact, the emitted photons will be randomly distributed over time and the detection system is then sensitive to the number of counts of detected photons and not their individual arrival times. For such a case, the sampling time of the apparatus is much longer than the decay time of the atom, and the exponential factor in equation (2.7.26) goes to zero. A second simplification results if the energy levels are well defined and resolvable by the equipment. The energy difference between the state transitions, $\omega_{21'}$ and $\omega_{2'1}$, vanish giving the steady-state form of equation (2.7.26) for resolvable lines as

$$C_{21} = \frac{e^2\omega_{21}^4}{c^3}\frac{1}{\gamma_{22'}}d\Omega\,. \tag{2.7.29}$$

2.8 Effects of Nuclear Spin

Since the results from the previous section pertain only to atoms with zero nuclear spin, these results must be amended for atoms with non-zero nuclear spin. The angular

momentum vector for the atom is now the sum of the orbital angular momentum vector, L, and the spin vector of the nucleus, I. The atom can therefore be characterized by the state vector $|\alpha(LI)FM\rangle$, where F is the total angular momentum, and M is the z-component of F. During the excitation process it is assumed that no particular spin orientation of the nucleus is favoured and the state vector is then essentially identical to the one used for the atom with no nuclear spin, but with the initial density matrix divided by 2I+1 to account for the unresolved nuclear spin states. Equation (2.7.28) can then accurately describe a non-zero nuclear spin atom if the quantum number L, and all its variations, is replaced by the total angular momentum quantum number F. Unfortunately, the dipole operators complicate the evaluation of equation (2.7.28) since they mediate transitions between the orbital angular momentum states, and not the total angular momentum. Therefore, before the Wigner-Eckart theorem can be applied to equation (2.7.16), the coupled angular momentum states $|(LI)FM\rangle$ must be uncoupled into a sum of states $|LM_J\rangle \otimes |IM_I\rangle$, by the transformation

$$\begin{aligned} |(LI)FM\rangle &= \sum_{M_J M_I} |LI; M_L M_I\rangle\langle LI; M_L M_I|(LI)FM\rangle \\ &= \sum_{M_L M_I} (-1)^{-L+I-M}(2F+1)^{1/2}\begin{pmatrix} L & I & F \\ M_J & M_I & -M \end{pmatrix} |LM_L\rangle \otimes |IM_I\rangle. \end{aligned} \qquad (2.8.1)$$

Applying the above equation to the matrix elements of the electric dipole operator gives

$$
\begin{aligned}
\langle (L_1 I) F_1 M_1 | r_\lambda | (L_2 I') F_2 M_2 \rangle = & \sum_{M_{L2} M_{L1} M_I' M_I} (-1)^{-L_2 - L_1 + M_2 + M_1 + I' + I} \left[(2F_2 + 1)(2F_1 + 1) \right]^{1/2} \\
& \langle L_1 M_{J1} | r_\lambda | L_2 M_{J2} \rangle \begin{pmatrix} L_2 & I' & F_2 \\ M_{L2} & M_I' & -M_2 \end{pmatrix} \\
& \begin{pmatrix} L_1 & I & F_1 \\ M_{L1} & M_I & -M_1 \end{pmatrix} \delta_{I,I'} \delta_{M_I', M_I} \\
= & \sum_{M_{L2} M_{L1} M_I} (-1)^{-L_2 + M_2 + M_1 + 2I - M_{L1}} \left[(2F_2 + 1)(2F_1 + 1) \right]^{1/2} \\
& \langle L_1 \| r_\lambda \| L_2 \rangle \begin{pmatrix} L_2 & I & F_2 \\ M_{L2} & M_I & -M_2 \end{pmatrix} \\
& \begin{pmatrix} L_1 & I & F_1 \\ M_{L1} & M_I & -M_1 \end{pmatrix} \begin{pmatrix} L_1 & 1 & L_2 \\ -M_{L1} & \lambda & M_{L2} \end{pmatrix} \\
= & (-1)^{1 + L_1 + I + F_1 + F_2 - M_1} \left[(2F_2 + 1)(2F_1 + 1) \right]^{1/2} \\
& \begin{pmatrix} F_1 & 1 & F_2 \\ -M_1 & \lambda & M_2 \end{pmatrix} \begin{Bmatrix} L_1 & F_1 & I \\ F_2 & L_2 & 1 \end{Bmatrix} \langle L_1 \| r_\lambda \| L_2 \rangle \delta_{I,I'},
\end{aligned}
\tag{2.8.2}
$$

where the contraction of the Wigner-6J symbol has been used to eliminate the sums over the magnetic quantum numbers.

Another complication arises when the density matrix of the initial excited state is expanded into the scattering cross sections for the magnetic sublevels, for example see equation (2.7.24). These cross sections are defined according to the orbital angular momentum, not the total angular momentum. To correct this, equation (2.8.1) is once again used to expand the total angular momentum states into a sum of orbital angular momentum states, or

$$
\begin{aligned}
\left\langle (L_{2'}I_2)F_{2'}M_{2'}\left|\rho_2^{\hat{k}}(0)\right|(L_2I_2)F_2M_2\right\rangle &= \sum_{L_{2'}L_2KQ}\left\langle (L_{2'}I_2)F_{2'}M_{2'}\left|T_Q^K(L_{2'}L_2)\right|(L_2I_2)F_2M_2\right\rangle \\
&\qquad \left\langle T_Q^K(L_{2'}L_2)^+\right\rangle^{\hat{k}} \\
&= \sum_{L_{2'}L_2KQ}\sum_{M_{L_2'}M_{L_2}M_{I_2}M_{I_2'}}\left\langle (L_{2'}I_2)F_{2'}M_{2'}\left|L_{2'}I_2;M_{L_2'}M_{I_2'}\right\rangle\right\langle L_2I_2;M_{L_2}M_{I_2}\left|(L_2I_2)F_2M_2\right\rangle\cdot \right. \\
&\qquad \left\langle L_{2'}I_2;M_{L_2'}M_{I_2'}\left|T_Q^K(L_{2'}L_2)\right|L_2I_2;M_{L_2}M_{I_2}\right\rangle\left\langle T_Q^K(L_{2'}L_2)^+\right\rangle^{\hat{k}} \\
&= \sum_{L_{2'}L_2KQ}\sum_{M_{L_2'}M_{L_2}M_{I_2}}\left\langle (L_{2'}I_2)F_{2'}M_{2'}\left|L_{2'}I_2;M_{L_2'}M_{I_2}\right\rangle\right\langle L_2I_2;M_{L_2}M_{I_2}\left|(L_2I_2)F_2M_2\right\rangle\cdot \right. \\
&\qquad \left\langle L_{2'}M_{L_2'}\left|T_Q^K(L_{2'}L_2)\right|L_2M_{L_2}\right\rangle\left\langle T_Q^K(L_{2'}L_2)^+\right\rangle^{\hat{k}} \\
&= \sum_{L_{2'}L_2KQ}(-1)^{1+L_{2'}+I_2+F_{2'}+F_2-M_{2'}}\left[(2F_{2'}+1)(2F_2+1)\right]^{1/2}\begin{pmatrix} F_{2'} & K & F_2 \\ -M_{2'} & Q & M_2\end{pmatrix} \\
&\qquad \begin{Bmatrix} L_{2'} & F_{2'} & I_2 \\ F_2 & L_2 & K\end{Bmatrix}\left\langle T_Q^K(L_{2'}L_2)^+\right\rangle^{\hat{k}}.
\end{aligned}
\tag{2.8.3}
$$

Chapter 3 Applications of the Theory

3.1 Introduction

The theory derived in Chapter 2 is applied to three different cases. All of the applications use information carried by emitted polarized photons to measure properties of the electron-atom collision. The scattered electrons are not measured, and the complete quantum knowledge of the collision process can not be determined. The first two applications analyze a two photon cascade from the D-state to the ground state for helium, and magnesium. The analysis of magnesium is complicated by the presence of isotopes with nuclear spin. The last application examines the scattering of electrons off of laser excited P-states, and into a D-state.

3.2 Photon-Photon Coincidence Measurements in Helium

As stated previously, the maximum number of unknowns in the scattering matrix for the incoherent excitation of a D state is three. The detection of the polarization of the $3D^1$-$2P^1$ photon, which is in the visible spectrum at 492 nm for helium, and the detection of the polarization of the $3D^1$-$2P^1$ photon in coincidence with the detection of the cascade transition $2P^1$-$1S^1$, gives two of the three needed independent observables. A third possible measurement is to determine the total scattering cross section, which would make it possible to extract the absolute scattering cross sections for the different magnetic sublevels. If the total scattering cross section is not available then it can be set to one, and the results are then relative.

The ground state of helium has zero atomic spin due to the closure of the S-level, and the lack of stable isotopes with spin. The analysis of the evolution of the excited atom can then be carried out using equation (2.7.4), which is repeated below,

$$\rho_{kk'} = \sum_{J_1 M_1} \left\langle 1;\hat{k}\left|\hat{U}_s(t_1)\rho_2^{\hat{k}}(0)\hat{U}_s^{+}(t_1)\right|1;\hat{k}'\right\rangle, \tag{3.2.1}$$

where

$$\begin{aligned}
\left\langle 1\left|\rho_{1,kk'}^{\hat{k}}(t_1)\right|1'\right\rangle &= \left\langle 1;\hat{k}\left|\hat{U}_s(t_1)\rho_2^{\hat{k}}(0)\hat{U}_s^{+}(t_1)\right|1';\hat{k}'\right\rangle \\
&= \sum_{L_2 M_2 L_{2'} M_{2'}} \left\langle 1;\hat{k}\left|\hat{U}_s(t_1)\right|2'\right\rangle\left\langle 2'\left|\rho_2^{\hat{k}}(0)\right|2\right\rangle\left\langle 2\left|\hat{U}_s^{+}(t_1)\right|1';\hat{k}'\right\rangle \\
&= \sum_{L_2 M_2 L_{2'} M_{2'}} C_{21,k}(t_1)\left\langle L_1 M_1\left|\vec{\varepsilon}_k\cdot\hat{r}\right|L_{2'} M_{2'}\right\rangle\left\langle L_{2'} M_{2'}\left|\rho_2^{\hat{k}}(0)\right|L_2 M_2\right\rangle \\
&\qquad \left\langle L_2 M_2\left|\vec{\varepsilon}_{k'}^{*}\cdot\hat{r}\right|L_{1'} M_{1'}\right\rangle \\
&= \sum_{L_2 M_2 L_{2'} M_{2'}} \sum_{KQ} C_{21,k}(t_1)\left\langle L_1 M_1\left|\vec{\varepsilon}_k\cdot\hat{r}\right|L_{2'} M_{2'}\right\rangle\left\langle L_2 M_2\left|\vec{\varepsilon}_{k'}^{*}\cdot\hat{r}\right|L_{1'} M_{1'}\right\rangle \\
&\qquad \left\langle T_Q^K(L_{2'} L_2)^{+}\right\rangle^{\hat{k}}\left\langle L_{2'} M_{2'}\left|T_Q^K(L_{2'} L_2)\right|L_2 M_2\right\rangle.
\end{aligned} \tag{3.2.2}$$

Due to the resolving power of current interference filters and the spacing of the helium spectral lines the apparatus can be made sensitive to specific singlet-to-singlet transitions. Such a limitation collapses the sum over L_2 and $L_{2'}$ to a single entry of L_2, the total angular momentum of the excited state. In equation (3.2.2), the quantum numbers are defined with the z-axis as the direction of propagation of the emitted photon. A more convenient frame of reference is the direction of propagation of the incident electrons. Using equation (2.4.8) the state multipoles can be expanded into a sum of multipoles whose frame of reference is the lab frame, or

$$\left\langle T_Q^K(L_2)^{-}\right\rangle^{\hat{k}} = \sum_q \left\langle T_q^K(L_2)^{+}\right\rangle^{lab} D_{Qq}^K(0\theta_k\varphi_k). \tag{3.2.3}$$

Now that the multipoles are defined in the scattering plane, the results of the symmetry considerations can be applied. Axial symmetry requires q to be zero, and the reflection invariance in the scattering plane causes K to be only even integers. Expanding the lab frame state multipoles gives

$$\begin{aligned}\left\langle T_0^K(L_2)^+\right\rangle^{lab} &= trace\left\{\rho_2^{lab}(0)T_0^K(L_2)^+\right\} \\ &= \sum_{M_{2'}M_2}\left\langle L_2M_{2'}\left|\rho_2^{lab}(0)\right|L_2M_2\right\rangle\left\langle L_2M_2\left|T_0^K(L_2)^+\right|L_2M_{2'}\right\rangle \\ &= \sum_{M_2}\left\langle L_2M_2\left|T_0^K(L_2)^+\right|L_2M_2\right\rangle\sigma(M_2) \end{aligned} \tag{3.2.4}$$

where the scattering cross sections have been substituted according to equation (2.3.10). Substituting the above formula into equation (3.2.2) results in a computational photon density matrix which is shown below for the steady state:

$$\begin{aligned}\rho_{kk'} &= \sum_{M_1}\sum_{M_2M_{2'}}\sum_{KQ}C_{21}\left\langle L_1M_1\left|\bar{\varepsilon}_k\cdot\hat{r}\right|L_2M_{2'}\right\rangle\left\langle L_2M_2\left|\bar{\varepsilon}_{k'}^*\cdot\hat{r}\right|L_1M_1\right\rangle\left\langle L_2M_{2'}\left|T_Q^K(L_2)\right|L_2M_2\right\rangle \\ &\quad \sum_{M_{2''}}\left\langle L_2M_{2''}\left|T_0^K(L_2)^+\right|L_2M_{2''}\right\rangle\sigma(M_{2''})D_{Q0}^K(0\theta_k\varphi_k) \\ &= \sum_{M_1}\sum_{M_2M_{2'}}\sum_{KQ}\sum_{M_{2''}}C_{21}(-1)^{L_1-M_1+3L_2-M_2-M_{2'}-M_{2''}}\left\langle 1\left\|r_{\lambda_{k'}}\right\|2\right\rangle\left\langle 2\left\|r_{\lambda_k}\right\|1\right\rangle(2K+1)\sigma(M_{2''})d_{Q0}^K(\theta_k) \\ &\quad \begin{pmatrix}L_1 & L_2 & 1\\ M_1 & -M_{2'} & -\lambda_k\end{pmatrix}\begin{pmatrix}L_2 & L_1 & 1\\ M_2 & -M_{1'} & -\lambda_{k'}\end{pmatrix}\begin{pmatrix}L_2 & L_2 & K\\ M_{2'} & -M_2 & -Q\end{pmatrix}\begin{pmatrix}L_2 & L_2 & K\\ M_{2''} & -M_{2''} & 0\end{pmatrix}. \end{aligned} \tag{3.2.5}$$

Using the above equation, and the third Stokes parameter, equation (2.2.7d), the polarization of the emitted radiation is calculated to be

$$\begin{aligned}P &= -\frac{\left(\rho_{-1,1}+\rho_{1,-1}\right)}{\rho_{1,1}+\rho_{-1,-1}} \\ &= -\frac{6Sin^2(\theta_k)(\sigma(0)+\sigma(1)-2\sigma(2))}{\left(3Cos(2\theta_k)-7\right)\sigma(0)+\left(3Cos(2\theta_k)-15\right)\sigma(1)-2\left(3Cos(2\theta_k)+9\right)\sigma(2)}, \end{aligned} \tag{3.2.6}$$

which was evaluated using Mathematica™. The density matrix elements should be integrated over the azimuthal angle, φ_k, before finding the polarization, to account for the lack of a defined scattering plane. However, due to the proper choice of symmetry conditions, the matrix elements are independent of the angle, and therefore the constant term is simply canceled. The Mathematica™ file used to calculate equation (3.2.6) can be found in Appendix 1. The maximum polarization is obtained by setting a detector at $\theta_k = \pi/2$, which gives a polarization of

$$P = \frac{3(\sigma(0) + \sigma(1) - 2\sigma(2))}{5\sigma(0) + 9\sigma(1) + 6\sigma(2)}, \tag{3.2.7}$$

and is in agreement with the literature, for example see Percival and Seaton (Percival1958). The solid angle of the detector will have a tendency to wash out the polarization, and will be investigated in Chapter 5.

Following the procedure outlined in section (2.7), the time evolution of the atom after it has made the transition to the P-state is given by

$$\rho^{\hat{n}}_{1,kk'}(t;t_1) = \hat{U}_s(t;t_1)\rho^{\hat{n}}_{1,kk'}(t_1)\hat{U}^{+}_s(t;t_1). \tag{3.2.8}$$

To accommodate the change in the quantization axis the density matrix $\rho^{\hat{n}}_{1,kk'}(t_1)$ must be written in terms of the previously derived matrices $\rho^{\hat{k}}_{1,kk'}(t_1)$.To do this, $\rho^{\hat{n}}_{1,kk'}(t_1)$ is expanded into irreducible spherical tensors,

$$\rho^{\hat{n}}_{1,kk'} = \sum_{KQ} \left\langle T^K_Q(J)^{+} \right\rangle^{\hat{n}} T^K_Q(J), \tag{3.2.9}$$

and then, using equations (2.3.8) and (2.3.9), the state multipoles are transformed into the $\hat{k}$ direction using the lab frame as an intermediate step. This ensures that all angles are referenced to the lab frame, and

$$\begin{aligned}
\rho^{\hat{n}}_{1,kk'} &= \sum_{KQ} \left\langle T^K_Q(L)^+ \right\rangle^{\hat{n}} T^K_Q(L) \\
&= \sum_{KQ} \left(\sum_{Q_{lab}} \left\langle T^K_{Q_{lab}}(L)^+ \right\rangle^{lab} D^K_{QQ_{lab}}(0\theta_n\vartheta_n) \right) T^K_Q(L) \\
&= \sum_{KQ} \left(\sum_{Q_{lab}Q_k} \left\langle T^K_{Q_k}(L)^+ \right\rangle^{\hat{k}} D^K_{Q_kQ_{lab}}(0\theta_k\vartheta_k)^* D^K_{QQ_{lab}}(0\theta_n\vartheta_n) \right) T^K_Q(L).
\end{aligned} \tag{3.2.10}$$

Once again making use of equation (2.7.29), the density matrix for the emitted P-S photon is

$$\begin{aligned}
\rho_{nn'.kk'} &= \sum_{L_1 M_1 L_1 M_1} C_{10}(t_2) \left\langle L_0 M_0 \middle| \bar{\varepsilon}_n \cdot \bar{r} \middle| L_{1'} M_{1'} \right\rangle \left\langle L_{1'} M_{1'} \middle| \rho^{\hat{n}}_{1.kk'} \middle| L_1 M_1 \right\rangle \left\langle L_1 M_1 \middle| \bar{\varepsilon}^*_{n'} \cdot \bar{r} \middle| L_0 M_0 \right\rangle \\
&= \sum_{L_1 M_1 L_1 M_1 KQ} C_{10}(t_2) \left\langle L_0 M_0 \middle| \bar{\varepsilon}_n \cdot \bar{r} \middle| L_{1'} M_{1'} \right\rangle \left\langle L_1 M_1 \middle| \bar{\varepsilon}^*_{n'} \cdot \bar{r} \middle| L_0 M_0 \right\rangle \cdot \\
&\left(\sum_{Q_{lab}Q_k} \left\langle T^K_{Q_k}(L_1)^+ \right\rangle^{\hat{k}} D^K_{Q_kQ_{lab}}(0\theta_k\varphi_k)^* D^K_{QQ_{lab}}(0\theta_n\varphi_n) \right) \left\langle L_{1'} M_{1'} \middle| T^K_Q(L_1) \middle| L_1 M_1 \right\rangle
\end{aligned} \tag{3.2.11}$$

where the state multipoles are found according to

$$\left\langle T^K_Q(L_1)^+ \right\rangle^{\hat{k}} = \sum_{M_{1'} M_1} \left\langle L_{1'} M_{1'} \middle| \rho^{\hat{k}}_{1,kk'} \middle| L_1 M_1 \right\rangle \left\langle L_1 M_1 \middle| T^K_Q(L_1)^+ \middle| L_{1'} M_{1'} \right\rangle. \tag{3.2.12}$$

Combining equations (3.2.5), (3.2.11), and (3.2.12) gives the final form for the density matrix as

$$\rho_{nn',kk'} = \sum_{M_1,M_1KQ}\sum_{Q_{lab}Q_k} C_{10}\langle 0|\bar{\varepsilon}_n\cdot\bar{r}|1'\rangle\langle 1'|T_Q^K(L_1)|1\rangle\langle 1|\bar{\varepsilon}^*_{n'}\cdot\bar{r}|0\rangle D^K_{Q_kQ_{lab}}(0\theta_k\varphi_k)^* D^K_{QQ_{lab}}(0\theta_n\varphi_n)$$
$$\sum_{M_{1''}M_{1'''}}\langle 1''|\rho^{\hat{k}}_{1,kk'}|1'''\rangle\langle 1'''|T^K_{Q_k}(L_1)^+|1''\rangle$$
$$= \sum_{M_1,M_1KQ}\sum_{Q_{lab}Q_k}\sum_{M_{1'''}M_{1''}} C_{10}\langle 0|\bar{\varepsilon}_n\cdot\bar{r}|1'\rangle\langle 1'|T^K_Q(L_1)|1\rangle\langle 1|\bar{\varepsilon}^*_{n'}\cdot\bar{r}|0\rangle\langle 1'''|T^K_{Q_k}(L_1)^+|1''\rangle \qquad (3.2.13)$$
$$\sum_{M_2,M_2K_2Q_2}\sum_{M_{2''}} C_{21}\langle 1''|\bar{\varepsilon}_k\cdot\bar{r}|2'\rangle\langle 2'|T^{K_2}_{Q_2}(L_2)|2\rangle\langle 2|\bar{\varepsilon}^*_{k'}\cdot\bar{r}|1'''\rangle\langle 2''|T^{K_2}_0(L_2)^+|2''\rangle$$
$$D^K_{Q_kQ_{lab}}(0\theta_k\varphi_k)^* D^K_{QQ_{lab}}(0\theta_n\varphi_n) D^{K_2}_{Q_20}(0\theta_k\varphi_k)\sigma(M_{2''}).$$

The elements of the resulting photon density matrix are dependent upon both of the emitted photons. If the first photon decay is not measured then the resulting photon density matrix could be found by finding the intensity of the D-P transition, equation (2.2.7a) , and then integrating over all related angles. Doing so would of course erase all knowledge of the initial D state. Measuring both photons in coincidence preserves the knowledge of the D state. If the polarization of the D-P transition photon is measured in coincidence with the intensity of the P-S transition then the expected polarization is found from the density matrix

$$\rho'_{kk'} = \rho_{1,1kk'} + \rho_{-1,-1kk'}. \qquad (3.2.14)$$

The resulting formula is independent of the previously found polarization for the D-P transition, equation (3.2.6). The solution of equation (3.2.13), using the Mathematica™ program found in Appendix 1, gives

$$P_{Coinc} = \frac{-(\rho'_{1,-1}+\rho'_{-1,1})}{\rho'_{1,1}+\rho'_{-1,-1}}$$
$$= \frac{(7-\cos(2\Delta))\sigma(0)-6\sigma(2)}{(9+\cos(2\Delta))\sigma(0)+12\sigma(1)+6\sigma(2)} \qquad (3.2.15)$$

for

$$\theta_k = \frac{\pi}{2}$$
$$\theta_n = \frac{\pi}{2}$$
$$\varphi_n = \varphi_k + \Delta$$

where Δ is the difference between the zenith angles of the two detectors. If the two photon detectors are π radians apart then the coincidence polarization becomes

$$P_{Coinc} = \frac{3(\sigma(0) - \sigma(2))}{5\sigma(0) + 6\sigma(1) + 3\sigma(2)}, \tag{3.2.16}$$

which agrees with the work of Mikosza(Mikosza1996). The polarization measurements give two of the three independent equations required to determine the individual integrated scattering cross sections. If the sum of the integrated cross sections is set to unity,

$$1 = \sigma(0) + 2\sigma(1) + 2\sigma(2), \tag{3.2.17}$$

then the corresponding values for the cross sections are

$$\sigma(0) = \frac{(3P + 15)(P_{Coinc} - 3) + 48}{(P - 3)(3P_{Coinc} - 5)} \tag{3.2.18a}$$

$$\sigma(1) = \frac{(5P + 13)(11 - 5P_{Coinc}) - 128}{5(P - 3)(3P_{Coinc} - 5)} \tag{3.2.18b}$$

$$\sigma(2) = \frac{(P - 5)(5P_{Coinc} - 9) + 120}{25(P - 3)(3P_{Coinc} - 5)}. \tag{3.2.18c}$$

3.3 Photon-Photon Coincidence Measurements in Magnesium

Magnesium is an alkali-earth metal with a twelve proton nucleus, and is the eighth most abundant element in the Earth's crust. It occurs naturally in three isotopes, the most abundant of which has zero nuclear spin. Properties of the magnesium isotopes are given below in Table 3.1.

Table 3.1: Naturally occurring isotopes in magnesium. The number of nucleons is given by A, and the number of protons by Z (Heath1986).

A	Z	Natural Abundance	Nuclear Spin
24	12	78.99%	0
25	12	10.00%	5/2
26	12	11.01%	0

Since magnesium has a low molecular weight, the orbital angular momentum is still a good quantum number and the analysis for the isotopes with zero nuclear spin is identical to that of helium. The singlet D-P transition, $3s3p\text{-}3s(^2S)4d$, is in the visible spectrum with a wavelength of 552.8 nm, while the singlet P-S transition, $3s^2\text{-}3s(^2S)3p$, is in the ultra-violet region with a wavelength of 285.2 nm.

For the A = 25 magnesium isotope the analysis has to be carried out using the methods described in section 2.8 since it has non-zero nuclear spin. Modifying equation (3.2.5) and inserting equations (2.8.2) and (2.8.3), gives the density matrix describing the P-State as

$$\left\langle 1\left|\rho^{\hat{k}}_{1,kk'}\right|1'\right\rangle = \sum_{F_2 M_2 F_{2'} M_{2'}} C_{21}\left\langle F_1 M_1\left|\vec{\varepsilon}_k\cdot\hat{r}\right|F_{2'} M_{2'}\right\rangle\left\langle F_{2'} M_{2'}\left|\rho^{\hat{k}}_2\right|F_2 M_2\right\rangle$$
$$\left\langle F_2 M_2\left|\vec{\varepsilon}^{\,*}_{k'}\cdot\hat{r}\right|F_{1'} M_{1'}\right\rangle$$
$$= \frac{1}{2I_2+1}\sum_{F_2 M_2 F_{2'} M_{2'}}\sum_{KQ}\sum_{M_{L_2'} M_{L_2} M_{I_2}} C_{21}\left\langle F_1 M_1\left|\vec{\varepsilon}_k\cdot\hat{r}\right|F_{2'} M_{2'}\right\rangle \tag{3.3.1}$$
$$\left\langle F_2 M_2\left|\vec{\varepsilon}^{\,*}_{k'}\cdot\hat{r}\right|F_{1'} M_{1'}\right\rangle\left\langle F_{2'} M_{2'}\,\middle|\, L_2 I_2; M_{L_2'} M_{I_2}\right\rangle$$
$$\left\langle L_2 I_2; M_{L_2} M_{I_2}\,\middle|\, F_2 M_2\right\rangle\left\langle L_2 M_{L_2'}\left|T^K_Q(L_2)\right|L_2 M_{L_2}\right\rangle$$
$$\sum_{M_{2''}}\left\langle L_2 M_{2''}\left|T^K_0(L_2)^+\right|L_2 M_{2''}\right\rangle\sigma(M_{2''})D^K_{Q0}(0\theta_k\varphi_k),$$

where the photon density matrix is

$$\rho^{25}_{kk'} = \sum_{F_1 M_1}\left\langle F_1 M_1\left|\rho^{\hat{k}}_{1,kk'}\right|F_1 M_1\right\rangle. \tag{3.3.2}$$

The calculation of equation (3.3.2) was carried out with the program contained in Appendix 2. Mathematica™ was not used to do the calculation due to the complexity of the expression and the inefficiency of Mathematica™ when doing non-symbolic calculations. The results of the calculation are

$$\rho_{1,-1} = \rho_{-1,1} = 0.08044\sigma(2) - 0.04056\sigma(1) - 0.03988\sigma(0) \tag{3.3.3}$$
$$\rho_{1,1} = \rho_{-1,-1} = 0.10000\sigma(2) + 0.15000\sigma(1) + 0.08333\sigma(0).$$

To find the polarization of the D-P transition due to the contributions from all of the isotopes, a weighted sum of the isotope polarization density matrices is formed, and the equation is solved for the resulting polarization, or

$$\rho_{kk'} = 0.7899\rho^{24}_{kk'} + 0.1000\rho^{25}_{kk'} + 0.1101\rho^{26}_{kk'}, \tag{3.3.4}$$

and

$$P = -\frac{(\rho_{1,-1} + \rho_{-1,1})}{\rho_{1,1} + \rho_{-1,-1}}. \tag{3.3.5}$$

The final expression for the polarization is therefore

$$P = \frac{2.939\sigma(0) + 2.943\sigma(1) - 5.883\sigma(2)}{5\sigma(0) + 9\sigma(1) + 6\sigma(2)}. \tag{3.3.6}$$

Equation (3.3.6) is almost identical to the corresponding equation for helium, equation (3.2.7). The effect of the hyper-fine splitting has been to decrease the measured polarization.

The decay of the P-state for the odd isotope is characterized by

$$\begin{aligned}\rho^{25}_{nn',kk'} = \sum_{M_{0'}M_0} \sum_{F_{1'}M_{1'}F_1M_1KQ} \sum_{Q_{lab}Q_k} & C_{10}\left\langle I_0 M_{0'}\left|\vec{\varepsilon}_n \cdot \vec{r}\right|F_{1'}M_{1'}\right\rangle\left\langle F_1 M_1\left|\vec{\varepsilon}^{\,*}_{n'} \cdot \vec{r}\right|I_0 M_0\right\rangle \\ & \left\langle F_{1'}M_{1'}\left|T^K_Q\left(F_{1'}F_1\right)\right|F_1M_1\right\rangle D^K_{Q_kQ_{lab}}\left(0\theta_k\varphi_k\right)^* D^K_{QQ_{lab}}\left(0\theta_n\varphi_n\right) \\ & \sum_{M_{1''}M_{1'''}} \left\langle F_{1'}M_{1''}\left|\rho^{\hat{k}}_{1,kk'}\right|F_1M_{1'''}\right\rangle\left\langle F_1M_{1'''}\left|T^K_{Q_k}\left(F_{1'}F_1\right)^+\right|F_{1'}M_{1''}\right\rangle,\end{aligned} \tag{3.3.7}$$

which is a modification of equation (3.2.13). Once again, a weighted sum is required to incorporate all of the magnesium isotopes into a single density matrix, and for the case where the polarization of the P-S photon is not observed

$$\begin{aligned}\rho'_{kk'} &= \rho_{1,1kk'} + \rho_{-1,-1kk'} \\ &= 0.7899\left(\rho^{24}_{1,1kk'} + \rho^{24}_{-1,-1kk'}\right) + 0.1000\left(\rho^{25}_{1,1kk'} + \rho^{25}_{-1,-1kk'}\right) + 0.1101\left(\rho^{26}_{1,1kk'} + \rho^{26}_{-1,-1kk'}\right)\end{aligned} \tag{3.3.8}$$

The computer program in Appendix 2 was used to calculate equation (3.3.7). The results of the analysis are

$$\begin{aligned}\rho^{25}_{1,-1} = \rho^{25}_{-1,1} &= 0.01667\sigma(2) - 0.01667\sigma(0) \\ \rho^{25}_{1,1} = \rho^{25}_{-1,-1} &= 0.01667\sigma(2) + 0.03333\sigma(1) + 0.02778\sigma(0).\end{aligned} \tag{3.3.9}$$

The final expression for the magnesium photon-photon coincidence measurement is therefore

$$P_{coinc} = \frac{3\sigma(0) - 3\sigma(2)}{5\sigma(0) + 6\sigma(1) + 3\sigma(2)}, \tag{3.3.10}$$

which is identical to the photon-photon coincidence calculation for helium presented in section 3.2. Equation (3.3.10) implies that the coincidence measurement of the D-P-S cascade transition is independent of the de-polarizing effects of the odd isotopes. The polarization of the D-P and P-S transitions, however, are effected by the presence of the odd isotopes. The polarization of the P-S transition in magnesium for just the odd isotope (A = 25) is

$$P_{A=25} = 0.775\frac{\sigma(0) - \sigma(1)}{\sigma(0) + \sigma(1)}, \tag{3.3.11}$$

where the polarization of the equivalent even isotope transition is

$$P_{even} = \frac{\sigma(0) - \sigma(1)}{\sigma(0) + \sigma(1)}. \tag{3.3.12}$$

3.4 Electron Scattering off of Laser Excited P-States

So far I have shown what information can be obtained about the scattering amplitudes for a ground state to a D-state electron impact excitation, without the detection of the scattered electrons. A similar exercise can be carried out for the electron excitation of a D-state off of a pre-excited P-state. The preparation of the initial P-state can be effectively accomplished via laser pumping. A laser provides enough energy resolution to selectively choose the appropriate transition, and by controlling the polarization of the light beam, the initial populations of the magnetic sublevels can be chosen. The laser orientation with respect to the electron beam is shown in Figure 3.1.

The initial density matrix for the system describes the ground state atom and the purely polarized laser beam, or

$$\rho_{in}^{\hat{k}} = \frac{1}{2S_i+1}\sum_{M_i}\sum_{\lambda\lambda'} A_{\lambda\lambda'}\left|\hat{k}\omega\lambda; S_i M_i\right\rangle\left\langle\hat{k}\omega\lambda'; S_i M_i\right|, \tag{3.4.1}$$

where the coefficients $A_{\lambda\lambda'}$ are the density matrix elements for a purely polarized light beam given by equation (2.2.9), and the quantization axis is along the direction of propagation of the photons. The time evolution of the initial system, as usual, is given by

$$\rho_{in}^{\hat{k}}(t) = U(t)\rho_{in}^{\hat{k}}U^{+}(t), \tag{3.4.2}$$

and the resulting excited states are found to be

$$\left\langle L'M'\left|\rho_{in}^{\hat{k}}(t)\right|LM\right\rangle = \frac{1}{2S_i+1}\sum_{M_i}\sum_{\lambda\lambda'} A_{\lambda\lambda'}\left\langle L'M'\left|U(t)\right|\hat{k}\omega\lambda; S_i M_i\right\rangle \left\langle\hat{k}\omega\lambda'; S_i M_i\left|U^{+}(t)\right|LM\right\rangle. \tag{3.4.3}$$

The partial evaluation of the time evolution operator bra-ket gives,

$$\left\langle L'M'\left|\hat{U}(t)\right|\hat{k}\omega\lambda' 00\right\rangle = W_{L'0}(t)\frac{e}{\hbar}\left(\frac{2\pi\hbar}{\omega_k}\right)^{1/2}\omega_{L'0}\left\langle L'M'\left|\vec{\varepsilon}_k\cdot\hat{r}\right|00\right\rangle, \tag{3.4.4}$$

where the derivation is analogous to that for equation (2.7.19), and the ground state is assumed to have zero spin. With the application of the above equation, equation (3.4.3) becomes

$$\left\langle L'M'\left|\rho_{in}^{\hat{k}}(t)\right|LM\right\rangle = C_{L0}(t)\sum_{\lambda\lambda'} A_{\lambda\lambda'}\left\langle L'M'\left|\vec{\varepsilon}_k\cdot\hat{r}\right|00\right\rangle\left\langle 00\left|\vec{\varepsilon}_{k'}\cdot\hat{r}\right|LM\right\rangle, \tag{3.4.5}$$

after having been integrated over the radiation frequency, as in equation (2.7.27). If the laser is operated continuously then the steady state form of equation (3.4.5) is required, and

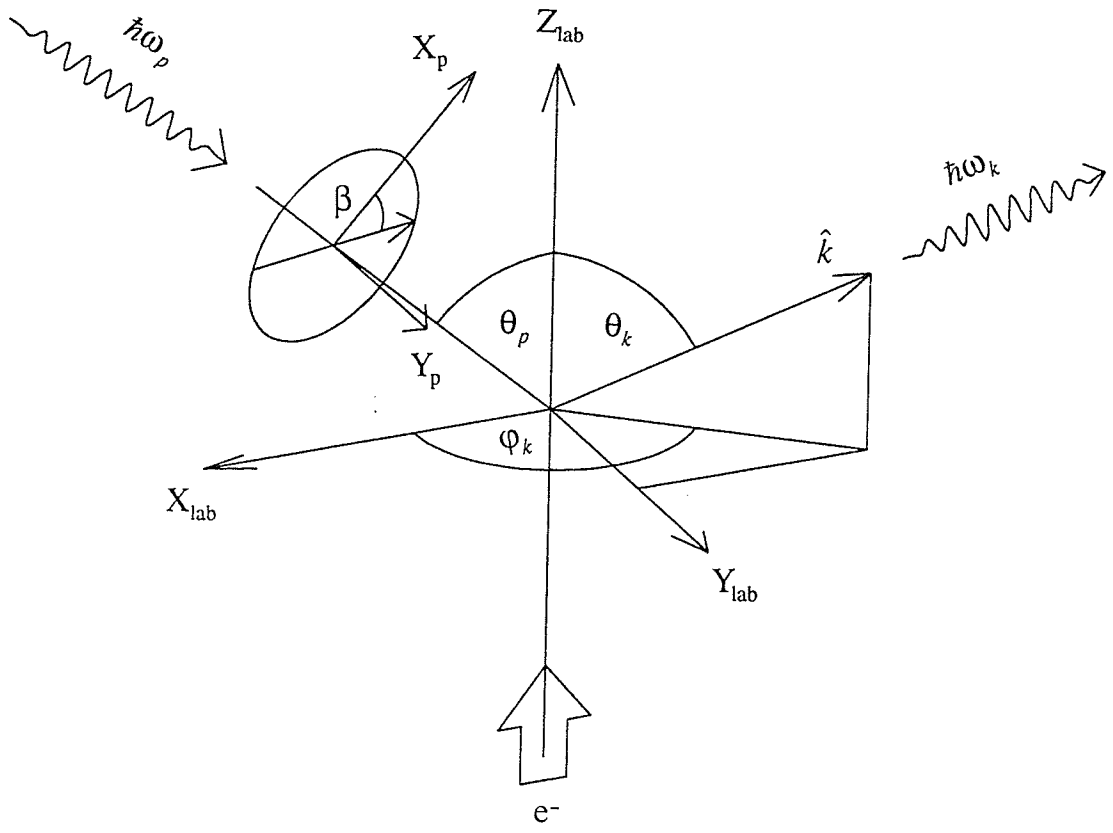

Figure 3.1: Orientation of the laser beam axis in comparison with the electron beam axis where the polarization of the laser is given by the angle β from the laser's x-axis and the phase difference δ between the two orthogonal polarization axes (not shown)

$$\left\langle L'M'\left|\rho_{in}^{\hat{k}}(t)\right|LM\right\rangle = C_{L0}\sum_{\lambda\lambda'} A_{\lambda\lambda'}\left\langle L'M'\left|\vec{\varepsilon}_k\cdot\hat{r}\right|00\right\rangle\left\langle 00\left|\vec{\varepsilon}_{k'}^{*}\cdot\hat{r}\right|LM\right\rangle. \tag{3.4.6}$$

The above equation gives the density matrix for the P-state atoms which have been excited by a purely polarized laser beam. Before electron scattering off of the P-state atoms can be discussed, the atomic density matrix must be rewritten with the quantization axis along the electron beam axis. Expanding the density matrix into state multipoles gives

$$\begin{aligned}\left\langle T_Q^K(L'L)^+\right\rangle^{\hat{k}} &= \sum_{M'M}\left\langle L'M'\left|\rho_{in}^{\hat{k}}\right|LM\right\rangle\left\langle L'M'\left|T_Q^K(L'L)^+\right|LM\right\rangle \\ &= \sum_{\lambda\lambda'} A_{\lambda\lambda'}\sum_{M'M}\left\langle L'M'\left|T_Q^K(L'L)^+\right|LM\right\rangle C_{L0}\left\langle L'M'\left|\vec{\varepsilon}_k\cdot\hat{r}\right|00\right\rangle \\ &\qquad \left\langle 00\left|\vec{\varepsilon}_{k'}^{*}\cdot\hat{r}\right|LM\right\rangle \\ &= \sum_{\lambda\lambda'} A_{\lambda\lambda'}\left\langle T_Q^K(L'L)^+\right\rangle_{\lambda\lambda'}^{\hat{k}}\end{aligned} \tag{3.4.7}$$

where I have defined the set of state multipoles to be

$$\left\langle T_Q^K(L'L)^+\right\rangle_{\lambda\lambda'}^{\hat{k}} = \sum_{M'M}\left\langle L'M'\left|T_Q^K(L'L)^+\right|LM\right\rangle C_{L0}\left\langle L'M'\left|\vec{\varepsilon}_k\cdot\hat{r}\right|00\right\rangle\left\langle 00\left|\vec{\varepsilon}_{k'}^{*}\cdot\hat{r}\right|LM\right\rangle. \tag{3.4.8}$$

Using the notation defined in Figure 3.1, the state multipoles redefined along the electron beam axis are

$$\begin{aligned}\left\langle T_q^K(L'L)^+\right\rangle^{lab} &= \sum_Q\left\langle T_Q^K(L'L)^+\right\rangle^{\hat{k}} D_{Qq}^K(0\theta_k\varphi_k)^* \\ &= \sum_{\lambda\lambda'} A_{\lambda\lambda'}\sum_Q\left\langle T_Q^K(L'L)^+\right\rangle_{\lambda\lambda'}^{\hat{k}} D_{Qq}^K(0\theta_k\varphi_k)^* \\ &= \sum_{\lambda\lambda'} A_{\lambda\lambda'}\left\langle T_q^K(L'L)^+\right\rangle_{\lambda\lambda'}^{lab}\end{aligned} \tag{3.4.9}$$

with the corresponding density matrix

$$\rho_{ox}^{lab} = \sum_{\lambda\lambda'} A_{\lambda\lambda'}\sum_{L'LKQ}\left\langle T_Q^K(L'L)^+\right\rangle_{\lambda\lambda'}^{lab} T_Q^K(L'L). \tag{3.4.10}$$

The optically pumped atomic states interact with the incident electrons according to the transition operator and

$$\rho_{ex}^{lab} = \hat{T}\rho_{ox,e}^{lab}\hat{T}^{+}, \tag{3.4.11}$$

where the combined optically excited state and incident electron density matrix is given by the combination of the density matrices ρ_{ox}^{lab}, and

$$\rho_{e}^{lab} = \frac{1}{2}\sum_{m_e} |\vec{p}m_e\rangle\langle\vec{p}m_e|, \tag{3.4.12}$$

to give

$$\begin{aligned}\rho_{ox,e}^{lab} &= \frac{1}{2}\sum_{\lambda\lambda'} A_{\lambda\lambda'} \sum_{L'LKQ} \left\langle T_Q^K(L'L)^{+}\right\rangle_{\lambda\lambda'}^{lab} \sum_{m_e} T_Q^K(L'L)|\vec{p}m_e\rangle\langle\vec{p}m_e| \\ &= \frac{1}{2}\sum_{\lambda\lambda'} A_{\lambda\lambda'} \sum_{L'LKQ} \left\langle T_Q^K(L'L)^{+}\right\rangle_{\lambda\lambda'}^{lab} \sum_{m_e M'M} (-1)^{L'-M'}(2K+1)^{1/2}\begin{pmatrix} L' & L & K \\ M' & -M & -Q\end{pmatrix} \cdot \\ &\qquad |\vec{p}m_e L'M'\rangle\langle\vec{p}m_e LM|\end{aligned} \tag{3.4.13}$$

The density matrix elements for the electron excited states are therefore equal to

$$\begin{aligned}\left\langle L_{2'}M_{2'}\left|\rho_{ex}^{lab}\right|L_2M_2\right\rangle &= \frac{1}{4}\sum_{\lambda\lambda'} A_{\lambda\lambda'} \sum_{L'LKQ} \left\langle T_Q^K(L'L)^{+}\right\rangle_{\lambda\lambda'}^{lab} \sum_{m_e' m_e M'M} (-1)^{L'-M'}(2K+1)^{1/2} \cdot \\ &\qquad \begin{pmatrix} L' & L & K \\ M' & -M & -Q\end{pmatrix} \left\langle \vec{p}'m_e' L_{2'}M_{2'}\left|\hat{T}\right|\vec{p}m_e L'M'\right\rangle \\ &\qquad \left\langle \vec{p}m_e LM\left|\hat{T}^{+}\right|\vec{p}'m_e' L_2M_2\right\rangle \\ &= \sum_{\lambda\lambda'} A_{\lambda\lambda'} \sum_{L'LKQ} \left\langle T_Q^K(L'L)^{+}\right\rangle_{\lambda\lambda'}^{lab} \sum_{M'M} (-1)^{L'-M'}(2K+1)^{1/2} \cdot \\ &\qquad \begin{pmatrix} L' & L & K \\ M' & -M & -Q\end{pmatrix} f\left(L_{2'}M_{2'};L'M'\right) f\left(L_2M_2;LM\right)^{*}\end{aligned} \tag{3.4.14}$$

where the lack of electron spin analysis, both preparation and detection, has been taken into account, and absorbed into the definition of the scattering amplitudes. The above equation gives the density matrix elements for the excited D state, and is equivalent to the initial D state population in equation (2.3.17). The analysis for the time evolution of an

excited D state can now be used to find the polarization of the D-P transition, or even the cascade transition D-P-S.

The symmetry conditions derived in section (2.5) must be reevaluated for the laser excited P-state system. The symmetry of the problem will change depending upon the orientation of the exciting laser, or in other words, the orientation of the excited P-state dipole. Therefore, the system will not generally be axially symmetric and off-diagonal elements of the density matrix will no longer necessarily be zero. The reflection invariance symmetry, however, is still applicable. Reflection invariance applied to equation (3.4.14) gives

$$\begin{aligned}\left\langle L_{2'}M_{2'}\middle|M^{+}M\rho_{ex}^{lab}M^{+}M\middle|L_2M_2\right\rangle=&\frac{1}{4}\sum_{\lambda\lambda'}A_{\lambda\lambda'}\sum_{L'LKQ}\left\langle T_Q^K(L'L)^{+}\right\rangle_{\lambda\lambda'}^{lab}\cdot\\ &\sum_{m_e'm_eM'M}(-1)^{L'-M'}(2K+1)^{1/2}\begin{pmatrix}L' & L & K\\ M' & -M & -Q\end{pmatrix}\left\langle L_{2'}M_{2'};\vec{p}'m_e'\middle|M^{+}\hat{T}M\middle|L'M';\vec{p}m_e\right\rangle\\ &\left\langle LM;\vec{p}m_e\middle|M^{+}\hat{T}^{+}M\middle|L_2M_2;\vec{p}'m_e'\right\rangle\\ &=\sum_{\lambda\lambda'}A_{\lambda\lambda'}\sum_{L'LKQ}\left\langle T_Q^K(L'L)^{+}\right\rangle_{\lambda\lambda'}^{lab}\cdot\\ &\sum_{M'M}(-1)^{L'-M'}(2K+1)^{1/2}\begin{pmatrix}L' & L & K\\ M' & -M & -Q\end{pmatrix}(-1)^{L_{2'}+L_2+L'+L-M_{2'}-M_2-M'-M}\\ &f\left(L_{2'}-M_{2'};L'-M'\right)f\left(L_2-M_2;L-M\right)^{*},\end{aligned}\tag{3.4.15}$$

or

$$\begin{aligned}f\left(L_{2'}M_{2'};L'M'\right)f\left(L_2M_2;LM\right)=(-1)^{M_{2'}+M_2+M'+M}&f\left(L_{2'}-M_{2'};L'-M'\right)\\ &f\left(L_2-M_2;L-M\right).\end{aligned}\tag{3.4.16}$$

The density matrix for the de-excitation to the P state is found by a direct application of equations (2.7.17) and (3.4.14) to give

$$
\begin{aligned}
\rho_{kk'} &= \sum_{M_1}\sum_{M_2 M_{2'}} C_{21}\left\langle L_1 M_1\middle|\bar{\varepsilon}_k\cdot\hat{r}\middle|L_2 M_{2'}\right\rangle\left\langle L_2 M_{2'}\middle|\rho_{ex}^{\hat{k}}\middle|L_2 M_2\right\rangle\left\langle L_2 M_2\middle|\bar{\varepsilon}_{k'}^{*}\cdot\hat{r}\middle|L_1 M_1\right\rangle \\
&= \sum_{M_1}\sum_{M_2 M_{2'}}\sum_{KQq} C_{21}\left\langle L_1 M_1\middle|\bar{\varepsilon}_k\cdot\hat{r}\middle|L_2 M_{2'}\right\rangle\left\langle L_2 M_2\middle|\bar{\varepsilon}_{k'}^{*}\cdot\hat{r}\middle|L_1 M_1\right\rangle\left\langle L_2 M_{2'}\middle|T_Q^K(L_2)\middle|L_2 M_2\right\rangle \\
&\qquad \left\langle T_q^K(L_2)^{+}\right\rangle^{lab} D_{Qq}^{K}(0\theta_k\varphi_k) \\
&= \sum_{M_1}\sum_{M_2 M_{2'}}\sum_{KQq} C_{21}\left\langle L_1 M_1\middle|\bar{\varepsilon}_k\cdot\hat{r}\middle|L_2 M_{2'}\right\rangle\left\langle L_2 M_2\middle|\bar{\varepsilon}_{k'}^{*}\cdot\hat{r}\middle|L_1 M_1\right\rangle\left\langle L_2 M_{2'}\middle|T_Q^K(L_2)\middle|L_2 M_2\right\rangle \\
&\qquad \sum_{M_{2''}M_{2'''}}\left\langle L_2 M_{2''}\middle|T_q^K(L_2)^{+}\middle|L_2 M_{2'''}\right\rangle\left\langle L_2 M_{2''}\middle|\rho_{ex}^{lab}\middle|L_2 M_{2'''}\right\rangle D_{Qq}^{K}(0\theta_k\varphi_k).
\end{aligned}
\tag{3.4.17}
$$

The actual polarization of the emitted radiation is, of course,

$$
P = -\frac{\rho_{1,-1}+\rho_{-1,1}}{\rho_{1,1}+\rho_{-1,-1}}, \tag{3.4.18}
$$

where

$$
\rho_{kk'} = \sum_{M_1}\left\langle L_1 M_1\middle|\rho_{1,kk'}\middle|L_1 M_1\right\rangle. \tag{3.4.19}
$$

If the scattered electrons are not detected then the density matrix elements must be averaged over the zenith angle before the polarization can be calculated.

Before solving for equation (3.4.19) it is instructive to see what combinations of density matrix elements of the P-state can be chosen with the pumping laser. Finding the matrix elements of equation (3.4.10), the excited P-state density matrix given in the lab frame, for the three laser orientations $\theta_L = 0$, $\theta_L = \pi/4$, and $\theta_L = \pi/2$ yields

$$
\theta_L = 0 \qquad \begin{pmatrix} \frac{1}{6}\left(1-\sin(2\beta)\sin(\delta)\right) & 0 & -\frac{1}{6}\left(\cos(2\beta)+I\cos(\delta)\sin(\beta)\right) \\ 0 & 0 & 0 \\ -\frac{1}{6}\left(\cos(2\beta)-I\cos(\delta)\sin(\beta)\right) & 0 & \frac{1}{6}\left(1+\sin(2\beta)\sin(\delta)\right) \end{pmatrix} \tag{3.4.20a}
$$

$$\theta_{l,} = \pi/4 \qquad \begin{pmatrix} \frac{1}{24}\left(3-\cos(2\beta)-2\sqrt{2}\sin(2\beta)\sin(\delta)\right) & -\frac{\cos(\beta)}{6\sqrt{2}}\left(\cos(\beta)+1\sqrt{2}\sin(\beta)e^{1\delta}\right) & \frac{1}{24}\left(1-3\cos(2\beta)-12\sqrt{2}\sin(2\beta)\sin(\delta)\right) \\ -\frac{\cos(\beta)}{6\sqrt{2}}\left(\cos(\beta)-1\sqrt{2}\sin(\beta)e^{-1\delta}\right) & \frac{\cos^2(\beta)}{6} & \frac{\cos(\beta)}{6\sqrt{2}}\left(\cos(\beta)+1\sqrt{2}\sin(\beta)e^{-1\delta}\right) \\ \frac{1}{24}\left(1-3\cos(2\beta)+12\sqrt{2}\sin(2\beta)\sin(\delta)\right) & \frac{\cos(\beta)}{6\sqrt{2}}\left(\cos(\beta)-1\sqrt{2}\sin(\beta)e^{1\delta}\right) & \frac{1}{24}\left(3-\cos(2\beta)+2\sqrt{2}\sin(2\beta)\sin(\delta)\right) \end{pmatrix} \quad (3.4.20b)$$

$$\theta_L = \pi/2 \qquad \begin{pmatrix} \frac{\sin^2(\beta)}{6} & -\frac{I\sin(2\beta)e^{I\delta}}{6\sqrt{2}} & \frac{\sin^2(\beta)}{6} \\ \frac{I\sin(2\beta)e^{-I\delta}}{6\sqrt{2}} & -\frac{1}{3}\cos^2(\beta) & \frac{I\sin(2\beta)e^{-I\delta}}{6\sqrt{2}} \\ \frac{\sin^2(\beta)}{6} & -\frac{I\sin(2\beta)e^{I\delta}}{6\sqrt{2}} & \frac{\sin^2(\beta)}{6} \end{pmatrix} \tag{3.4.20c}$$

When the laser beam is inline with the electron beam, $\theta_L = 0$, the density matrix is in its simplest form since the geometry is axially symmetric, though the excited P-state is not necessarily axially symmetric. Note that when circularly polarized light is used, see Figure 3.2, the matrix collapses to a single element, either $\rho_{1,1}$ or $\rho_{-1,-1}$ depending upon the photon's direction of rotation. Another single element density matrix is possible if, in the perpendicular laser beam direction, $\theta_L = \pi/2$, the polarizer is oriented along the electron beam axis, or $\beta = n\pi$, see Figure 3.3. Such a system is axially symmetric due to the alignment of the P-state along the electron beam, and the density matrix collapses to the element $\rho_{0,0}$. Note that for $\beta = \pi/2$ the P-state is orientated perpendicular to the electron beam for all of the different azimuthal laser directions, for example see Figure 3.4, and hence all three density matrices are the same.

The two axially symmetric systems in Figure 3.2 and Figure 3.3 are the easiest to analyze, and hence a good place to start. Using the Mathematica™ program given in Appendix 1 the appropriate polarization density matrices were generated by calculating equation (3.4.19). Since the scattering amplitudes are dependent upon both the initial and final states the following change of notation will be implemented

$$f\left(L_f, M_f; L_i, M_i\right) f\left(L_f, M_f'; L_i, M_i'\right)^* = f_{M_f', M_i'}^{M_f, M_i}. \tag{3.4.21}$$

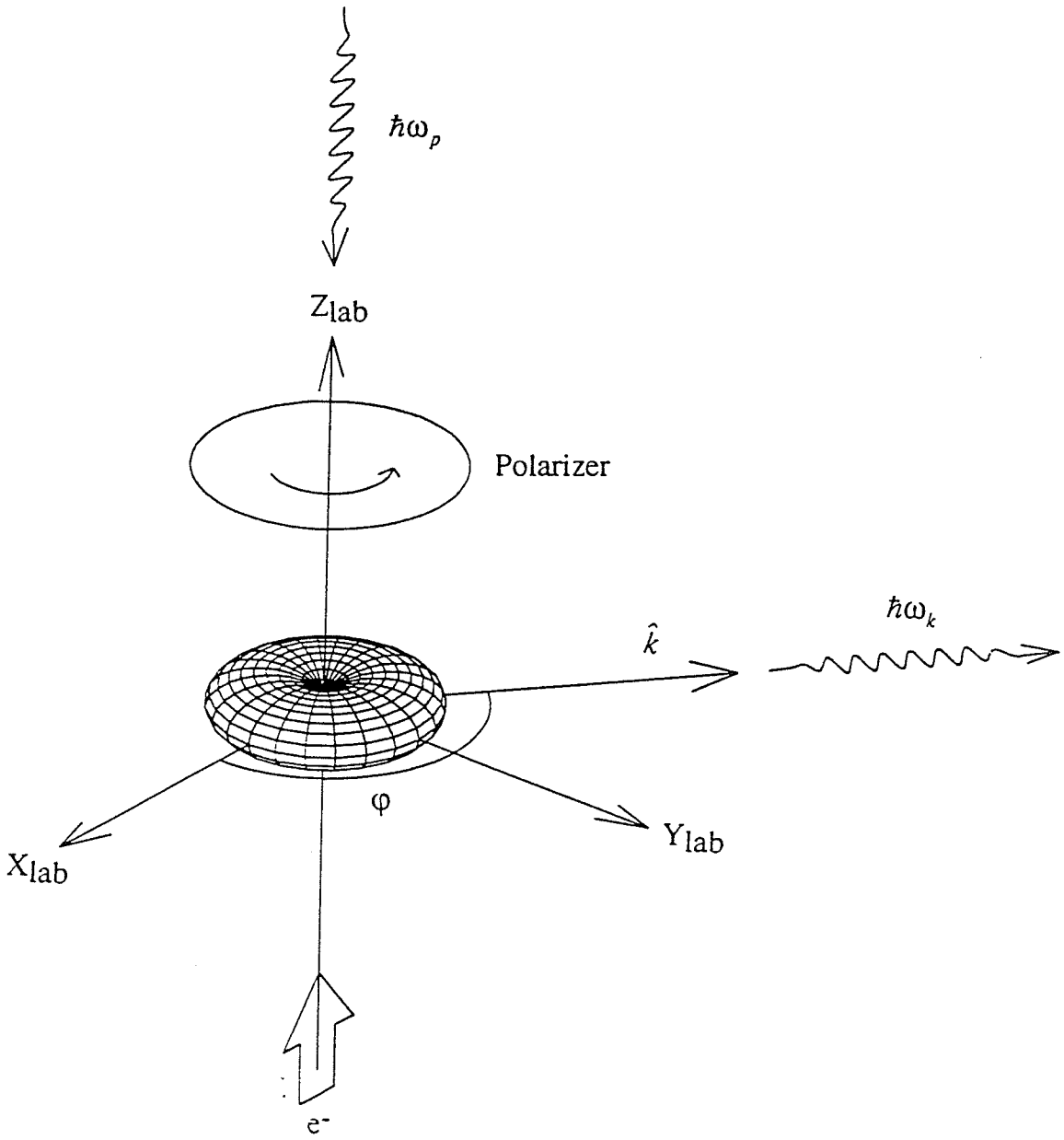

Figure 3.2: Circularly polarized light is produced by a laser inline with the electron beam axis and viewed at 90° to the electron beam. The excited atom state is shown.

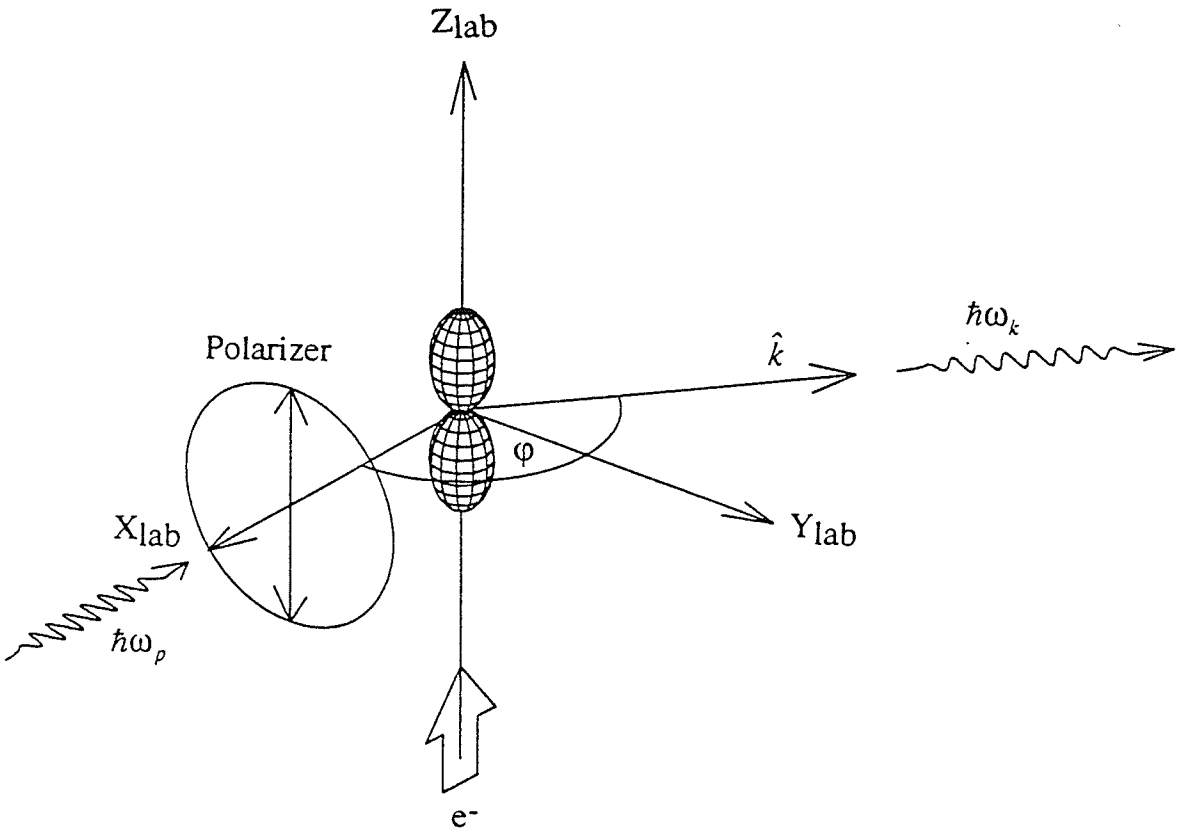

Figure 3.3: Linearly polarized light exciting a P-state dipole along the electron beam. Incident laser light produced perpendicular to the electron beam axis, but with the polarization axis along the beam, causes a the P-state to be orientated along the electron beam.

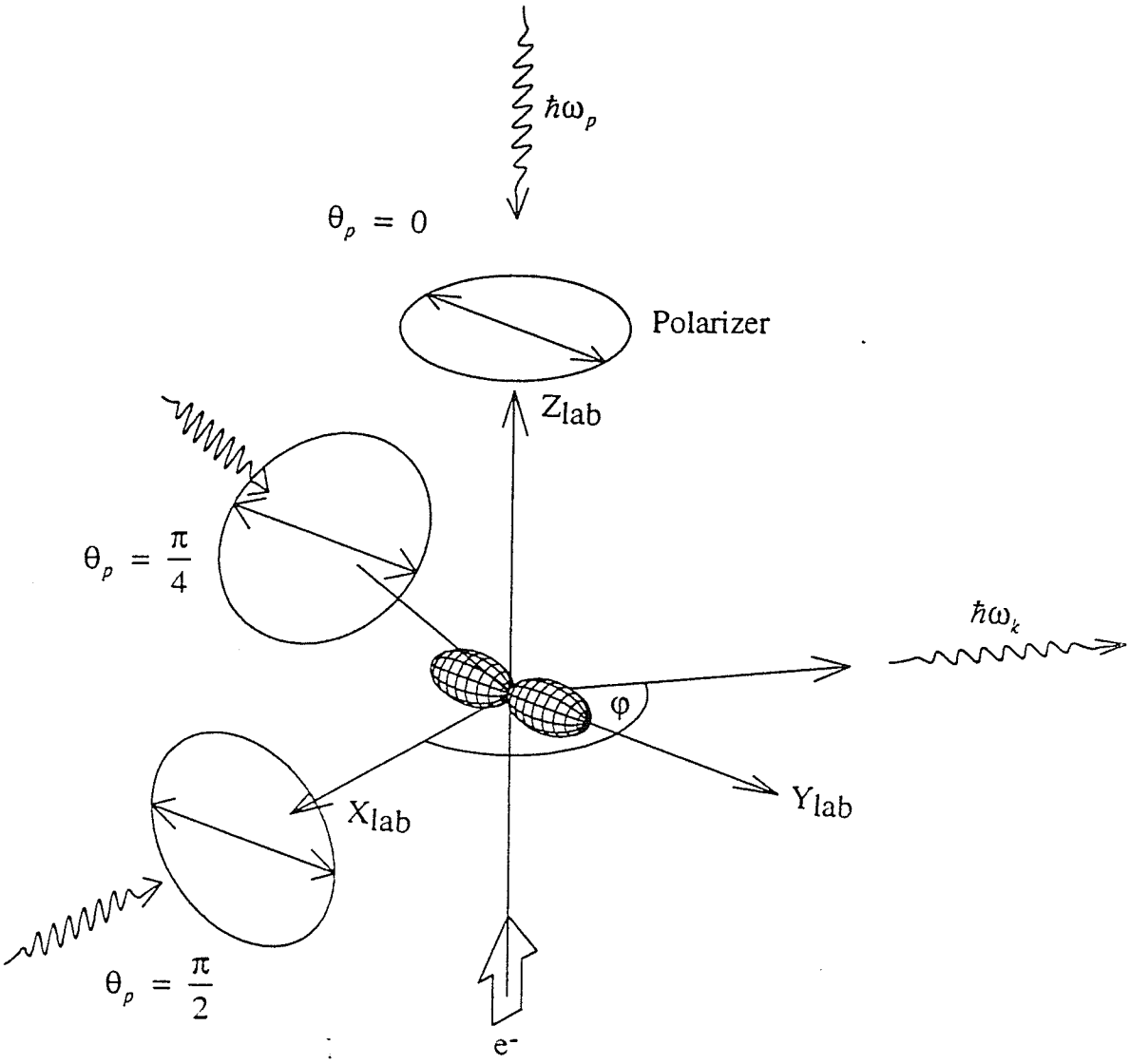

Figure 3.4: Linearly polarized light exciting a P-state dipole perpendicular to the electron beam. Laser polarization perpendicular to the electron beam axis results in the same physical excitation of the aligned P-state for various orientations.

The resulting Stokes parameters for the setup as defined by Figure 3.2 are

$$\begin{aligned} n_1 &= 0 \\ n_2 &= 0 \\ n_3 &= \frac{3\left(f_{01}^{01} + f_{\pm 11}^{\pm 11} - 2f_{\pm 21}^{\pm 21}\right)}{5f_{01}^{01} + 9f_{\pm 11}^{\pm 11} + 6f_{\pm 21}^{\pm 21}}, \end{aligned} \tag{3.4.22}$$

where

$$f_{\pm i1}^{\pm i1} = \frac{f_{i1}^{i1} + f_{-i1}^{-i1}}{2}. \tag{3.4.23}$$

If the polarization in equation (3.4.24) is compared to the previously derived equation for the helium D-P transition, equation (3.1.7), then it is apparent that their forms are identical. This is true even though the electron is scattering off of an anisotropic M=1 P-state, and not the isotropic ground state. It is interesting that the scattering amplitudes for excitation to the $M_f = \pm 2$ sublevels appear as a single term , as do the $M_f = \pm 1$ sublevels. This suggests that the paired terms might be inseparable, and will therefore reduce the total number of independent parameters that can be measured. A diagram showing the available energy level transitions is in Figure 3.5.

The Stokes parameters for the second setup (Figure 3.3) are

$$\begin{aligned} n_1 &= 0 \\ n_2 &= 0 \\ n_3 &= \frac{-6f_{20}^{20} + 3f_{10}^{10} + 3f_{00}^{00}}{6f_{20}^{20} + 9f_{10}^{10} + 5f_{00}^{00}}. \end{aligned} \tag{3.4.24}$$

Once again the results are identical to the polarization for the Helium D-P transition. This time, however, the scattering amplitudes are due to scattering off of the M = 0 P-state.

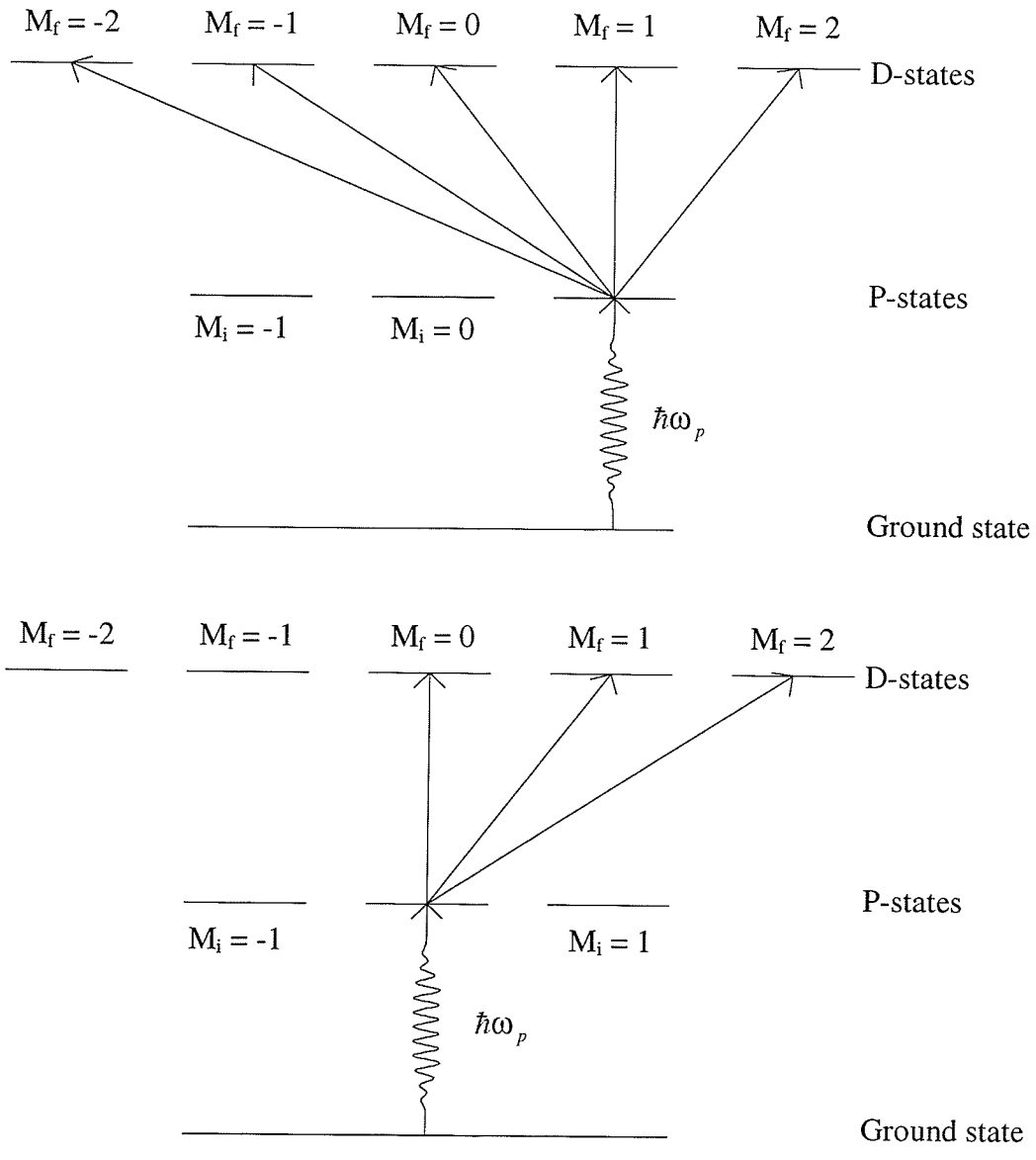

Figure 3.5: Energy level transitions available from the laser excited P-states

The scattering amplitudes

$$f_{\pm 20}^{\pm 20} = \frac{f_{20}^{20} + f_{-20}^{-20}}{2}, \tag{3.4.25}$$

and

$$f_{\pm 10}^{\pm 10} = \frac{f_{10}^{10} + f_{-10}^{-10}}{2}, \tag{3.4.26}$$

do not appear in equation (3.4.24) due to the symmetry defined by equation (3.4.16).

The solution to Equation (3.4.19) for the general case of a circularly polarized laser in a direction defined by (θ_p,φ_p) and a detector with a position defined by $(\theta_k,\varphi_p+\Delta)$ yields

$$\begin{aligned}
In_1 &= -4\sin(2\Delta)\cos(\theta_k)\sin^2(\theta_p)\left(3f_{-1-1}^{11} + 2\sqrt{6}\,\mathrm{Re}\left[f_{0-1}^{21}\right]\right) \\
In_2 &= 0 \\
In_3 &= 3\sin^2(\theta_k)\left[\sin^2(\theta_p)\left(f_{00}^{00} + f_{10}^{10} - 2f_{20}^{20}\right) + \left(1+\cos^2(\theta_p)\right)\left(f_{01}^{01} + f_{\pm 11}^{\pm 11} - 2f_{\pm 21}^{\pm 21}\right)\right] \\
&\quad -\cos(2\Delta)\sin^2(\theta_p)\left(1+\cos^2(\theta_k)\right)\left(\frac{3}{2}f_{-1-1}^{11} + \sqrt{6}\,\mathrm{Re}\left[f_{0-1}^{21}\right]\right),
\end{aligned} \tag{3.4.27a}$$

where the intensity, I, is

$$\begin{aligned}
I = &\left(2+3\sin^2(\theta_k)\right)\left[\sin^2(\theta_p)f_{00}^{00} + \left(1+\cos^2(\theta_p)\right)f_{01}^{01}\right] + \\
&3\left(2+\sin^2(\theta_k)\right)\left[\sin^2(\theta_p)f_{10}^{10} + \left(1+\cos^2(\theta_p)\right)f_{\pm 11}^{\pm 11}\right] + \\
&6\left(1+\cos^2(\theta_k)\right)\left[\sin^2(\theta_p)f_{20}^{20} + \left(1+\cos^2(\theta_p)\right)f_{\pm 21}^{\pm 21}\right] + \\
&\cos(2\Delta)\sin^2(\theta_k)\sin^2(\theta_p)\left(\frac{3}{2}f_{-1-1}^{11} + \sqrt{6}\,\mathrm{Re}\left[f_{0-1}^{21}\right]\right).
\end{aligned} \tag{3.4.27b}$$

If either the laser or the detector is orientated along the electron beam axis then the relative angle Δ in the density matrix elements must be integrated over a full revolution since the relative angle will no longer be defined. Two off-diagonal terms are evident in

equation (3.4.27) and both are dependent upon the relative angle Δ. The contributions from these elements disappear as soon as axial symmetry is restored to the system.

The solution to equation (3.4.19) for the general case of a linearly polarized laser orientated in a direction defined by (θ_p,φ_p) and a detector with a position defined by $(\theta_k,\varphi_p+\Delta)$ gives

$$\begin{aligned} In_1 &= -4\sin(2\Delta)\cos(\theta_k)\cos^2(\theta_p)\left(3f_{-1-1}^{11}+2\sqrt{6}\,\mathrm{Re}\left[f_{0-1}^{21}\right]\right) \\ In_2 &= 0 \\ In_3 &= 3\sin^2(\theta_k)\left[\sin^2(\theta_p)\left(f_{00}^{00}+f_{10}^{10}-2f_{20}^{20}\right)+\cos^2(\theta_p)\left(f_{01}^{01}+f_{\pm11}^{\pm11}-2f_{\pm21}^{\pm21}\right)\right] \\ &\quad -\cos(2\Delta)\cos^2(\theta_p)\left(1+\cos^2(\theta_k)\right)\left(\frac{3}{2}f_{-1-1}^{11}+\sqrt{6}\,\mathrm{Re}\left[f_{0-1}^{21}\right]\right), \end{aligned} \tag{3.4.28a}$$

where the intensity, I, is

$$\begin{aligned} I = &\left(2+3\sin^2(\theta_k)\right)\left[\sin^2(\theta_p)f_{00}^{00}+\cos^2(\theta_p)f_{01}^{01}\right]+ \\ &3\left(2+\sin^2(\theta_k)\right)\left[\sin^2(\theta_p)f_{10}^{10}+\cos^2(\theta_p)f_{\pm11}^{\pm11}\right]+ \\ &6\left(1+\cos^2(\theta_k)\right)\left[\sin^2(\theta_p)f_{20}^{20}+\cos^2(\theta_p)f_{\pm21}^{\pm21}\right]+ \\ &\cos(2\Delta)\sin^2(\theta_k)\cos^2(\theta_p)\left(\frac{3}{2}f_{-1-1}^{11}+\sqrt{6}\,\mathrm{Re}\left[f_{0-1}^{21}\right]\right). \end{aligned} \tag{3.4.28b}$$

For the linearly polarized laser beam, the relative angle Δ is well defined until the P-state electric dipole is aligned with the electron beam ($\theta_p = \pi/2$) or when the detector is aligned along the electron beam. The difference between equations (3.4.27a) and (3.4.28a) is due to the extra dipole component contained within the circularly polarized laser beam. The beam can be split into two orthogonal components. The component which is in the laser/electron beam plane is identical to the dipole caused by the linearly polarized beam, while the component which is perpendicular to the plane is equivalent to the dipole shown in Figure 3.4.

The number of independent parameters, as indicated by equations (3.4.27) and (3.4.28), is eight. Three of the parameters, $\{ f_{20}^{20}, f_{10}^{10}, f_{00}^{00} \}$, are simply the scattering cross sections for excitation out of the M = 0 P-state. Three more, $\{ f_{\pm 21}^{\pm 21}, f_{\pm 11}^{\pm 11}, f_{01}^{01} \}$, are the scattering cross sections for excitation out of the M=1 P-state. Two of these scattering processes, $f_{\pm 21}^{\pm 21}$ and $f_{\pm 11}^{\pm 11}$, do not discern between their target states even though the contributions from the different processes are anisotropic. The last two parameters, f_{0-1}^{21} and f_{-1-1}^{11}, are off-diagonal elements which only contribute when the axial symmetry has been destroyed by the orientation of the P-state dipoles, M=±1.

The number of independent measurements required to completely characterize the D-state atomic density matrix created by electron scattering off of a laser excited P-state is eight. The number of independent parameters available for measurement in equations (3.4.27) and (3.4.28) is five. This becomes obvious when either of the equations is rearranged. For example, equation (3.4.28) can be rewritten as

$$\begin{aligned} In_1 &= -8\sin(2\Delta)\cos(\theta_k)\cos^2(\theta_p)\gamma \\ In_2 &= 0 \\ In_3 &= 3\sin^2(\theta_k)\left[\sin^2(\theta_p)\alpha_0 + \cos^2(\theta_p)\alpha_1\right] - \cos(2\Delta)\cos^2(\theta_p)\left(1+\cos^2(\theta_k)\right)\gamma, \end{aligned} \tag{3.4.29a}$$

and

$$\begin{aligned} I = {} & \sin^2(\theta_p)\left[\beta_0 + \sin^2(\theta_k)\alpha_0\right] + \cos^2(\theta_p)\left[\beta_1 + \sin^2(\theta_k)\alpha_1\right] + \\ & \cos(2\Delta)\sin^2(\theta_k)\cos^2(\theta_p)\gamma, \end{aligned} \tag{3.4.29b}$$

where

$$\alpha_i = f_{0i}^{0i} + f_{\pm 1i}^{\pm 1i} - 2f_{\pm 2i}^{\pm 2i}$$
$$\beta_i = 5f_{0i}^{0i} + 9f_{\pm 1i}^{\pm 1i} + 6f_{\pm 2i}^{\pm 2i} \qquad (3.4.29c)$$
$$\gamma = \frac{3}{2} f_{-1-1}^{11} + \sqrt{6}\,\mathrm{Re}\left[f_{0-1}^{21}\right].$$

Since a common factor can be divided out from the numerator and denominator of the polarization, there are only four independent parameters contained in equation (3.4.29). A fifth parameter can be obtained by either setting the total cross section for the transition to one, or by measuring it. The measurement of the polarized D-P transition is, therefore, not sufficient to fully determine the D-state density matrix populated from a laser excited P-state. I propose that in order to fully characterize the D-state density matrix, the polarization of the D-P transition must also be measured in coincidence with the P-S cascade transition, or in coincidence with the scattered electron.. This is analogous to the measurement procedure required to fully characterize the D-state density matrix which has been excited from the ground state.

Chapter 4 Apparatus

4.1 Introduction

The apparatus was built to perform photon-photon coincidence measurements. It is capable of measuring the polarization of a visible photon, and will be capable of measuring the polarization of the visible photon in coincidence with an ultra-violet photon. The general setup of the apparatus is illustrated in Figure 4.1. The interaction region is formed by the intersection of the electron beam, the atom beam, and the optical axis.

4.2 Vacuum System

The main vacuum chamber is an aluminium block 10 ½ by 10 ½ by 15 inches with a 9 ½ inch diameter hole bored through its length. The ends are capped with aluminium plates, the one on the front actually being a capped cylinder which increases the available volume. A four inch Varian diffusion pump provides the required vacuum and is exhausted by a Duo Seal Model 1402 roughing pump by the Welch Scientific Company. The chamber can be isolated from the diffusion pump by a pneumatically operated gate valve and roughed directly via a separate inlet. At low pressures, $< 10^{-4}$ torr, an ion gauge is used to measure the chamber pressure, at higher pressures there are 2 available thermocouple gauges, one before the diffusion pump exhaust valve, and the second after. The lowest pressure measured with the above system was approximately 9×10^{-8} torr. The system is shown in Figure 4.2 There are six flanges attached to the main chamber which are used to interface to the outside: two on the top and two on each side. Two of the flanges are used solely for electrical connections, and another contains two quarter inch

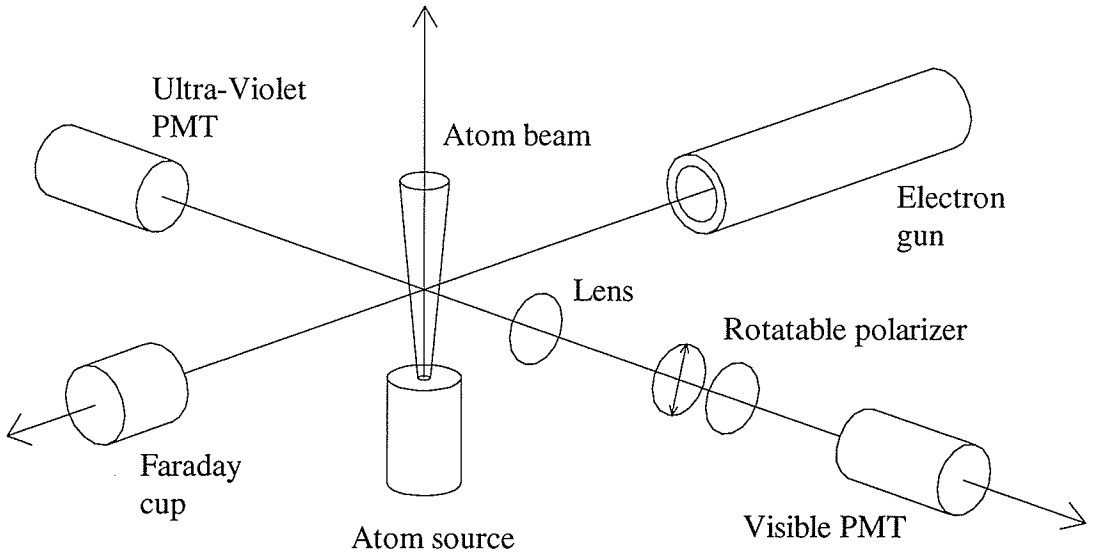

Figure 4.1: The general setup of the experiment. The interaction region is defined by the interception of the three orthogonal axes.

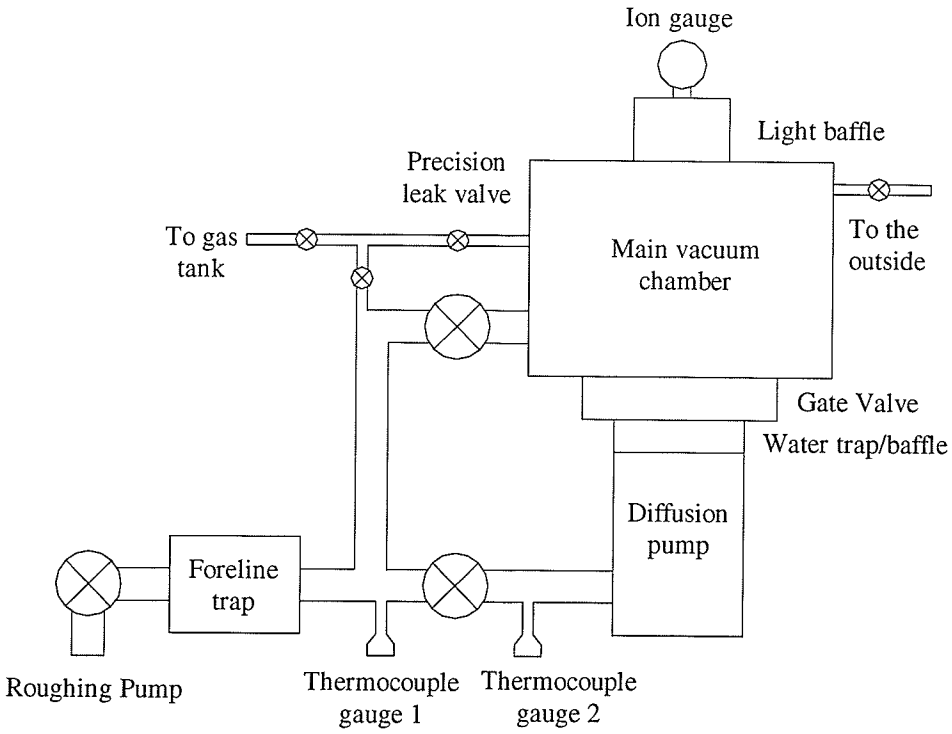

Figure 4.2: Block diagram of the vacuum chamber

stainless steel pipe feedthroughs to allow the regulated supply of a target gas into the chamber. The flange which holds the ion gauge also incorporates a light baffle to prevent any outside light from entering the chamber. Another flange holds the internal ultra-violet photo-multiplier tube and also provides for cooling and electrical connections, or contains a 1 ½ inch diameter quartz window with the PMT being mounted on the outside. The last flange contains a 1 ½ inch diameter glass window enabling the visible florescence to enter the external optics setup. The birefringence of such windows has been investigated by Li and was found to be undetectable (Li). The flanges form a vacuum seal to the main chamber by using Viton o-rings, while most connections onto the flanges are made via a Conflat Flange seal..

A number of safety circuits have been built to minimize the risk of a catastrophic event. The first main system is triggered by the ion-gauge pressure surpassing a set trigger point. Once this pressure is exceeded, the power to the electron gun filament supply, the high voltage supply for the UV photo-multiplier tube, and the actual ion-gauge are automatically shut off. The chamber is also isolated from the diffusion pump by the closing of the gate valve, and the diffusion pump is itself isolated from the roughing pump by the closing of a valve. A second system tests for water leaking from the cooling lines of the diffusion pump, and in such an event shuts off the water supply and the power to the diffusion pump heater.

4.3 Electron Gun

The electron gun was designed by A. Chutjian at the Jet Propulsion Laboratory and its design is detailed in his 1979 paper(Chutjian1979). The goal of the design was to

create an electron gun which could focus at a fixed region over a large range of electron energies. A further requirement was that the tuning of the gun over the wide range of electron energies could be accomplished with the variation of only one potential.

The lenses used in the gun are simply created by a potential difference between two isolated conductive cylinders. The field varying region between the cylinders accelerate or decelerate the incident electrons in a manner similar to an optical lens focusing light. The electrostatic lenses can be approximately modeled as a thick lens with focal points f_1 and f_2, which are measured with respect to the principal planes H_1 and H_2. The object focused by a lens is best represented as two limiting apertures, a window and a pupil. The window is defined to be a physically limited source which emits a constant flux of electrons. The image formed by the source is then limited by the pupil which defines the half angles of the rays (Figure 4.3). The image formation by a thick lens is illustrated in Figure 4.4. The linear and angular magnification factors for a thick lens are given by

$$M_L = \frac{x_2}{x_1} = \frac{f_2 - q}{f_2} = \frac{f_1}{f_1 - p}, \tag{4.3.1}$$

and

$$M_\theta = \frac{\theta_1}{\theta_2} = \frac{f_1 - p}{f_2} = \frac{f_1}{f_2 - q}, \tag{4.3.2}$$

where p and q are the object and image distances respectively, defined with respect to the principal planes. The ray-transfer matrix method, described by DiChio (DiChio1973), was used by Chutjian to design the lens elements. The matrix method is just an application of the optical ray tracing matrix methods used to analyze optical elements discussed, for example, by Klein and Furtak (Klein1986).

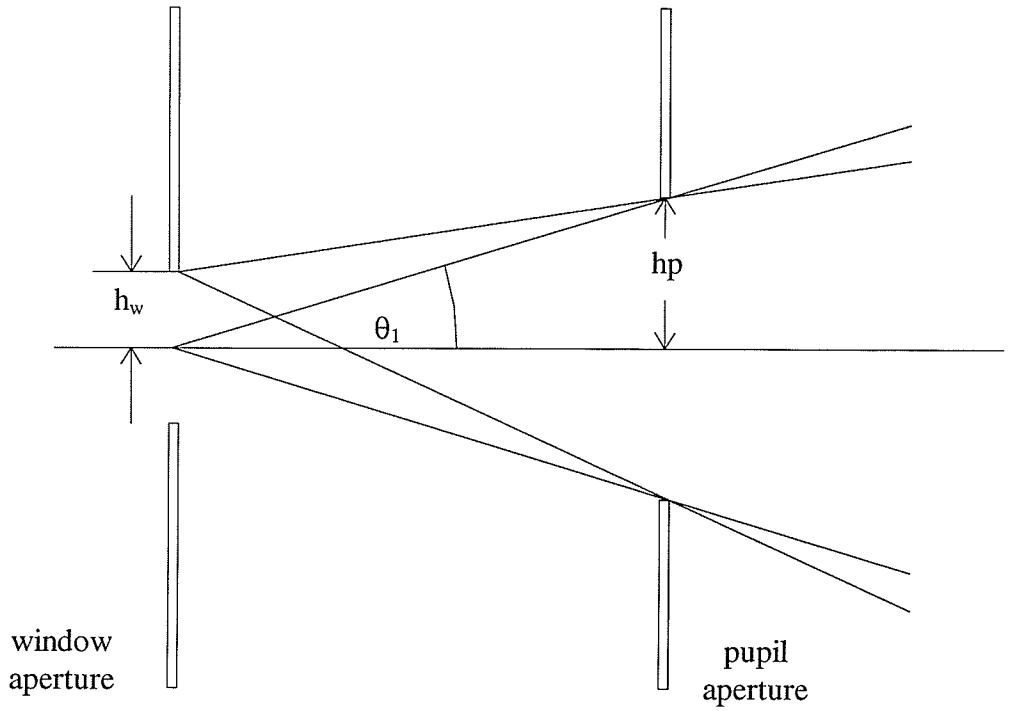

Figure 4.3: An image defined by a window and a pupil. Adapted from (Li1996).

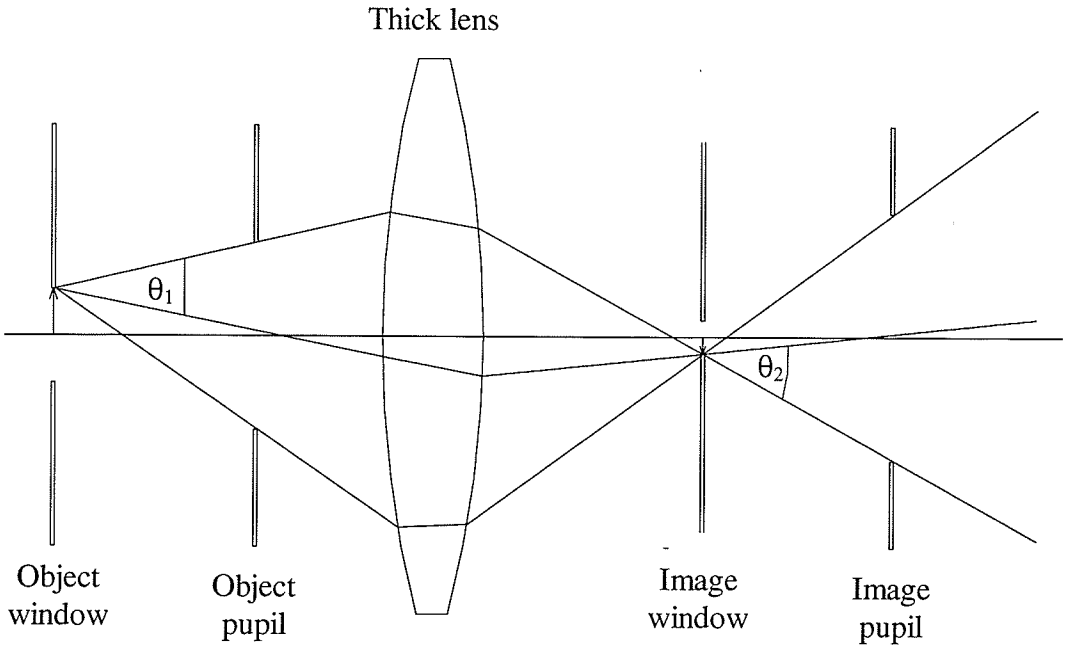

Figure 4.4: The formation of an image window and pupil by a thick lens. Adapted from (Li1996).

The first lens in the gun (Figure 4.5) is a Pierce extraction diode which forms the first image of the hairpin filament defined by the window w_1 and the pupil p_1. The next lens is placed with its focal point roughly located at w_1 and the emitted rays are therefore mostly parallel. A spatter aperture is located within the parallel portion of the electron beam to limit any aberrations. The purpose of lenses two and three is to place a secondary image defined by w_2 and p_2 at the focal point of the variable zoom lens system. The zoom lens is created by the focusing of lenses four and five, and the window w_2 is capable of being focused at w_3, the interaction region, for a large range of energies ,2 eV to 1800 eV.

The electron gun routinely supplied 1-2 μA of current over a wide range of energies, 15 eV to 350 eV. At lower energies, less than 15 eV, the overall current output decreased and the gun required more than the adjustment of the single focusing element to retune after a change in operating energy. The Faraday cup used to measure the electron flux consisted of two concentric surfaces. The inner diameter of the first was 0.083 inches, while the diameter of the second was 0.112 inches. A normal current distribution was 1 μA on the inner cup, and less than 100 nA on the outer cup. The energy resolution of the gun was directly determined by the energy resolution of the cathode since no energy analyzer was used. The electrons' energy profile for emission by a thermionic cathode is given by the Boltzmann equation

$$I(E) = I_0 \frac{2E^{1/2}}{\pi^{1/2}(kT)^{3/2}} e^{-\frac{E}{kT}}, \tag{4.3.3}$$

where E is the kinetic energy of the emitted electrons and T is the cathode temperature. A measure of the electron beam energy resolution is the full width at half maximum of equation (4.3.3), or

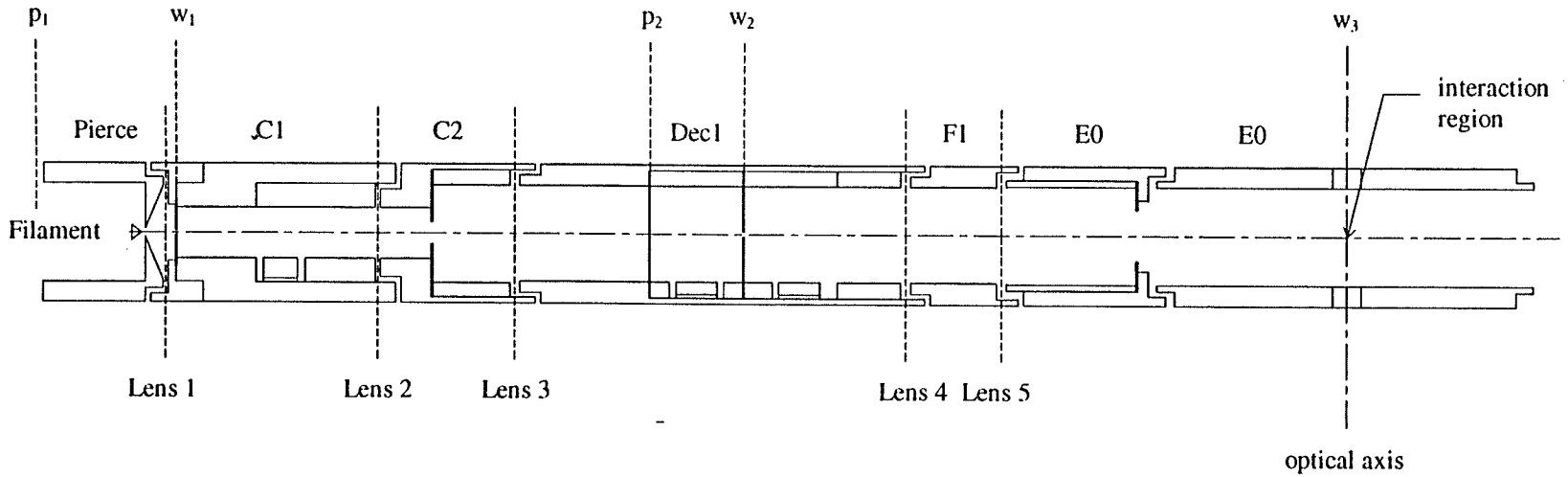

Figure 4.5: The electron gun elements and the interaction chamber. The lenses are located along with the real images of the filament. Also shown is the interaction region defined by the electron beam axis and the optical axis.

$$\Delta E = 1.79kT. \tag{4.3.4}$$

For a normal operating temperature of 3000°K the resolution of the electron gun is approximately 0.5 eV.

The power supply for the gun was made by Yufei Li, and consists of separate supplies for each gun element all biased off of the cathode bias power supply. A block diagram of the electron gun power supply is shown in Figure 4.6. The last element of the gun and the interaction region are grounded, and therefore, the cathode bias supply is negative with respect to ground. To enable the electron gun to be switched on and off remotely, a background switching circuit was developed which can be installed in series with these existing power supplies. The circuit, depicted in Figure 4.7, was designed to switch voltages less than 450 V with a minimum of effort. The switching speed of the circuit is limited by the high voltage opto-isolators, MOC8204, which take at most 5 μS to change state. The circuit is essentially an up/down counter whose sequence will ensure that both power supplies are isolated. The RC combination at the input to the CLR pins guarantees that the flip-flops will turn on in a safe state.

The electron gun is capable of sweeping the impact energy of the electrons over a 10 Volt range due to the ramp output of the ORTEC MCS computer card. To increase the range of the ramp a simple non-inverting op-amp circuit was built. The circuit, shown in Figure 4.8, provides the operator with the options of by-passing the ramp or applying a 10 V, 20 V, or 30 V sweep. The ramp is only capable of increasing monotonically over the set range.

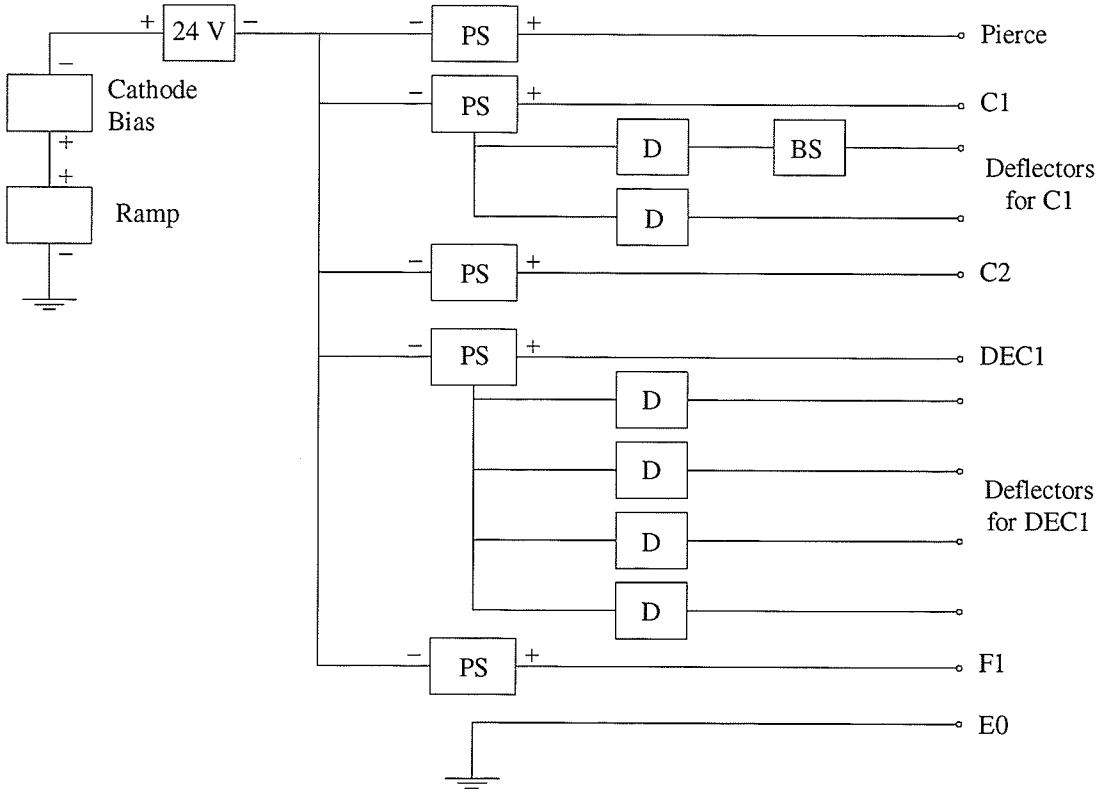

PS: Gun element power supply capable of 0-330 V

D: Deflector power supply, ±12 V on top of the element

BS: Background switching circuit

Figure 4.6: A block diagram of the electron gun power supply. The deflector potentials are not mounted in serial with the parent element, but utilize some of the same circuitry to guarantee their voltages are centered around the parent.

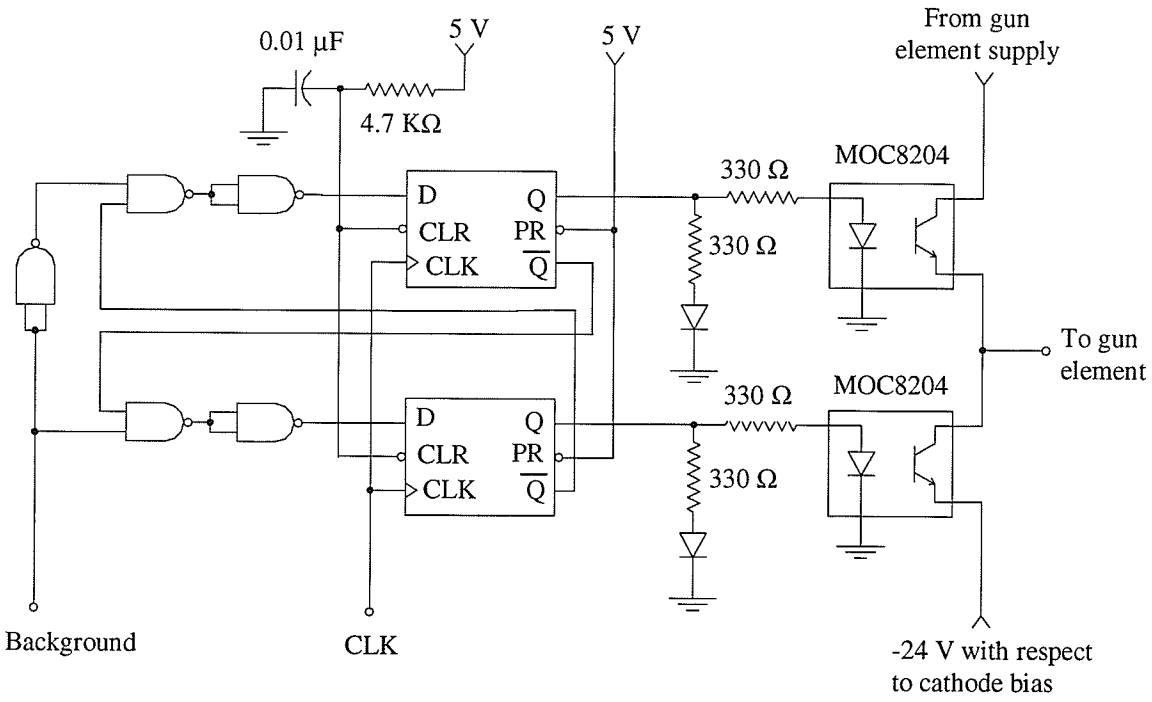

Figure 4.7: The background switching circuit capable of switching a gun element from its operating potential to a different potential. The 'Background' signal line determines which supply is connected to the element: high - normal gun element supply; low - -24 V with respect to cathode bias.

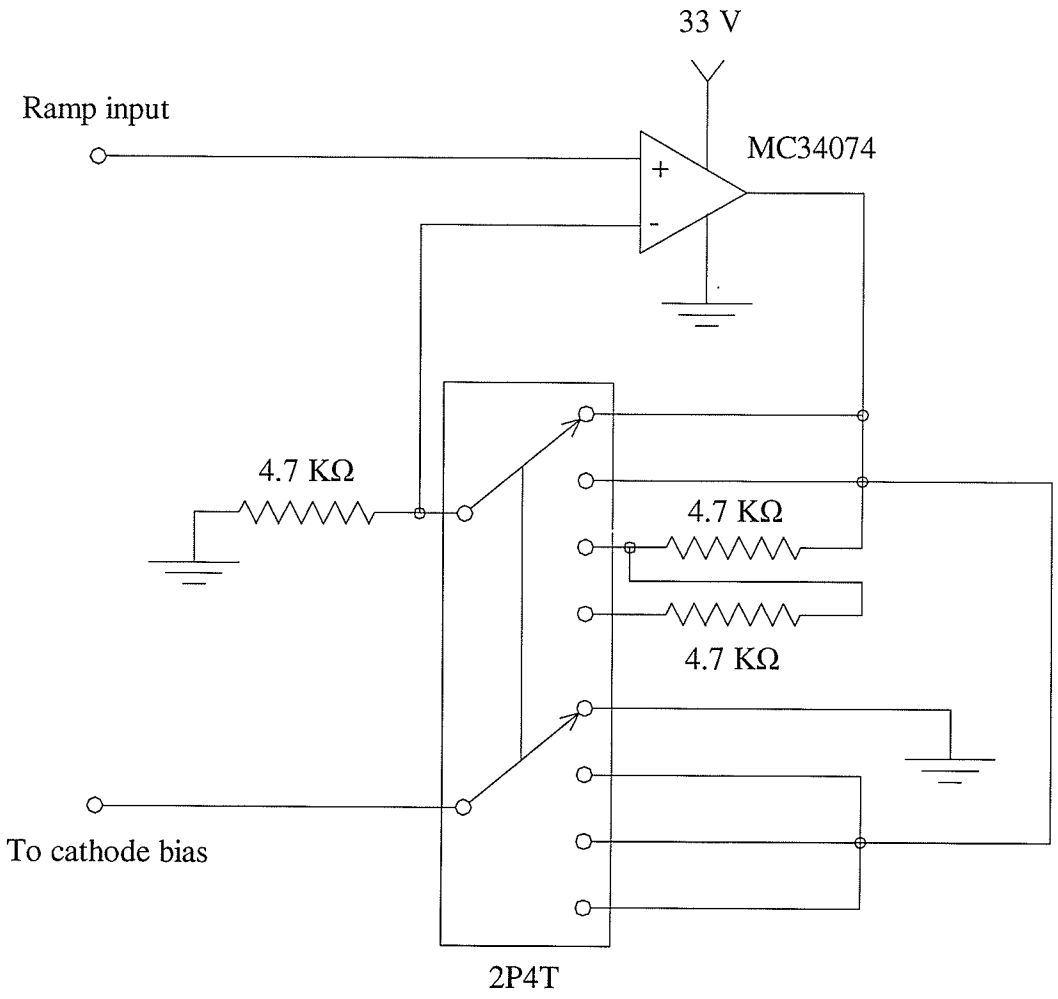

Figure 4.8: The ramp amplification circuit. The ramp input is a 0-10 V signal from the MCS pc card. The amplified signal acts as a base voltage for the cathode bias. The possible voltage ranges are 0 V, 10 V, 20 V, and 30 V.

4.4 Atom Sources

4.4.1 Helium

The two different atoms which will be investigated, helium and magnesium, require two completely different delivery systems. The helium is supplied to the interaction region via a molybdenum tube with an inside diameter of 2 mm, and a length of 2 inches. Molybdenum is used for this purpose because it is completely non-magnetic and a good conductor. The flow of gas through the needle is limited by a Varian variable leak-valve capable of supplying leak rates as small as $1x10^{-10}$ Torr-litres per second. To ensure a clean supply of helium, the entire gas delivery system can be pumped on to remove any contaminants. The alignment of the gas needle to the interaction region is accomplished by aligning a needle, inserted down the shaft of the tube, with two sets of orthogonal apertures. The first set of apertures is defined by the Pierce element of the electron gun and the final element constituting the Faraday cup. The second axis is determined by the set of apertures which define the optical path.

4.4.2 Magnesium

The supply of magnesium to the interaction region requires more effort. To produce a metal vapour beam the magnesium must be heated to approximately 530 °C. The oven that is used to heat the magnesium is shown in Figure 4.9. The heater used, a 400 W element made by ARi Industries Inc., is a 2-wire coaxial element which is wrapped around the magnesium chamber. The coaxial nature of the element significantly reduces the magnetic fields emitted by the oven due to the high currents involved. To insulate the

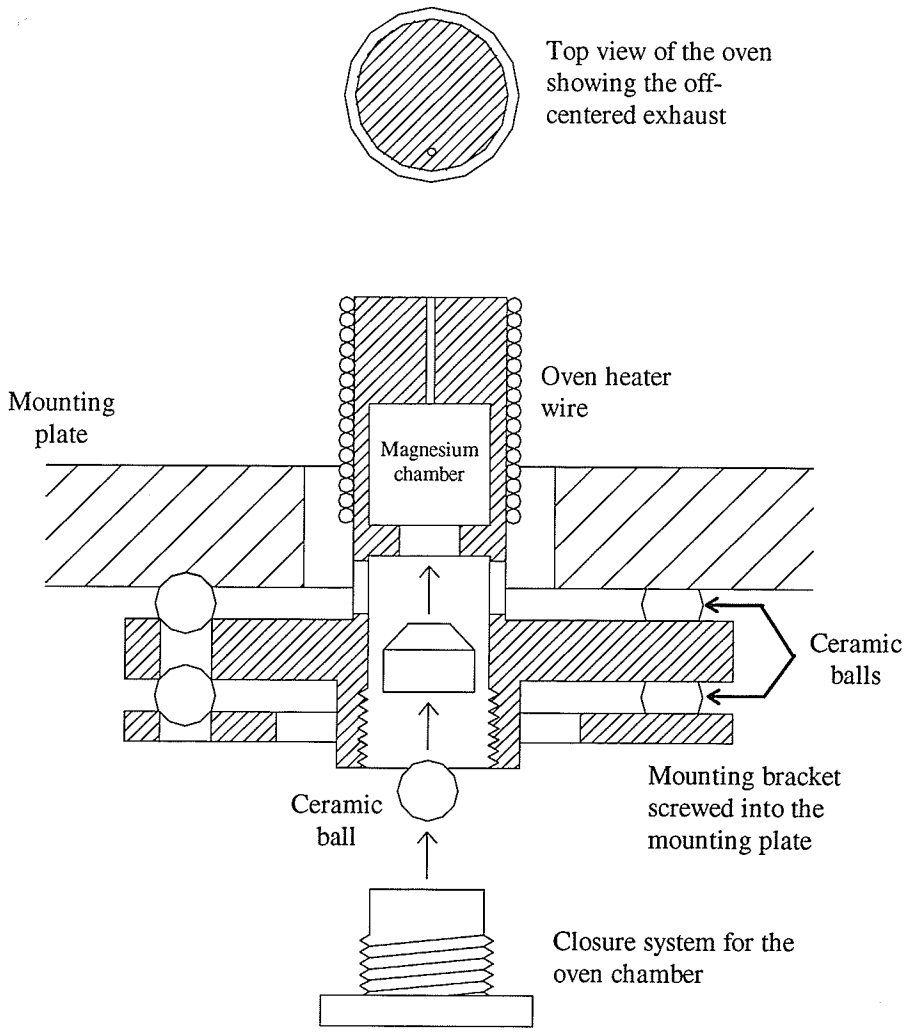

Figure 4.9: Magnesium oven. The magnesium oven is mounted underneath the electron gun. The magnesium chamber is sealed with a stainless steel plug. The ceramic balls and the holes drilled in the oven walls helped to minimize heat loss.

main chamber from the rest of the oven the amount of conductive metal was reduced by drilling holes in the cylinder walls and by using ceramic balls as spacers between the mounting bracket and oven, and the mounting plate and oven. The ceramic balls also serve to accurately position the oven since they sit in hemispherical depressions which have been drilled into the mounting plate. A major concern in designing the oven was ensuring there was a long enough exhaust hole to aid in collimating the metal vapour beam. However, if the chamber heats up prior to the exhaust tube then there is a danger of condensation forming on the exhaust walls and blocking it. To prevent this, the exhaust tube was off-centered and placed at the edge of the inner chamber. This ensured that the exhaust tube heated up at the same rate as the inner chamber walls.

4.5 Photon Detection Systems

4.5.1 Visible

The visible photon detector consists of a number of optical elements whose aim was to select a specific polarization of light at a specific frequency from the interaction region. The general setup is shown in Figure 4.10. The first element in the optical path was a 0.75 inch diameter lens with a focal length of 1.75 inches. The lens was placed so that the interaction region was located at its focal point. The interaction region was therefore focused at infinity, or equivalently, the diverging radiation, which was collected by the lens, was collimated into a non-diverging plane wave. With the atomic fluorescence no longer diverging, the distances between subsequent optical elements was no longer critical. The solid angle seen by the lens was 0.14 sr. After passing through the glass flange, the light was polarized by a sheet polarizer mounted in a rotating assembly. The

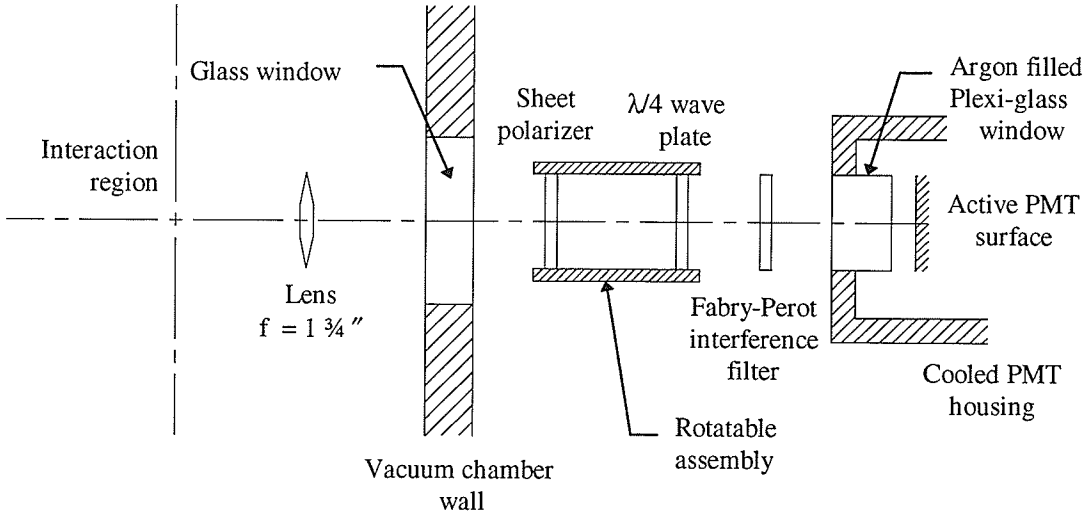

Figure 4.10: Optical path for the visible photon. The sheet polarizer and the quarter-wave plate can be rotated by an attached stepper motor.

assembly was rotated by a 200 step per revolution stepper motor geared down by a ratio of 3.56:1. The motor was controlled by the data acquisition computer and could be placed with an accuracy of 0.5°. Since there was no encoder on the shaft of the motor to provide a feedback as to the polarizer's position, the motor was only rotated in one direction, and its position was calibrated every rotation by an optical switch. Also mounted within the rotating assembly was a quarter-wave plate which had its fast axis mounted at a 45° angle to that of the polarizer. This arrangement changed the linearly polarized light into circularly polarized light which negated any polarization sensitivity that the subsequent elements had.

The last optical element before the photo-multiplier tube was a Fabry-Perot interference filter, a band-pass filter, with maximum transmission at the wavelength of interest. Shown in Figure 4.11 is a percent transmission curve for the 492 nm filter used with helium. The closest adjacent line in helium was at 502 nm, and was therefore well rejected by the filter. The interference filter used to measure the 553 nm transition in magnesium had a FWHM of 10 nm centred at 550 nm. The closest transition to the 553 nm spectral line was at 518 nm, and was therefore also rejected. Fabry-Perot interference filters are sensitive to the direction of the incident light since the effective length of the interference cavity is increased for light rays which are not normal to the filter. The increased cavity length increases the frequency of the transmission maximum and increases the bandwidth of the filter. The plane wave produced by the initial collimating lens reduced the angular spread of the light and therefore minimized the amount of non-normal light incident on the filters. The last optical element was the actual photo-

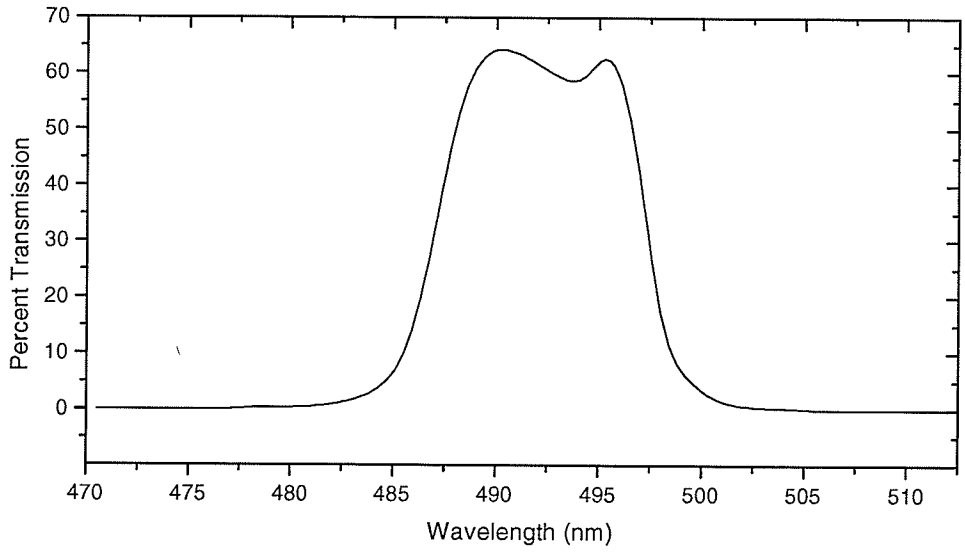

Figure 4.11: 492 nm bandpass filter

multiplier tube, EMI 9658R. The tube was enclosed in a Peltier cooled, hermetically sealed enclosure, a TE-206TSRF made by Products for Research Inc. The cooled tube had an improved dark count, which for an operating voltage of 1100 V was approximately 90 Hz. The wavelength sensitivity range for the 9658R was from 300 to 900 nm with a peak sensitivity at 370 nm.

4.5.2 Ultra-Violet

The ultra-violet photon detector was mounted inside the vacuum chamber in a stainless steel container. Since the detection system had to operate when the oven was at 535 °C, the normal operating temperature of magnesium oven, the container was cooled by an enclosing stainless steel water cooling line. Stainless steel was chosen for the tubing to minimize the risk of a rupture when under vacuum, since the lab has found copper tubing to be susceptible to corrosion.

Two different UV photon detectors were required to measure the ultra-violet P to S transitions in helium and magnesium. The high energy of the helium transition, 21.2 eV, required the use of an electron multiplier tube. The dynodes of the EMT are coated with an active film of processed alumina which emits an electron upon the absorption of a photon. The quantum efficiency for a device with a processed aluminium oxide coating is reported to be 14% for an incident wavelength of 58.4 nm (Canfield1987). The P-S transition in magnesium emits a photon of lower energy, 4.35 eV. A conventional UV photo-multiplier tube, Hamamatsu R2078, with a spectral range of 160 to 320 nm, and a peak sensitivity at 240 nm was used. The quantum efficiency of the detector was reported to be 10% for the 285 nm spectral line (Hamamatsu1997). The view cone for the detector

is formed by an aperture (diameter = 3/8 “) mounted on the stainless steel container, and the physical extent of the interaction region. The extent of the interaction region is approximated to be a 3 mm cube.

4.6 Data Acquisition System

As mentioned previously the photon detection was accomplished by using photon-multiplier tubes (PMT), or in the case of the high energy ultra-violet transition in helium, an electron multiplier tube. The output from both of the aforementioned devices was similar, and consisted of small negative current pulses caused by the cascade of electrons through the device. The detection electronics for both of the photon detectors for magnesium is shown in Figure 4.12. The difference in the detection electronics for the visible and ultra-violet photons was due to the use of the EC&G preamplifier/discriminator which outputs a TTL or ECL pulse without the need for a separate amplifier stage and a single channel analyzer.

The setup for helium was almost the same as for magnesium, the only difference was a change in the de-coupling circuit which extracted the current pulse from the electron multiplier tube. Since the electron multiplier tube can measure energetic particles including ions, and electrons, the entrance aperture of the device was grounded to limit the electric field intensity, and the anode was maintained at a large positive potential. Photon multiplier tubes, however, cannot measure charged particles, and a large negative potential was applied to the cathode, leaving the anode at ground. The latter scheme was convenient since the detected pulses were measured at the anode, and therefore, did not need to be separated from the large DC component of the EMT power supply.

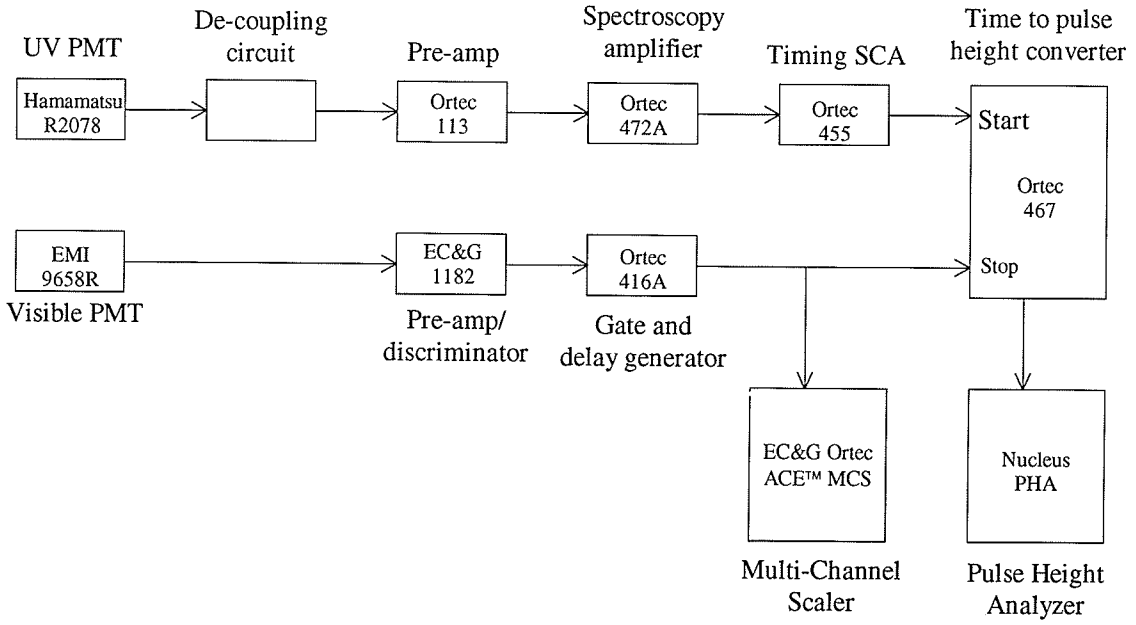

Figure 4.12: Detection electronics. The separate detection paths for the visible and ultra-violet detectors converge at the time to pulse height converter. The PHA was used to bin the coincidence signal according to pulse height. The MCS was used to collect excitation functions and to measure the polarization of the visible signal.

The signal which contains the polarization of the D-P transition can be measured directly after the visible photon pre-amplifier/discriminator stage with the multi-channel scalar. The exact method of measuring the polarization, either accumulating signal at the maximum and minimum of the signal or mapping out the entire polarization curve, was not limited by the apparatus and can be accommodated by the controlling hardware. The second measurement of interest, the polarization of the visible photon measured in coincidence with the ultra-violet photon, used the time to pulse height converter to generate a pulse train of varying height. The ultra-violet transition, whose intensity was over an order of magnitude greater than the intensity of the visible transition, was used to start the time to pulse height converter. If the time to pulse height converter did not time out before a pulse from the visible transition arrived at the stop input, then a pulse whose height was dependent upon the time difference was sent to the pulse height analyzer and binned into one of 1024 channels.

The operation of the apparatus was controlled by an IBM compatible computer which interfaced with the equipment via a digital input/output computer card. The card, a PCL-720, had 32 digital input and output channels and three 16-bit programmable counters. The hierarchy of the control system used is shown in Figure 4.13. The I/O card controlled the advancement of the MCS data channels and the stepper motor with the help of additional onboard circuitry. The extra circuitry, shown in Figure 4.14, enabled the software to control individually which devices were being advanced and also enabled the 'End of rotation' signal to stop any further motor rotation once an optical switch on the rotator was triggered.

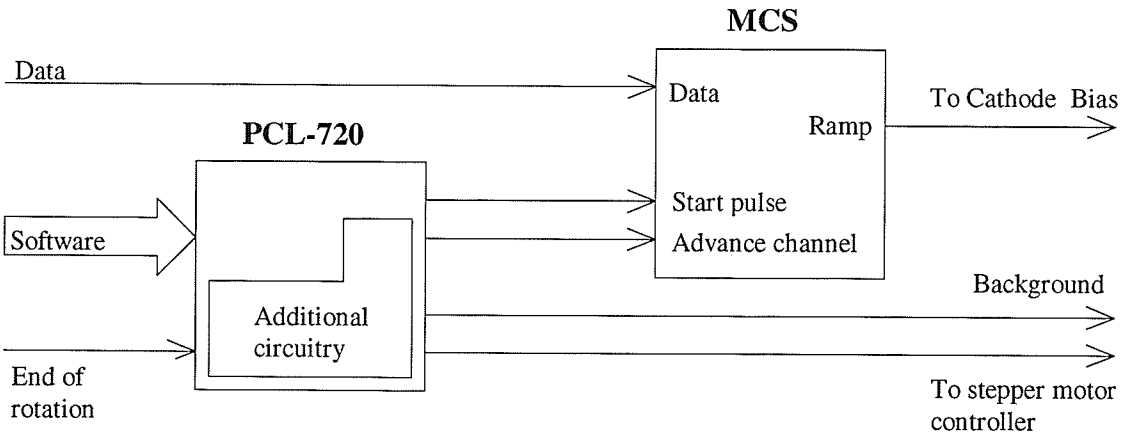

Figure 4.13: The controller hierarchy. The software controls the PCL-720, which in turn enables the advancement of the MCS and/or the stepper motor. The rotation of the stepper motor can be stopped by the 'End of Rotation' signal.

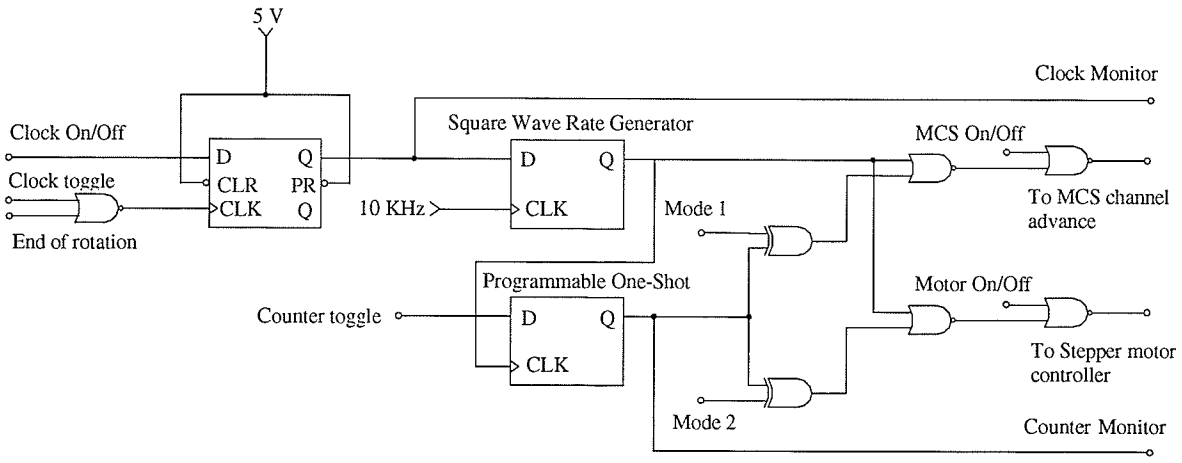

Figure 4.14: Onboard I/O card controller circuit. The signals 'Mode 1' and 'MCS On/Off' were used to enable the advancement of the MCS channel, while the signals 'Mode 2' and 'Motor On/Off' were used to advance the motor. The motor rotation can be stopped automatically by the rotator if the 'Clock On/Off' signal is low, and the rotator sends the 'End of rotation' signal.

The square wave generator and the programmable one-shot modules in Figure 4.14 are two of the three available counters on the PCL-720. The square wave rate generator used the 10 KHz signal as a base clock and generated a variable clock to be used by the other circuitry. The rate of the variable clock output was set by a programmable 16-bit register. The square wave rate generator can be turned on by a high signal at 'D'. The variable clock signal can be stopped by the 'End of rotation' signal supplied by the rotator if the 'Clock On/Off' signal had previously been set low. The current status of the generator was read with the 'Clock monitor' signal line. The second counter operated in a programmable one-shot mode, and was used to generate a pulse train whose length was predetermined by a 16-bit register. This enabled the stepper motor and/or the MCS to be advanced by a specified number of pulses. The clock to the counter was supplied by the output of the variable clock pulse generator, and the counting sequence was initiated by a pulse on the 'Counter toggle' line. The state of the counter was determined with the 'Count monitor' signal line. The truth table for controlling which component of the system was to be advanced is given in Table 4.1. The program which controlled the hardware is included in Appendix 3.

Due to addressing conflicts within the computer, the PHA card had to be installed in a separate data acquisition computer. The communication required to synchronize the computers was accomplished with the existing I/O card and a separate controller program which manipulated the PHA. The separate controlling program enabled the data from the time to pulse height converter to be placed into two separate memory groups. The first memory group contained the polarization which was

Table 4.1: Truth table for the controller circuit. The operation is analogous for the MCS advancement. The first column refers to whether a pulse train is currently being generated by the programmable one-shot counter module.

Programmable one-shot	Programmable one-shot: Q	Square wave rate generator: Q	Mode 1	Motor On/Off	To stepper motor controller
Not counting	1		0	X	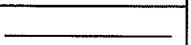
	1		1	1	
	1		1	0	
	1	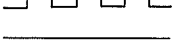	X	X	
Counting	0	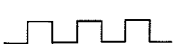	0	1	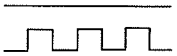
	0	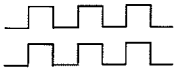	0	0	
	0	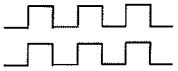	1	X	
	0	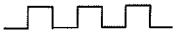	X	X	

parallel to the electron beam, and the second contained the polarization which was perpendicular to the electron beam. The program is included in Appendix 4.

Chapter 5 Preliminary Results

5.1 1s4d-1s2p Transition in Helium

The initial diagnostics for the polarization sensitivity of the apparatus were performed with the 1s4d-1s2p singlet transition in helium since there is a large amount of readily available data for this transition. For example, McFarland (McFarland1967) has determined the polarization for electron impact energies ranging from 24 to 550eV, while Raan *et al.*(Raan1970) have measured the polarization with electron energies of up to 1000eV. To date, however, there have been no D-P-S photon-photon coincidence measurements made involving the 492 nm spectral line. The only published results of a double photon coincidence measurement have been presented by Mikosza *et al.* (Mikosza1995) for the 1s3d-1s2p-$1s^2$ helium transition and Williams *et al.*(Williams1993) for the hydrogen n=3 levels.

The apparatus described in Chapter 4 was used to measure the polarization of the 492 nm transition in helium. The incident electron energy ranged from the excitation threshold of the D-state, 23.76 eV, to 350 eV. The vacuum chamber was maintained at a background pressure of approximately $3x10^{-5}$ torr during the measurements, but the actual density of the helium in the interaction region could not be determined with the apparatus. The electron gun was tuned so that 1.0 μA was measured on the inner Faraday cup, and only 75 nA on the outer Faraday cup. The actual data were taken by continuously rotating the polarizer and collecting the processed visible photon signal with the Ortec MCS card. The background signal due to the dark count of the PMT and any ambient

light was measured by repeating the polarization measurement, but with the electron gun turned off. Since the average collection time for a polarization measurement was approximately 15 minutes and the background signal rate was extremely stable. It was, therefore, not necessary to continuously alternate the polarization and background measurements in order to eliminate error accumulation. At 40 eV an average photon count was 8 KHz with a background signal of approximately 90 Hz. Examples of the data collected, with the background already subtracted, are shown in Figure 5.1, 5.2, and 5.3. The three figures depict the extremes of polarization measured. At 43.6 eV the polarization was near its maximum (Figure 5.1), while at approximately 303.6 eV the polarization underwent a sign change and was almost equal to zero (Figure 5.2). The polarization maintained a negative slope until the limits of the cathode bias power supply was reached at 353.6 eV (Figure 5.3) and data collection stopped.

The entire collection of polarization measurements taken for the 492 nm helium transition is shown in Figure 5.4, along with previous measurements taken by Raan *et al.* (Raan1970). The energy scale in Figure 5.4 was determined by measuring the excitation function of the ultra-violet $1s2p\text{-}1s^2$ transition as shown in Figure 5.5. The threshold of excitation is sharply defined by the steep drop-off in the UV count rate. A straight line was fitted to the incline and the intercept was used to shift the energy scale to the proper threshold excitation energy. The accuracy of the excitation function energy scale was guaranteed by noting two energies off of the digital multi-meter at set places in the energy sweep. The threshold energy, as shown by Figure 5.5, is 24.7±0.9 eV, while the accepted value is 21.24 eV. The energy scales in Figures 5.1 through 5.4 have already had the 3.5 eV voltage shift applied. The measured

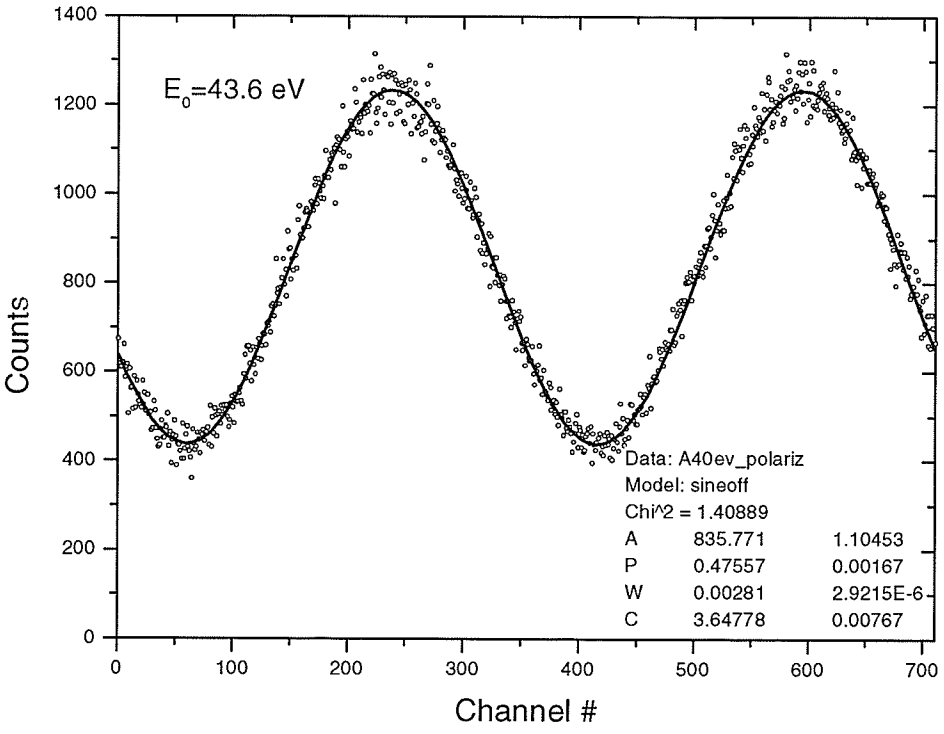

Figure 5.1: Intensity as a function of 'Channel #' for the He singlet-singlet transition 1s4d-1s2p at an impact energy of $E_0 = 43.6$ eV. The fitting results are given in the bottom corner of the graph for the equation $A(1+p\cos(2\pi w x + C))$. The parameter p is the polarization of the signal.

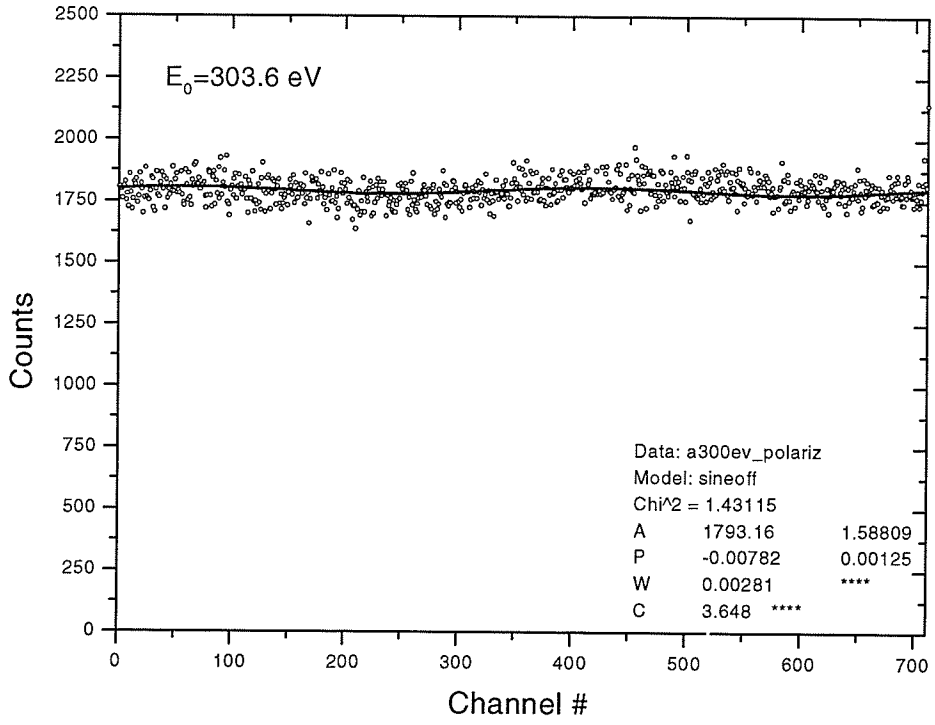

Figure 5.2: Intensity as a function of 'Channel #' for the He singlet-singlet transition 1s4d-1s2p at an impact energy of E_0 = 303.6 eV. The fitting results are given in the bottom corner of the graph for the equation $A(1+p\cos(2\pi w x + C))$. The parameter p is the polarization of the signal.

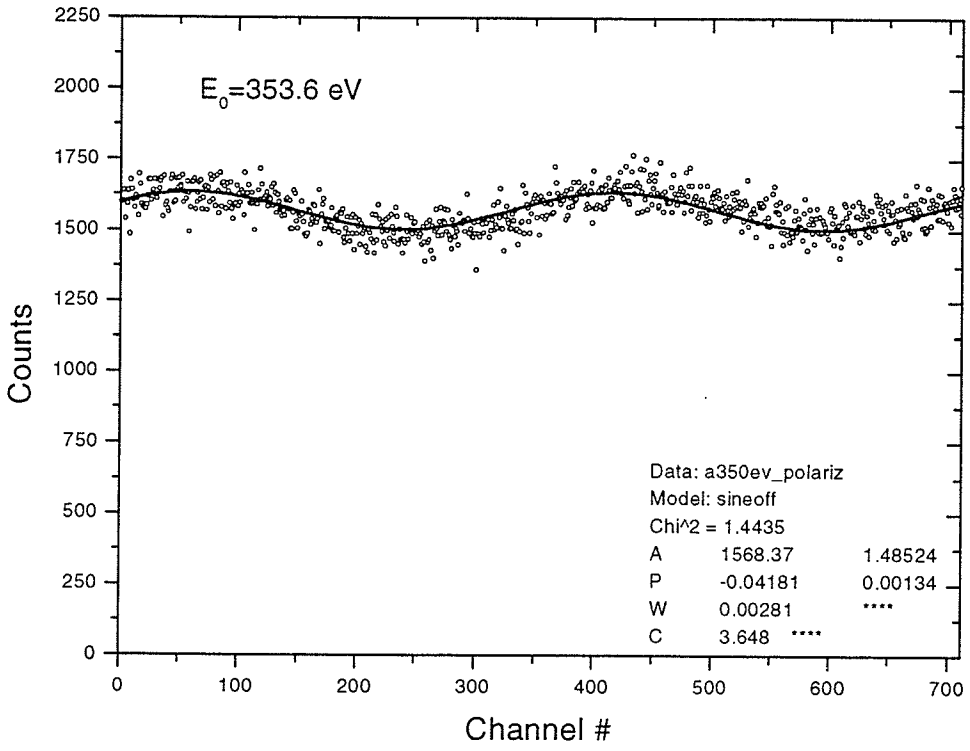

Figure 5.3: Intensity as a function of 'Channel #' for the He singlet-singlet transition 1s4d-1s2p at an impact energy of E_0 = 353.6 eV. The fitting results are given in the bottom corner of the graph for the equation $A(1+p\cos(2\pi w x + C))$. The parameter p is the polarization of the signal.

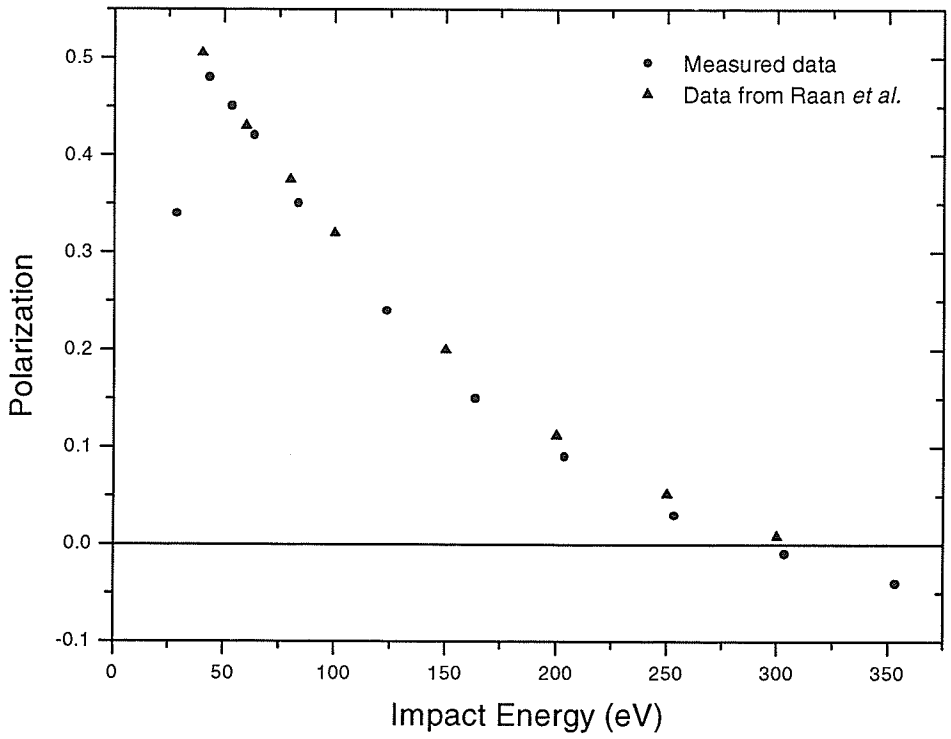

Figure 5.4: The polarization function for the He singlet-singlet 1s4d-1s2p transition as found in this work and as found by Raan *et al.* (Raan1970).

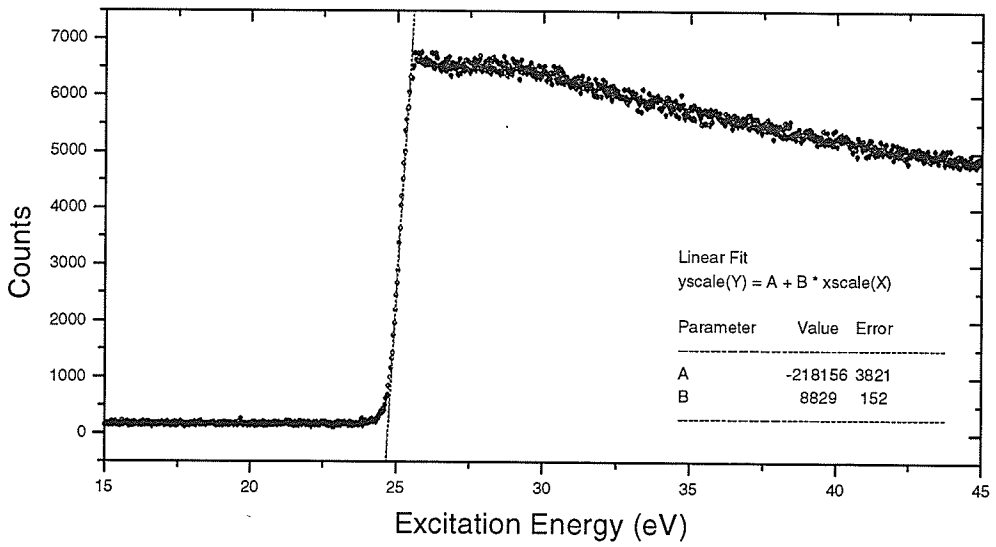

Figure 5.5: The excitation function for the ultra-violet 1s2p-1s2 singlet-singlet transition in helium.

polarization curve shows good agreement with the measurements by Raan *et al.*(Figure 5.4). Although discrepancies between the two curves become noticeable at higher energies, Heddle has noted that the polarization measurements of other authors for the 492 nm line also diverge (Clout1971, McFarland1967, Raan1970) and is probably a result of the small cross sections which occur at the higher energies (Heddle1989). The polarization minimum near the threshold has been noted previously by McFarland (McFarland1967) and similar minima have been observed for the 389.9 nm, 438.8 nm, and 501.6 nm spectral lines of helium (McFarland1964). The polarization minimum is not a general feature of all spectral lines and has not been observed in the lithium and sodium resonance lines (Haidt1965).

5.1.1 Analysis of the Depolarization Effects on the 1s4d-1s2p Transition in Helium

There are four main mechanisms for the depolarization of the fluorescence caused by electron impact excitation. The four mechanisms are the anisotropic polarization sensitivity of the apparatus, the alignment of the atomic state vectors due to external electric and magnetic fields, the cascade population of the D-state from more energetic states, and the absorption and re-emission of the fluorescence.

The polarization sensitivity of the apparatus can be caused by the finite solid angle measured by the photon detectors, and the inherent polarization sensitivity of some of the equipment. Since the electrons were not detected, the experiment was axially symmetric and the emitted polarized light was independent of the zenith angle (assuming the electron beam was the z-axis). The depolarization can therefore only be dependent upon the azimuthal angle seen by the detector (Figure 5.6). The dependence of the measured

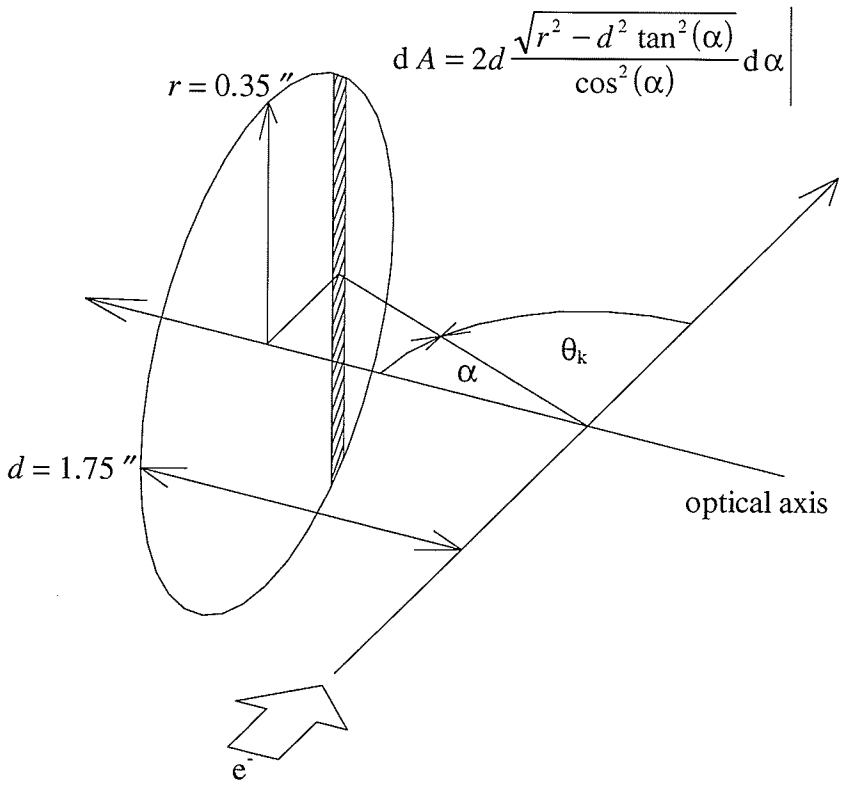

Figure 5.6: Effect of the detector's view cone on the polarization. The view cone of the detector defined by a detector of radius *r*. The distance between the electron beam axis and the detector is *d*. In the experiment the detector is actually the collimating lens (f = *d*) which then focuses the interaction region at infinity.

polarization on the orientation of the detector was previously calculated in section 3.2 and is given by equation (3.2.6), or

$$P = -\frac{6\sin^2(\theta_k)(\sigma(0)+\sigma(1)-2\sigma(2))}{(3\cos(2\theta_k)-7)\sigma(0)+(3\cos(2\theta_k)-15)\sigma(1)-2(3\cos(2\theta_k)+9)\sigma(2)}.$$

A measure of the sensitivity of the polarization to the finite solid angle can be calculated if equation (3.2.6) is integrated over the detector view cone for sample values of the scattering cross sections. The polarization, rewritten in terms of the angle, α (Figure 5.6), and rearranged gives

$$P = \frac{6\cos^2(\alpha)(\sigma(0)+\sigma(1)-2\sigma(2))}{6\cos^2(\alpha)(\sigma(0)+\sigma(1)-2\sigma(2))+(4\sigma(0)+12\sigma(1)+24\sigma(2))} \qquad (5.1.1)$$
$$= \frac{\frac{a}{b}\cos^2(\alpha)}{1+\frac{a}{b}\cos^2(\alpha)},$$

where

$$a = 6(\sigma(0)+\sigma(1)-2\sigma(2)), \qquad (5.1.2)$$

and

$$b = 4\sigma(0)+12\sigma(1)+24\sigma(2). \qquad (5.1.3)$$

Integrating over the detector's view cone, and normalizing by the detector area yields the corrected polarization

$$P_{corrected} = \frac{1}{\pi r^2}\int_0^{\tan^{-1}\left(\frac{r}{d}\right)}\left(\frac{\frac{a}{b}\cos^2(\alpha)}{1+\frac{a}{b}\cos^2(\alpha)}\right)4d\,\frac{\sqrt{r^2-d^2\tan^2(\alpha)}}{\cos^2(\alpha)}\,d\alpha. \qquad (5.1.4)$$

The detector would be polarization insensitive if the coefficient a/*b* was zero, or

equivalently, if the measured polarization was zero. The detector would also be insensitive to the polarization if *a/b* was much larger than one. Since the total scattering cross section requires that

$$1 = \sigma(0) + 2\sigma(1) + 2\sigma(2)$$

for the relative cross sections, the maximum and minimum values for *a/b* occur when

$$\frac{a}{b}_{\min} = -0.5, \text{ or } \sigma(2) = 0.5, \tag{5.1.5}$$

and

$$\frac{a}{b}_{\max} = 1.5, \text{ or } \sigma(0) = 1. \tag{5.1.6}$$

The coefficient a/b_{max} corresponds to the theoretical limit for the relative cross sections at the threshold excitation energy. The coefficient a/b_{min} does not necessarily relate to a physically realizable case but will still supply a bound on the system. The percentage difference between the numerical integration of equation (5.1.4) and equation (5.1.1) with $\alpha = 0$ is shown in Figure (5.7). The calculations show that the effect of the detectors view cone on the polarization of the fluorescence is less than 2% for any impact energy.

The polarization sensitivity of the optical elements must also be accounted for. The optical elements before the polarizer, the collimating lens and the glass window, are essentially polarization insensitive, and will not affect the polarization. After the polarizer, the optical elements are the quarter wave plate, the Fabry-Perot interference filter and the

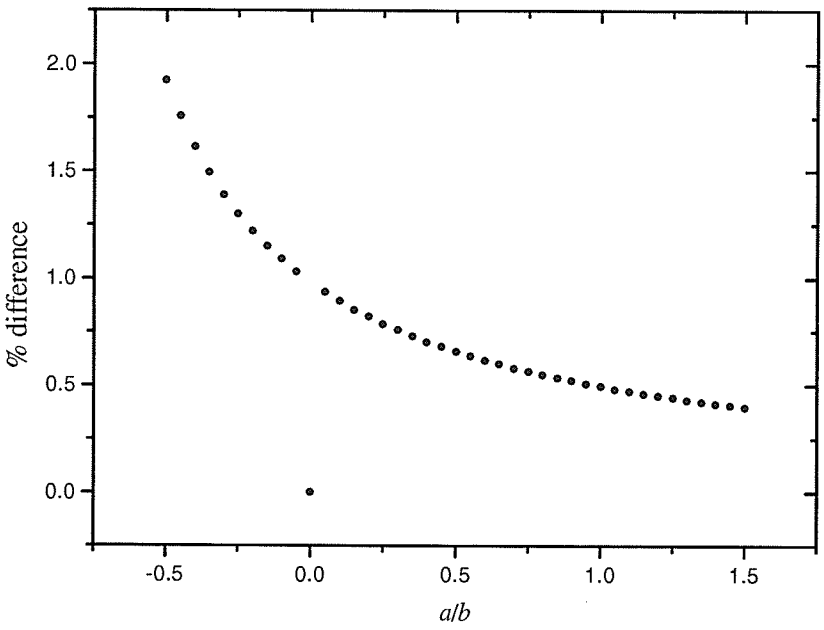

Figure 5.7: The polarization sensitivity of the detector as a function of the coefficient a/b.

PMT (Figure 4.8). The Fabry-Perot interference filter is sensitive to the polarization of the incident light if the incident rays are not perpendicular to the filter. The transmitted wavelength is also dependent upon the incident direction of the light since the effective length of the interference cavity is dependent upon the light's direction. The interference filter works by causing destructive interference between reflected waves in a cavity (Figure 5.8). The reflectance of a surface is polarization dependent and for a plane dielectric boundary, the reflection and transmission coefficients for perpendicular polarization are, respectively,

$$\Gamma_{\perp} = \frac{n_2 \cos\theta_i - n_1 \cos\theta_t}{n_2 \cos\theta_i + n_1 \cos\theta_t} \qquad (5.1.7)$$

$$\tau_{\perp} = \frac{2n_2 \cos\theta_i}{n_2 \cos\theta_i + n_1 \cos\theta_t},$$

and for parallel polarization are, respectively,

$$\Gamma_{\parallel} = \frac{n_2 \cos\theta_t - n_1 \cos\theta_i}{n_2 \cos\theta_t + n_1 \cos\theta_i} \qquad (5.1.8)$$

$$\tau_{\parallel} = \frac{2n_2 \cos\theta_i}{n_2 \cos\theta_t + n_1 \cos\theta_i}.$$

Since the light must undergo multiple reflections before being fully transmitted, the important quantity is the difference between the two reflection coefficients. The perpendicular and parallel reflection coefficients are graphed for a light-air interface in Figure 5.9. To remove the polarization sensitivity, the linearly polarized light can be converted into circularly polarized light. The circularly polarized light will still lose intensity when traversing the filter, but the loss will be constant and independent of the initial linearly polarized light. As mentioned earlier in section 4.5, a quarter wave plate

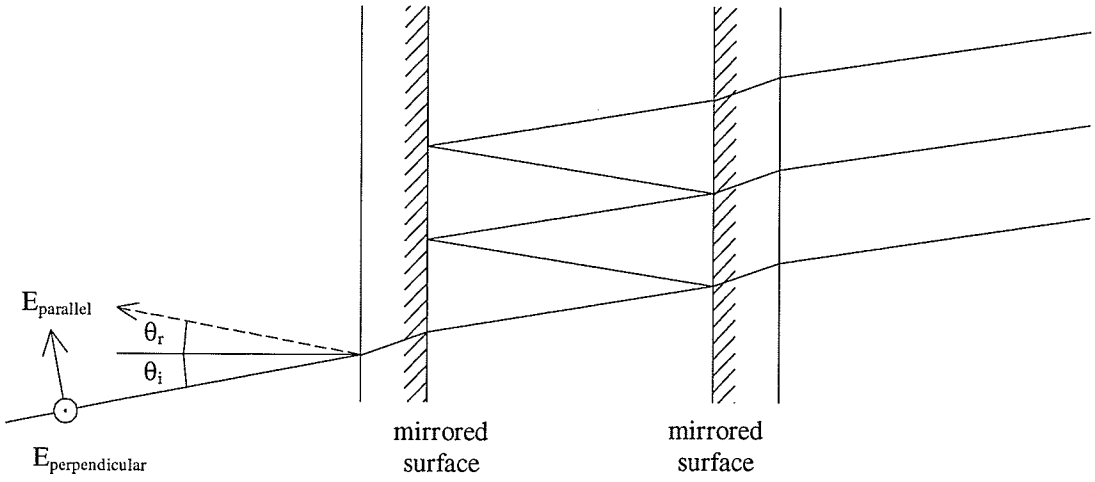

Figure 5.8: The cavity of an interference filter and the reflections due to an arbitrary incident light ray. The cavity is formed by two mirrored surfaces.

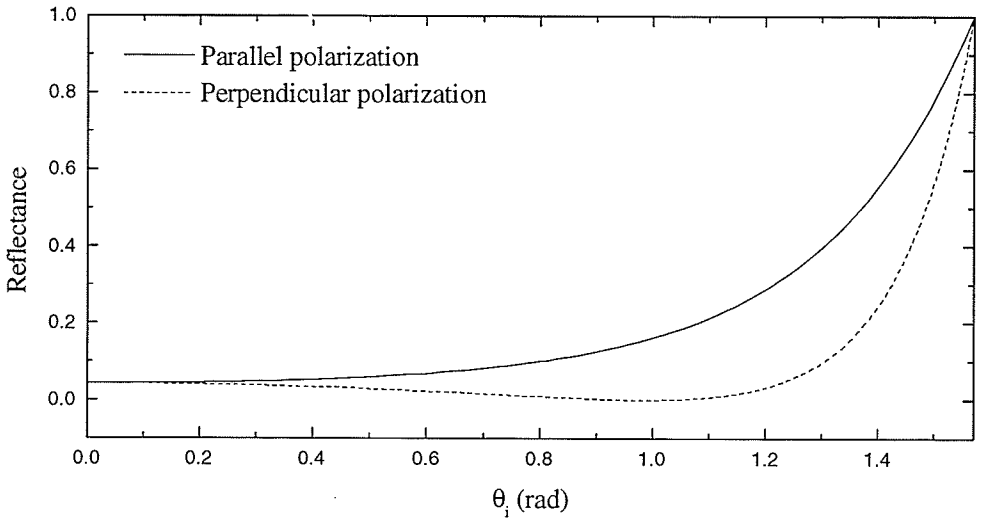

Figure 5.9: The reflectance for the parallel and perpendicular polarizations for an air-glass interface.

with its fast axis oriented at 45° to the linearly polarized light will convert the linearly polarized light into circularly polarized light.

A consequence of not ensuring that the apparatus is polarization insensitive is shown in Figure 5.10. The figure shows the fitted polarization curves for the helium 492 nm transition before the insertion of the quarter wave plate. The fitted curves have had their offset intensities removed. From the figure it is clear that as the electron impact energy increases, a noticeable phase shift develops between each measurement. The actual cause of the effect has not been determined. It is not due to misalignment of the interaction region with the photon axis, since the focusing of the electron gun had no effect upon the measured phase shifts. The problem was solved, however, by inserting the quarter wave plate. The effect might have easily been missed if the polarization data had been collected by the more traditional method of only recording data with the polarizer parallel and perpendicular to the electron beam.

Another cause of depolarization is the alignment of the atomic state vectors due to the presence of external electric and magnetic fields. If a small magnetic field is present then the angular momentum vectors precess about the direction of the field at the Larmor frequency of the excited states. This is an important effect for long lived states since there is ample time for the momentum vectors to precess, therefore destroying the polarization before the state has time to decay to a lower lying state. If the state is short lived then it can decay before there is time for precession. The depolarization of light due to an applied magnetic field was discovered by Hanle in 1924, and is commonly called the Hanle

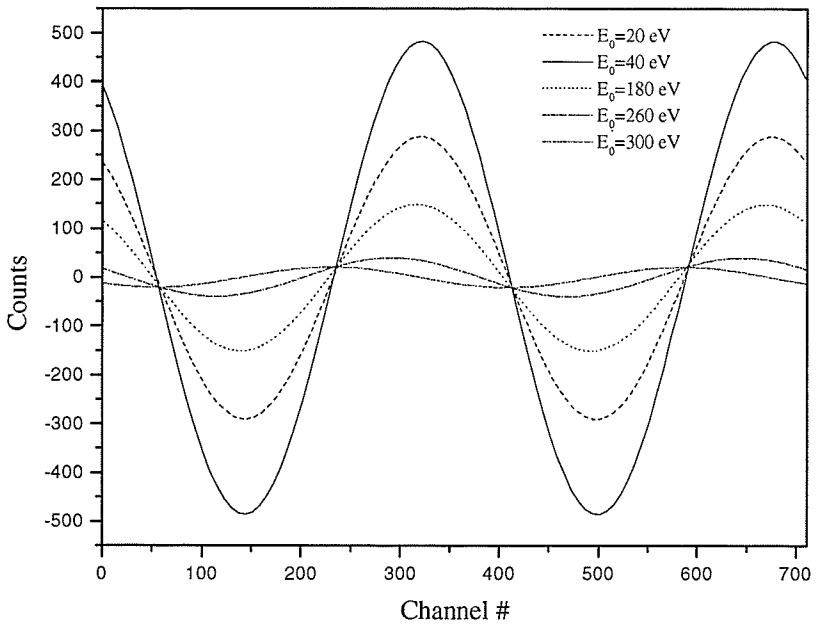

Figure 5.10: The phase shift caused by a sensitivity to linearly polarized light. The phase shift is only dependent on the energy of the incident electrons.

effect (Hanle1924). The density matrix description of the Hanle effect can be found in Blum (Blum1981). The effect of an electric field on an atom is to force alignment of the charge cloud with the electric field to minimize the system's energy.

Electric fields can be easily shielded from the interaction region by a simple metal cage with a fixed potential. Generally it is harder to shield out magnetic fields. The normal method of shielding a region is to surround it with a substance of high permeability. The magnetic field energy is minimized if the field flows through the substance, therefore preventing field leakage into the interaction region. The alloy commonly used to shield out magnetic fields is called μ-metal and is manufactured by Advance Magnetics Inc.. To obtain an ideal μ-metal shield the alloy must be in one continuous piece and the effects of machining must be minimized by annealing the finished product. Due to the limited space in the vacuum chamber and a limited supply of μ-metal, the magnetic shielding for the apparatus was not in one continuous piece and it has therefore not been annealed. The magnetic field strength was minimized however, by de-Gaussing the apparatus with a large oscillating magnetic field produced by a set of Helmholzt coils before each experiment. Three sets of Helmholtz coils, one set per orthogonal direction, were also built to actively minimize the magnetic fields present. The coils also allowed the dependence of the polarization on the applied field to be measured. No effects due to the applied field were detected and therefore, the de-polarization due to magnetic fields was not considered important.

The analysis of the electron impact excitation of the D-state has been carried out using the assumption that the electrons are the only mechanism for exciting the D-state. In reality the D-state can also be populated by decay from higher lying energy states which

are also excited by electron impact. A thorough analysis would require calculating the contributions to the D-state density matrix from all of the upper levels which can cascade down into it. This is impractical since we have yet to characterize completely the D-state density matrix, and have acquired even less information about the more energetic states. An estimate of the cascade intensity can be made with the available data. Heddle and Gallagher (Heddle1989) have presented a method for empirically determining the cascade contribution to a state if the cascade contributions are known for some of the lower level transitions. The method is unsuitable for the current problem though since there are not enough data to fit a non-linear curve. The cross sections for the higher quantum number states decrease rapidly and it can therefore be assumed that a good approximation to the cascade intensity can be found by analyzing only the contributions from the two closest P-states. The energy level diagram for the transitions is shown in Figure 5.11. The 1s4p and 1s5p states can be populated directly from the ground state or from the metastable 1s2s state. The scattering cross sections are available for both the 1s4p and 1s5p states. The cross sections for the states at an impact energy of 100 eV and the radiative transition probabilities are given in Table 5.1.

Table 5.1: The total cross sections of helium (measured at 100 eV) and the radiative transition probabilities for the transitions which contribute to cascade population (Heddle1989, Wiese1969).

	λ (nm)	σ (10^{-20} cm^2)	$A_{i,j}$ (10^8 sec^{-1})
$1s^2$-1s4p	52.2	109	2.46
1s2s-1s4p	396.5	109	0.0717
$1s^2$-1s5p	51.6	56	1.28
1s2s-1s5p	361.4	56	0.0376
1s4p-1s4d	-	-	5.7×10^{-7}
1s5p-1s4d	-	-	0.00166

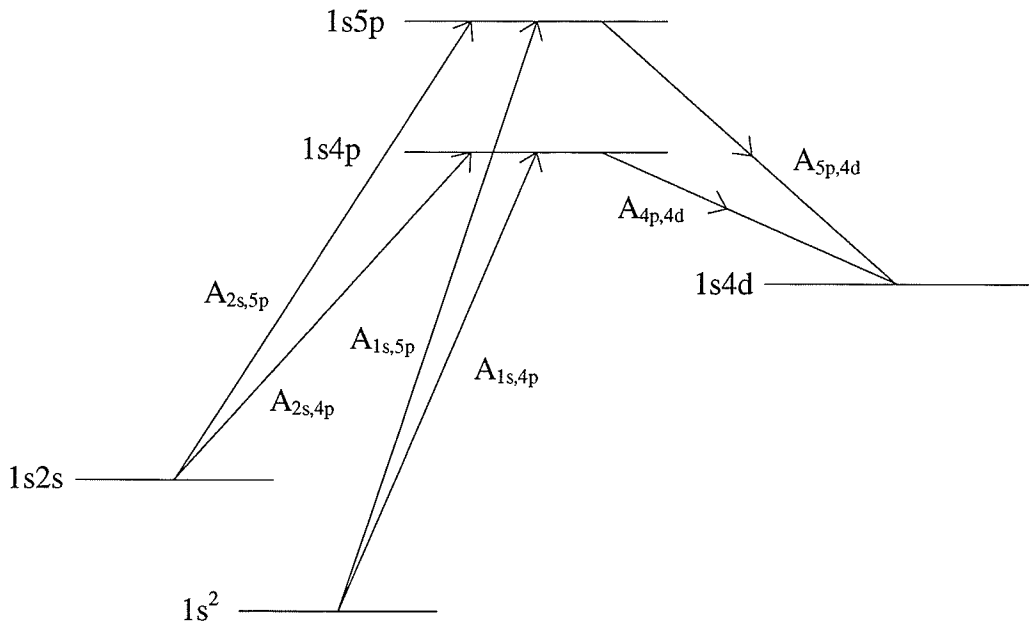

Figure 5.11: The energy level diagram for the cascade population of the 1s4d state. The radiative transition probabilities are also shown.

The cascade contribution is simply given by the proportion of the scattering cross section which feeds the 1s4d state. The proportion is determined by the ratio of the transition probabilities. A weighting factor must be applied to the terms which describe scattering out of the metastable 1s2s state since it is only populated by cascade from the higher lying states. Table 5.2 shows that the contribution from the 1s2s state will be small since the transition probabilities are much smaller than the $1s^2$ terms, and the metastable states will therefore be ignored. The cascade contribution is approximated as

$$\sigma_{cascade} = \sigma_{4p}\frac{A_{4p,4d}}{A_{1s,4p}} + \sigma_{5p}\frac{A_{5p,4d}}{A_{1s,5p}} \qquad (5.1.9)$$
$$= 0.073\times10^{-20}\ \mathrm{cm}^2\ ,$$

while the cross section for the 1s4d-1s2p transition at 100 eV is $9\text{x}10^{-20}$ cm^2 (Raan1989). The cascade population therefore contributes less than 1% to the excitation of the D-state, and the depolarization effects will be small.

The last potential cause for a depolarization of the emitted fluorescence is due to the re-absorption of the light by an atom, followed by its subsequent re-emission into a different solid angle and with a different polarization. The process, commonly called radiation trapping, is negligible for the D-P transition since a high population of the P-state is required to absorb the D-P radiation. The P-state is extremely short lived ($A_{1s,2p}$ = $17.99\text{x}10^8$ sec^{-1}) and therefore no significant population can be achieved to facilitate the radiation trapping. The pressure dependence of the polarization for the 492 nm transition was not observed with the current apparatus, and has been reported to be insignificant for the helium 492 nm transition by McFarland (McFarland1967). The process is important

for S-P transitions, since a large ground state population exists to trap resonance radiation.

5.2 3s4d-3s3p Transition in Magnesium

The 3s4d-3s3p transition in magnesium was measured in an analogous manner to the helium D-P transition. The major difference between the two measurements was the use of the oven to form a metal vapour beam. The oven normally operated at a temperature of 530°C which resulted in a background pressure of $3x10^{-6}$ Torr. The actual pressure inside the interaction region could not be measured. Since the ion gauge was not calibrated to measure magnesium, the background density was probably also a lot higher. The oven was maintained at the operating temperature by approximately 1.0 A of DC current. The black body radiation given off by the oven was detectable by the visible photon multiplier tube. Baffling inside the vacuum chamber was used to block the radiation, although some was still detected (Figure 5.12). The polarization of the radiation is presumably due to the many reflections off of metal surfaces that the light must have traversed before entering the PMT, in conjunction with a highly selective path. The data collection was carried out in an identical manner to the helium transition, though the energy scale covered was much smaller. The threshold energy for the ultra-violet transition is 4.35 eV, and the excitation function for the transition is given in Figure 5.13. The required energy shift is calculated to be 0.7±0.2 eV. The polarization of the emitted radiation as a function of energy is shown in Figure 5.14. No previous measurements of the polarization have been reported. The shape of the curve is similar to the helium transition though near threshold the behaviours differ. A minimum near the threshold is

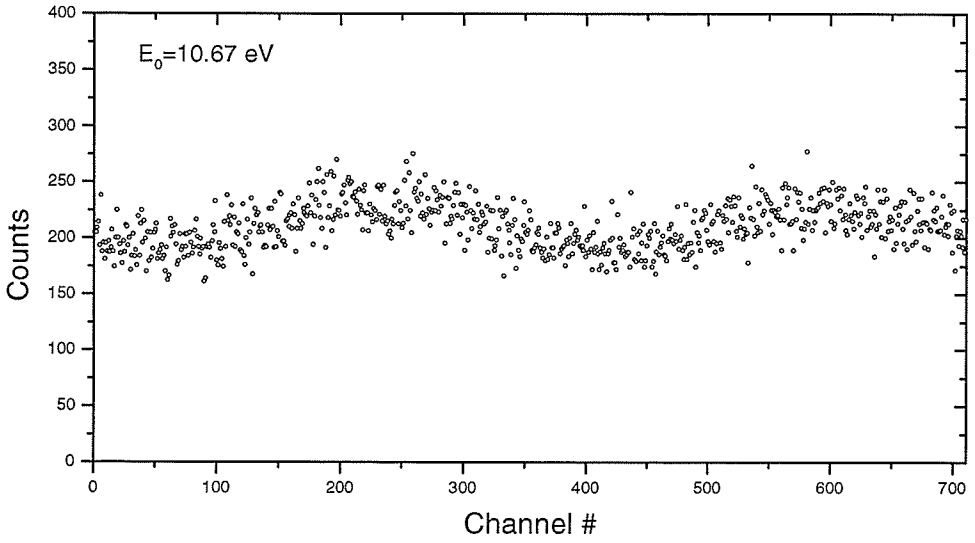

Figure 5.12: Polarized background signal attributed to the magnesium oven

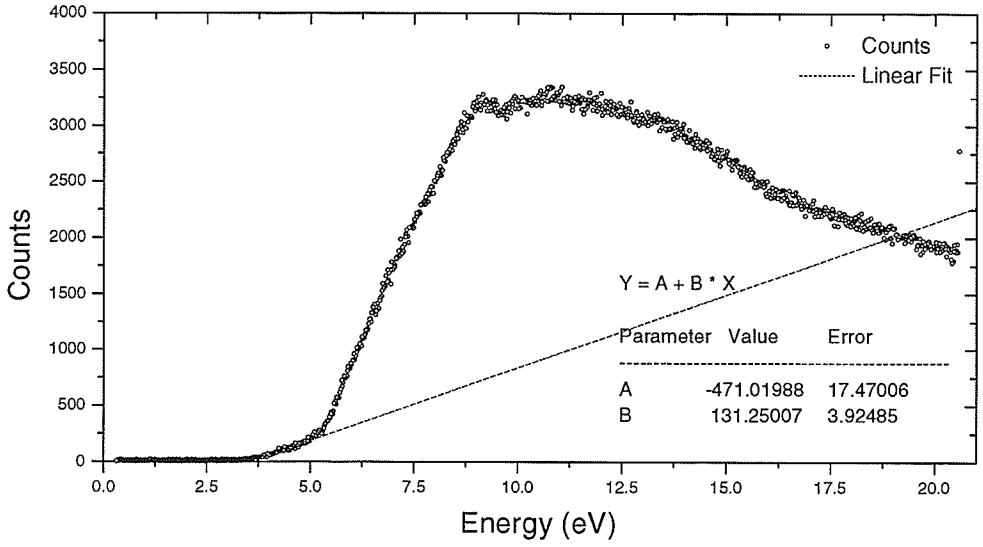

Figure 5.13: The excitation function for the ultra-violet $3s3p\text{-}3s^2$ singlet-singlet transition in magnesium. The results of the linear fit are given in the right-hand corner of the graph.

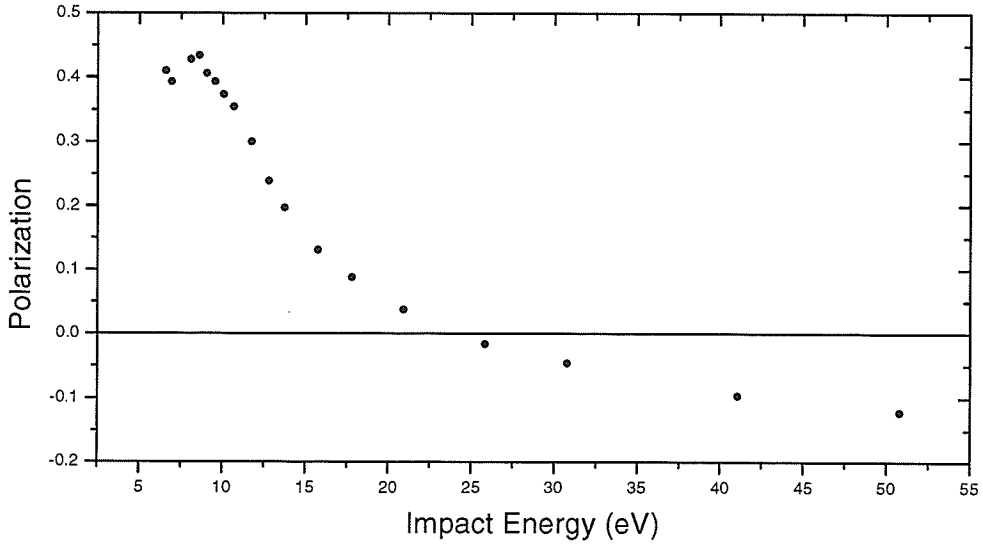

Figure 5.14: The measured polarization curve for the 552.8 nm 3s4d-3s3p singlet-singlet transition in magnesium

suggested by the data but the energy resolution of the electron gun is not adequate to resolve any structure.

5.2.1 Analysis of Depolarization Effects on the 3s4d-3s3p Transition in Magnesium

Of the four depolarization mechanisms discussed in section 5.1.1, only one needs to be re-addressed. The cascade contribution to the D-state must be re-evaluated for the 3s4d-3s3p magnesium transition. However, no data has been reported which would enable an analysis of the cascade contribution. The best estimate for the cascade contribution is therefore the previously calculated cascade population results for the helium D-P transition discussed in section 5.1.1.

5.3 Photon-Photon Coincidence Measurements

At the time of writing, a successful coincidence measurement had not been made. The general setup of the apparatus used to attempt the measurements has been discussed previously in Chapter 4. The coincidence measurement required finding the polarization of the D-P transition in coincidence with the P-S transition. Attention was focused on the magnesium photon-photon coincidence measurement due to the favourable total cross sections of the D-state. A simple calculation can be made to determine an expected rate of coincidence. Using the notation in Figure 2.4, the detected rate of emission from the D state is

$$\dot{N}_k = \sigma_2 \frac{nl_k i}{e} \kappa_k \frac{\Delta\Omega_k}{4\pi}, \qquad (1.1)$$

where

- σ_2 = total scattering cross section for level 2

l_k = length of the interaction region seen by the visible photon detector

$\Delta\Omega_k$ = solid angle of the visible photon detector

κ_k = quantum efficiency of the visible photon detector

n = atom beam density

i = electron beam current.

A similar expression can be written for the P-S transition

$$\dot{N}_n = (\sigma_1 + \sigma_2)\frac{nl_n i}{e}\kappa_n \frac{\Delta\Omega_n}{4\pi}, \tag{1.2}$$

which includes the cascade contribution from the D-state, assuming that the D-state cannot decay via a different transition. The coincidence rate is simply the portion of the D-P transition which is also detected by the ultra-violet detector or

$$\dot{N}_{coinc} = \sigma_2 \frac{nl_k i}{e}\kappa_n \frac{\Delta\Omega_n}{4\pi}\kappa_k \frac{\Delta\Omega_k}{4\pi}. \tag{1.3}$$

The coincidence rate can be rewritten in terms of the D-P photon count rate as

$$\dot{N}_{coinc} = \dot{N}_k \kappa_n \frac{\Delta\Omega_n}{4\pi}, \tag{1.4}$$

and an approximate value for the coincidence rate can be determined if the solid angle and quantum efficiency of the ultra-violet detector are known. The count rate of the visible photons has already been determined from the P-D polarization measurements. The solid angle seen by the UV detector is approximately 0.0013 sr, and according to the Hamamatsu catalogue, the quantum efficiency of the PMT is 10% (Hamamatsu1997). For a visible count rate of 1 KHz the coincidence signal should therefore be roughly 0.01 Hz, or 360 counts every ten hours. The background signal accumulated over a ten hour

period is of the same order of magnitude as the coincidence signal. This suggests that sufficient coincidence signal is present to resolve a coincidence peak in under 24 hours.

To check the timing of the visible and ultra-violet photon signals, a de-excitation timing curve was generated for each signal. The electron gun was repeatedly switched on and off , and the signal which switched the electron gun off also triggered the stop pulse on the time to height pulse converter. The start pulse to the time to height pulse converter was supplied by a delay generator fed by one of the photon detectors. The procedure is clarified in Figure 5.15. The switching of the electron gun at a frequency of 20 KHz was accomplished with the background switching circuit described in section 4.3. The timing diagrams for the visible and ultra-violet photons are shown in Figure 5.16. Ideally, the two graphs would have the same shape and be offset by the life time of the D-state or 0.7 ns. However, the two curves are offset by more than 20 μs and their shapes are not identical. The different profiles of the graphs were due to a misalignment of the ultra-violet detector. When the UV detector was aligned, the UV data profile mirrored the visible photon timing curve in Figure 5.15. The cause of the timing difference between the two signals has yet to be established.

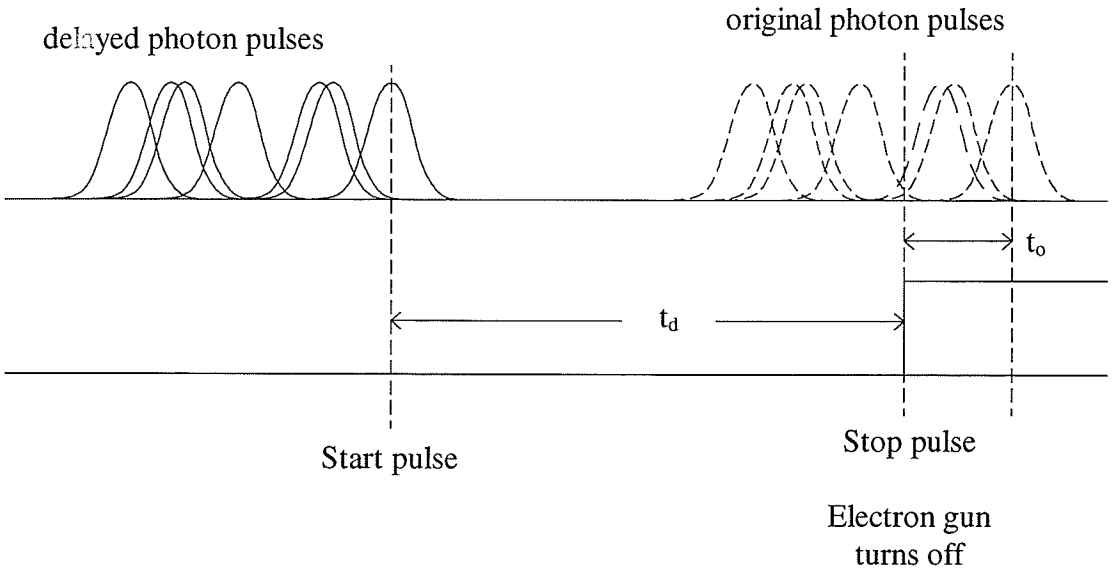

Figure 5.15: The timing procedure used to measure the timing curves of the photon transitions. The delayed pulses from a photon detector are used to start the timer. The stop pulse is supplied when the electron gun turns off. The original timing, t_o, is represented by the delayed time, t_d.

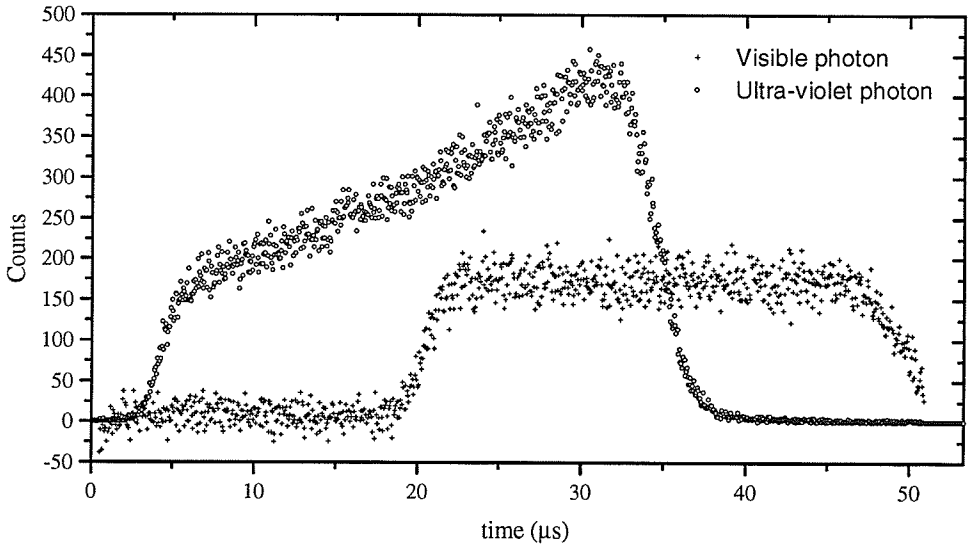

Figure 5.16: The timing curves for the visible and ultra-violet transitions of Mg. The shapes of the above curves should be the same, and the timing difference should be less than 1 ns. The difference in shape was caused by a misalignment of the ultra-violet detector.

Chapter 6 Summary

The measurement of polarized fluorescence emitted from electron impact excited atoms provides information on the relative populations of the magnetic sublevels for the excited atomic state. An overview of the theory required to describe the time evolution of excited atoms has been presented and has been used to calculate the contributions of the integrated scattering cross sections of the magnetic sublevels to the measured polarization. Three separate cases have been analyzed: the 1s4d-1s2p-$1s^2$ cascade transition in helium; the 3s4d-3s3p-$3s^2$ cascade transition in magnesium that required the inclusion of hyperfine splitting effects; the D-P transition as a result of electron scattering off of a laser excited P-state.

The first case, the 1s4d-1s2p-$1s^2$ cascade transition in helium, has been previously analyzed by Mikosza (Mikosza1996) and his results agree with the calculations in this work. The corresponding transition in magnesium, 3s4d-3s3p-$3s^2$, has also been analyzed in this work for all naturally occurring isotopes. The affects of the hyperfine splitting on the magnesium cascade transition did not result in a depolarization of the emitted fluorescence. However, the polarizations of the D-P and P-S transitions were affected by the hyperfine structure.

I have also shown that the laser excitation of a P-state removes the axial symmetry for a collision process in which the scattering plane has not been defined. The loss of axial symmetry resulted in the contribution of off-diagonal atomic density matrix elements to the calculated polarization. These results provide the background theory for a set of new

experiments which can be used to probe the scattering cross sections for excitation off of an excited atomic state.

The measurement of the polarization of the D-P transition, and the polarization of the D-P transition in coincidence with the P-S transition was shown to be sufficient to obtain relative measurements of the integrated scattering cross sections. The apparatus required to conduct the D-P-S cascade measurements has been constructed, and preliminary diagnostic testing of the apparatus, to ensure accurate polarization measurements, has been completed for the 1s4d-1s2p transition in helium. The measured polarization for the helium transition agreed with the previous measurements of Raan *et al.* (Raan1970). The polarization of the 3s4d-3s3p spectral line for magnesium was also measured. This measurement is the first of two measurements required to calculate the integrated scattering cross sections for the D-state of magnesium. The D-P-S coincidence measurement has yet to be realized. Initial diagnostic work has revealed a timing problem in the apparatus. Further diagnostic work is required before a photon-photon coincidence measurement can be made.

References

(Bartschat1981) K. Bartschat, K. Blum, G.F. Hanne, and J. Kessler, *J. Phys B: At. Mol. Phys.* **14**, 3761 (1981).

(Blum1981) K. Blum, *Density Matrix Theory and Applications* (Plenum, New York, 1981)

(Canfield1987) L.R. Canfield, and N. Swanson, *J. Res. Nat. Bureau Standards* **92**, 97 (1987).

(Chutjian1979) A. Chutjian, *Rev. Sci. Instrum.* **50**, 347 (1979).

(Clout1971) P.N. Clout, M.A. Haque, and D.W.O. Heddle, *J. Phys. E* **4**, 393 (1971).

(DiChio1974) D. DiChio, S.V. Natali, C.E. Kuyatt, and A. Galejs, *Rev. Sci. Instrum.* 45, 566 (1974).

(Fano1973) U. Fano, and J. Macek, *Rev. Mod. Phys.* **45**, 553 (1973).

(Haidt1965) D. Haidt, H. Kleinpoppen, and H. Kruger, *Proceedings of the Fourth International conference on the Physics of Electronic and Atomic Collisions*, Quebec, Canada, 1965 (Science Bookcrafters, New York, 1965).

(Hamamatsu1997) 1997 PMT Catalogue, Hamamatsu Inc.

(Hanle1924) W. Hanle, *Z. Phys.* **30**, 93 (1924).

(Heath1986) R.L. Heath, *CRC Handbook of Chemistry and Physics 67th Ed.*, R.C. Weast-*editor* (CRC Press, Florida, 1986), B-219.

(Heck1986) E.L. Heck and J.P. Gauntlett, *J. Phys. B: At. Mol. Phys.* **19**, 3633 (1986).

(Heitler1944) W. Heitler, *The Quantum Theory of Radiation: Second Ed.* (Oxford Press, London, 1944).

(Kazantsev1988) S.A. Kazantsev, N.Ya. Polynovskaya, L.N. Pyatnitskii, and S.A. Edel'man, *Sov. Phys. Usp.* **31**, 785 (1988).

(King1972) G.C.M. King, A. Adam, and F.H. Read, *J. Phys. B* **11**, L254 (1972).

(Klein1986) M.V. Klein, and T.E. Furtak, Optics: Second Ed. (John Wiley, New York, 1986).

(Li) Private correspondence.

(Li1996) Y. Li, 1996, Ph.D. thesis (University of Manitoba).

(Loudon1983) R. Loudon, *The Quantum Theory of Light: Second Ed.* (Clarendon Press, Oxford, 1983)

(Macek1974) J. Macek and I.V. Hertel, *J. Phys. B: At. Mol. Phys.* **7,** 2173 (1974).

(McFarland1964) R.H. McFarland, *Phys. Rev.* **133**, A986 (1964).

(McFarland1967) R.H. McFarland, *Phys. Rev.* **156**, 55 (1967).

(Mikosza1996) A.G. Mikosza, R. Hippler, J.B. Wang, and J.F. Williams, *Phys. Rev. A* **53**, 3287 (1996)

(Mizushima1970) M. Mizushima, *Quantum Mechanics of Atomic Spectra and Atomic Structure* (W.A. Benjamin, New York, 1970)

(Oppenheimer1927) J.R. Oppenheimer, *Z. Phys.* **43**, 27 (1927).

(Penney1932) W.G. Penney, *Proc. Nat. Acad. Sci.* **18**, (1932) 231

(Percival1958) L.C. Percival and M.J. Seaton, *Philos. Trans. R. Soc. London* **A251**, 113 (1958).

(Raan1970) A.F.J. Van Raan, J.P. De Jongh, J. Van Eck, and H.G.M. Heideman, *Physica* **53**, 45 (1970).

(Sakurai1994) J.J. Sakurai, *Modern Quantum Mechanics: Revised Ed.* (Addison-Wesley, New York, 1994)

(Taylor1972) J.R. Taylor, *Scattering Theory* (John Wiley, New York, 1972).

(Wang1992) J.B. Wang and J.F. Williams, *Comp. Phys. Com.* **75**, 275 (1993).

(Wang1995) J.B. Wang, J.F. Williams, A.T. Stelbovics, J.E. Furst, and D.H. Madison, *Phys. Rev. A* **52**, 2885 (1995).

(Wiese1966) W.L. Wiese, M.W. Smith, and B.M. Glennan, *Atomic Transition Probabilities Volume I: Hydrogen Through Neon* (National Bureau of Standards, Washington, 1966).

(Wiese1969) W.L. Wiese, M.W. Smith, and B.M. Miles, *Atomic Transition Probabilities Volume II: Sodium Through Calcium* (National Bureau of Standards, Washington, 1969).

(Zare1988) R.N. Zare, *Angular Momentum* (John Wiley, New York, 1988).

(Zetner1997) P.W. Zetner, S. Trajmar, S. Wang, I. Kanik, G. Csanak, R.E.H. Clark, J. Abdallah Jr., and J.C. Nickel, *J. Phys. B: At. Mol. Phys.* **30**, 5317 (1997).

Appendix 1 Mathematica™ Programs

Photon-Photon Coincidence Measurements for Helium

```
Off[ClebschGordan::phy]          /Turns off annoying messages/
Off[ClebschGordan::tri]

ifct[x_] := If[x ≥ 0, 1/(x!),0]

/Rotation matrix for a rotation about the y-axis by an angle θ, see Blum (Blum1981)/
d[j_,mp_,m_,θ_]:= d[j,mp,m,θ] = Sum[(-1)^(j-mp-k)((j+m)!(j-m)!(j+mp)!(j-mp)!)^(1/2)
      ifct[j-m-k] ifct[j-k-mp] ifct[m+mp+k] ifct[k]  Cos[θ/2]^(2k+m+mp)
      Sin[θ/2]^(2j-2k-m-mp), {k, 0, j+Abs[m]+Abs[mp]}]

/Rotation matrix for a general rotation defined by the Euler angles (γ,β,α)/
rot[j_,mp_,m_,γ_,β_,α_] := (Cos[mp γ]+I Sin[mp γ])d[j,mp,m,β](Cos[m α]+
      I Sin[m α])

/Conjugate of the rotation matrix/
Crot[j_,mp_,m_,γ_,β_,α_] := (Cos[mp γ]-I Sin[mp γ])d[j,mp,m,β]
      (Cos[m α]-I Sin[m α])

/Dipole operator matrix element/
DipoleElement[ja_,ma_,n_,jb_,mb_] := (-1)^(ja-ma) ThreeJSymbol[{ja,ma},{jb,-mb},
      {1,-n}]

/Irreducible tensor matrix element/
TensorElement[ja_,ma_,K_,Q_,jb_,mb_] := (-1)^(ja-ma) (2K+1)^(1/2)
      ThreeJSymbol[{ja,ma},{jb,-mb},{K,-Q}]

/Conjugate of the irreducible tensor matrix element/
TensorElementC[ja_,ma_,K_,Q_,jb_,mb_] := (-1)^(jb-mb) (2K+1)^(1/2)
      ThreeJSymbol[{jb,mb},{ja,-ma},{K,-Q}]

/Following equations are equivalent to equations (3.1.2),(3.1.3), and (3.1.4)/
DStateDensity[m2p_,m2_,θ_,φ_] := DStateDensity[m2p,m2,θ,φ] =
      Sum[If[EvenQ[K], TensorElementC[2,m,K,0,2,m]
      TensorElement[2,m2p,K,Q,2,m2] σ[Abs[m]] rot[K,Q,0,0, θ,φ],
      {m,-2,2}, {K,0,4}, {Q,-K,K}]

PStateDensity[m1p_,m1_,k_,kp_,θk_,φk_] := Sum[DipoleElement[1,m1p,k,2,m2p]
      DStateDensity[m2p,m2,θk,φk] DipoleElement[2,m2,-kp,1,m1],{m2p,-2,2},
      {m2,-2,2}]
```

```
/Following equations are equivalent to equation (3.1.12)/
PStateMulti[K_,Q_,k_,kp_,θk_,φk_] := Sum[TensorElementC[1,m1,K,Q,1,m1p]
        PStateDensity[m1p,m1,k,kp,θk,φk],{m1,-1,1},{m1p,-1,1}]

RotPStateMulti[K_,Q_,k_,kp_,θk_,φk_,θn_,φn_] :=
        Sum[PStateMulti[K,qk,k,kp,θk,φk] Crot[K,qk,ql,0,θk,φk]
        rot[K,Q,ql,0,θn,φn],{qk,-K,K},{ql,-K,K}]

/Following equations are equivalent to equation (3.1.13)/
RotPStateDensity[m1p_,m1_,k_,kp_,θk_,φk_,θn_,φn_] :=
        Sum[RotPStateMulti[K,Q,k,kp,θk,φk,θn,φn]
        TensorElement[1,m1p,K,Q,1,m1],{K,0,2},{Q,-K,K}]

SStateDensity[k_,kp_,θk_,φk_,n_,np_,θn_,φn_] :=  Sum[DipoleElement[0,0,n,1,m1p]
        RotPStateDensity[m1p,m1,k,kp,θk,φk,θn,φn]
        DipoleElement[1,m1,-np,0,0],{m1p,-1,1},{m1,-1,1}]

/Equivalent to equation (3.1.4)/
SStateMeasureable[k_,kp_,θk_,φk_,θn_,φn_] :=
        Sum[SStateDensity[k,kp,θk,φk,n,n,θn,φn], {n,-1,1,2}]

/To calculate the polarization density matrix for a D-P-S cascade transition with the D-P
detector at (θk,φk), and the P-S detector at (θn,φk+Δ)/
p = Table [SStateMeasureable[k,kp,θk,φk,θn,φk+Δ],{k,-1,1,2}, {kp,-1,1,2}]

/The Stokes parameters are/
Simplify[(-p[[1,-1]]-p[[-1,1]])/(p[[1,1]]+p[[-1,-1]])]
Simplify[(p[[1,1]]-p[[-1,-1]])/(p[[1,1]]+p[[-1,-1]])]
Simplify[I(-p[[1,-1]]+p[[-1,1]])/(p[[1,1]]+p[[-1,-1]])]

/To calculate the polarization density matrix for a D-P transition with the detector at
(θk,φk)/
PStatePhoton[k_,kp_,θk_,φk_] := Sum[PStateDensity[m1,m1,k,kp,θk,φk], {m1,-1,1}]

p1 = Table [PStatePhoton[k,kp,θk,φk], {k,-1,1,2}, {kp,-1,1,2}]

/The Stokes parameters are/
Simplify[(-p1[[1,-1]]-p1[[-1,1]])/(p1[[1,1]]+p1[[-1,-1]])]
Simplify[(p1[[1,1]]-p1[[-1,-1]])/(p1[[1,1]]+p1[[-1,-1]])]
Simplify[I(-p1[[1,-1]]+p1[[-1,1]])/(p1[[1,1]]+p1[[-1,-1]])]
```

Electron Scattering off of Laser Excited P-States

```
Off[ClebschGordan::phy]
Off[ClebschGordan::tri]

ifct[x_] := If[x ≥ 0, 1/(x!),0]

/Rotation matrix for a rotation about the y-axis by an angle θ/
d[j_,mp_,m_,θ_]:= d[j,mp,m,θ] = Sum[(-1)^(j-mp-k)((j+m)!(j-m)!(j+mp)!
        (j-mp)!)^(1/2) ifct[j-m-k] ifct[j-k-mp] ifct[m+mp+k] ifct[k]  Cos[θ/2]^(2k+m+mp)
        Sin[θ/2]^(2j-2k-m-mp), {k,0,j+Abs[m]+Abs[mp]}]

/Rotation matrix for a general rotation defined by the Euler angles (γ,β,α)/
rot[j_,mp_,m_,γ_,β_,α_] := (Cos[mp γ]+I Sin[mp γ])d[j,mp,m,β]
        (Cos[m α]+I Sin[m α])

/Conjugate of the rotation matrix/
Crot[j_,mp_,m_,γ_,β_,α_] := (Cos[mp γ]-I Sin[mp γ])d[j,mp,m,β]
        (Cos[m α]-I Sin[m α])

/Dipole operator matrix element/
DipoleElement[ja_,ma_,n_,jb_,mb_] := (-1)^(ja-ma) ThreeJSymbol[{ja,ma},{jb,-mb},
        {1,-n}]

/Irreducible tensor matrix element/
TensorElement[ja_,ma_,K_,Q_,jb_,mb_] := (-1)^(ja-ma) (2K+1)^(1/2)
        ThreeJSymbol[{ja,ma},{jb,-mb},{K,-Q}]

/Conjugate of the irreducible tensor matrix element/
TensorElementC[ja_,ma_,K_,Q_,jb_,mb_] := (-1)^(jb-mb) (2K+1)^(1/2)
        ThreeJSymbol[{jb,mb},{ja,-ma},{K,-Q}]

/purely polarized photon, equivalent to equation (2.2.16)/
A[1,1][β_,δ_] := (1 + Sin(2β)Sin(δ))/2
A[-1,1][β_,δ_] := (-Cos(2β) - I Sin(2β)Cos(δ))/2
A[1,-1][β_,δ_] := (-Cos(2β) + I Sin(2β)Cos(δ))/2
A[-1,-1][β_,δ_] := (1 - Sin(2β)Sin(δ))/2

/Equivalent to equation (3.3.7)/
PStateMulti[K_,Q_,β_,δ_] := PStateMulti[K,Q,β,δ] = Sum[(A[λ,λp][ β,δ]
        TensorElement[1, λ,K,-Q,1,- λp] DipoleElement[1, λ,λ,0,0]
        DipoleElement[1, λp, λp,0,0]], {λ,-1,1,2}, {λp,-1,1,2}]
```

```
/Equivalent to equation (3.3.9)/
RotPStateMulti[K_,Q_,θ_,φ_,β_,δ_] := Sum[PStateMulti[K,Qp, β,δ]
        Crot[K,Qp,Q,0, θ,φ], {Qp,-K,K}]

/Equivalent to equation (3.3.10)/
LaserPStateDensity[θ_,φ_,β_,δ_] :=  Table[Simplify[Sum[RotPStateMulti[K,Q, θ,φ,β,δ]
        TensorElement[1,m1,K,Q,1,m1p], {K,0,2}, {Q,-K,K}]], {m1,-1,1}, {m1p,-1,1}]

/Equivalent to equation (3.3.14)/
DStateDensity[m2p_,m2_,θ_,φ_,β_,δ_] := Sum[If[EvenQ[K+Q],
        RotPStateMulti[K,Q, θ,φ,β,δ] Sum[If[Abs[m+Q] ≤ 1,
        TensorElement[1,m+Q,K,Q,1,m] f[m2p,m+Q] Conj[f[m2,m]],0],
        {m,-1,1}], 0], {K,0,3}, {Q,-K,K}]

/Following equations are equivalent to equation (3.3.17)/
DStateMulti[K_,Q_,θ_,φ_,β_,δ_] := Sum[If[Abs[m2+Q] ≤ 2,
        DStateDensity[m2+Q,m2, θ,φ,β,δ]    TensorElementC[2,m2,K,Q,2,m2+Q],0],
        {m2, -2, 2}]

RotDStateMulti[K_,Q_,θk_,φk_,θp_,φp_,β_,δ_] :=
        Sum[DStateMulti[K,q,θp,φp,β,δ] rot[K,Q,q,0,θk,φk], {q,-K,K}]

RotDStateDensity[m2p_,m2_,θk_,φk_,θp_,φp_,β_,δ_] := Sum[If[Abs[m2-m2p] ≤
        K, TensorElement[2,m2p,K,m2p-m2,2,m2]
        RotDStateMulti[K,m2p-m2,θk,φk,θp,φp,β,δ], 0], {K,0,4}]

PStateDensity[m1p_,m1_,k_,kp_,θk_,φk_,θp_,φp_,β_,δ_] := If[Abs[m1p-k] ≤ 2,
        If[Abs[m1-kp] ≤ 2, DipoleElement[1,m1p,k,2,m1p-k]
        RotDStateDensity[m1p-k,m1-kp,θk,φk,θp,φp,β,δ]
        DipoleElement[2,m1-kp,-kp,1,m1],0],0]

/Equivalent to equation (3.3.19)/
PhotonDensity[k_,kp_,θk_,φk_,θp_,φp_,β_,δ_] :=
        Sum[PStateDensity[m1,m1,k,kp,θk,φk,θp,φp,β,δ], {m1, -1, 1}]

/To calculate the polarization density matrix elements for a system with a laser at (θp,φp)
and polarization defined by (β,δ), and a detector at (θk,φp+Δ)/

p = Table [Integrate[PhotonDensity[k,kp,θk,φp+Δ,θp,φp,β,δ],
        {φp, -π, π}], {k,-1,1,2}, {kp,-1,1,2}]

/The Stokes parameters are/

Simplify[(-p[[1,-1]]-p[[-1,1]])/(p[[1,1]]+p[[-1,-1]])]
```

```
Simplify[(p[[1,1]]-p[[-1,-1]])/(p[[1,1]]+p[[-1,-1]])]
Simplify[I(-p[[1,-1]]+p[[-1,1]])/(p[[1,1]]+p[[-1,-1]])]
```

Appendix 2 Photon-Photon Coincidence Programs for Magnesium

Two different programs were created to calculate separately the polarization for the D-P transition in magnesium, and the polarization of the coincidence measurement, D-P-S, for magnesium. The programs use analytical forms of the rotation matrices, Clebsch-Gordan coefficients and the Wigner-6j symbols presented by Zare (Zare1988). Note that there is a mistake in the analytical form of the Clebsch-Gordan coefficient printed in Zare, and the equation has been corrected for the programs.

Polarization of the D-P Transition in Magnesium

```
#include<math.h>
#include<stdlib.h>
#include<stdio.h>
#define PI 3.141592654
/*********************************************/

int ftoi(double num)
{
int i;

i = floor(num);

if (abs(num-i) > 0.5)
        i++;

return i;
};

/*********************************************/

double f(double num)

{
double answer=1.0;
```

```
int i;

i=ftoi(num);

if (i < 0)
        return 0.0;
else if (i <= 1)
        return 1.0;
else
    {
    while (i > 1)
        {
        answer=answer*i;
        i--;
        };
    return answer;
    };
};

/*******************************************/

double f_comb(double a, double b, double c)

{
return sqrt(f(a+b-c)*f(a-b+c)*f(-a+b+c)/f(a+b+c+1));
};

/*******************************************/

double threejs(double j1, double m1, double j2, double m2, double j3, double m3)

{
double answer,
     sum=0,
     tmp;

int k;

if (fabs(m1+m2+m3) <= 0.0001)
        {
        answer = pow(-1,ftoi(j1-j2-m3))*f_comb(j1,j2,j3)*sqrt(f(j1+m1)*f(j1-m1)*
                 f(j2+m2)*f(j2-m2)*f(j3+m3)*f(j3-m3));
        for (k=0;k<=(j1+j2+j3);k++)
                {
                tmp=f(j1+j2-j3-k)*f(j1-m1-k)*f(j2+m2-k)*
```

```
                f(j3-j2+m1+k)*f(j3-j1-m2+k)*f(k);
            if (fabs(tmp) >= 0.0001)
                sum+=pow(-1,k)/(tmp);
            };

        return answer*sum;
        }
else
        return 0;
};

/*******************************************/

double Rot(double j, double mp, double m, double theta)

{
double tmp,
    sum=0.0,
    answer;

int k;

answer = sqrt(f(j+m)*f(j-m)*f(j+mp)*f(j-mp));

for (k=0;k<=(fabs(m)+fabs(mp)+j);k++)
        {
        tmp = f(j-m-k)*f(j-k-mp)*f(m+mp+k)*f(k);

        if (fabs(tmp) >= 0.0001)
            sum += pow(-1,ftoi(j-mp-k))*pow(cos(theta/2),2*k+m+mp)*
                pow(sin(theta/2),2*j-2*k-m-mp)/tmp;
        };

return answer*sum;
};

/*******************************************/

double cg(double j1,double m1, double j2, double m2, double j3, double m3)

{
return pow(-1,ftoi(j1-j2+m3))*sqrt(2*j3+1)*threejs(j1,m1,j2,m2,j3,-m3);
};

/*******************************************/
```

```
double sixjs(double j1,double j2, double j3, double l1, double l2, double l3)

{
double tmp,
     sum=0;

int min,
   max,
   k;

min = -j1-j2-j3;
if (min > -j1-l2-l3)
        min = -j1-l2-l3;
if (min > -l1-j2-l3)
        min = -l1-j2-l3;
if (min > -l1-l2-j3)
        min = -l1-l2-j3;

max = j1+j2+l1+l2;
if (max < j2+j3+l2+l3)
        max = j2+j3+l2+l3;
if (max < (j3+j1+l3+l1))
        max = j3+j1+l3+l1;

for(k=abs(min);k<=max;k++)
        {
        tmp = f(k-j1-j2-j3)*f(k-j1-l2-l3)*f(k-l1-j2-l3)*f(k-l1-l2-j3)*
            f(j1+j2+l1+l2-k)*f(j2+j3+l2+l3-k)*f(j3+j1+l3+l1-k);
        if (fabs(tmp) >= 0.0001)
                sum+=pow(-1,k)*f(k+1)/tmp;
        };

sum *= f_comb(j1,j2,j3)*f_comb(j1,l2,l3)*f_comb(l1,j2,l3)*f_comb(l1,l2,j3);
return sum;
};

/*****************************************/

double DipoleElement(double fa, double ja, double ma, double n,
                     double fb, double jb, double mb, double i)

{
return pow(-1,ftoi(1+ja+i+fa+fb-ma))*sqrt((2*fa+1)*(2*fb+1))*threejs(fa,-ma,1,n,fb,mb)*
     sixjs(ja,fa,i,fb,jb,1);
```

```
};

/*******************************************/

double TensorElement(double ja, double ma, double k, double q,
                     double jb, double mb)

{
return pow(-1,ftoi(ja-ma))*sqrt(2*k+1)*threejs(ja,ma,jb,-mb,k,-q);
};

/*******************************************/

double TensorElementC(double ja, double ma, double k, double q,
                      double jb, double mb)

{
return pow(-1,ftoi(jb-mb))*sqrt(2*k+1)*threejs(jb,mb,ja,-ma,k,-q);
};

/*******************************************/

void main()

{
double  m2pp=-1,
      m2=-2,
      f1,
      ml2,
      mi2,
      f2,
      f2p,
      sum2=0;

int    K=0,
       n=1,
       np=-1,
       x=-1,
       xp=-1;

for(n=-1;n<=1;n+=2)
for(np=-1;np<=1;np+=2)
for(m2pp=-2;ftoi(m2pp)<=2;m2pp++) {
 for(K=0;K<=4;K+=2)
  if(abs(ftoi(np-n)) <= K)
```

```
  for(ml2=-2;ftoi(ml2)<=2;ml2++)
   for(mi2=-2.5;ftoi(mi2-0.5)<=2;mi2+=1.0)
    for(f1=1.5;ftoi(f1-0.5)<=3;f1+=1.0)
     for(f2=0.5;ftoi(f2-0.5)<=4;f2+=1.0)
      for(f2p=0.5;ftoi(f2p-0.5)<=4;f2p+=1.0)
       if (np+ml2+mi2 <= f1+0.1)
        if (np-n+ml2+mi2 <= f2+0.1)
         if (ml2+mi2 <= f2p+0.1)
          if (np-n+ml2 <= 2)
           sum2 += DipoleElement(f1,1,np+ml2+mi2,n,f2p,2,np-n+ml2+mi2,2.5)*
                   DipoleElement(f1,1,np+ml2+mi2,np,f2,2,ml2+mi2,2.5)*
                   cg(2,np-n+ml2,2.5,mi2,f2p,np-n+ml2+mi2)*
                   cg(2,ml2,2.5,mi2,f2,ml2+mi2)*
                   TensorElement(2,np-n+ml2,K,np-n,2,ml2)*
                   TensorElementC(2,m2pp,K,0,2,m2pp)*
                   Rot(K,np-n,0,PI/2.0);

 printf("\nn=%d np=%d m2=%f sum=%f \n",n,np,m2pp,sum2);
 sum2=0.0;
 };

};
```

Polarization of the Coincidence Measurement in Magnesium (D-P-S)

```
#include<math.h>
#include<stdlib.h>
#include<stdio.h>

#define PI 3.141592654

double f[31];

/*****************************************/

int ftoi(double num)

{
int i;

i = floor(num);

if (fabs(num-i) > 0.5)
        i++;
```

```
return i;
};

/*********************************************/

double factorial(double num)

{
double answer=1.0;

int i;

i=ftoi(num);

if (i < 0)
        return 0.0;
else if (i <= 1)
        return 1.0;
else
    {
    while (i > 1)
        {
        answer=answer*i;
        i--;
        };
    return answer;
    };
};

/*********************************************/

double f_comb(double a, double b, double c)

{
return sqrt(f[15+ftoi(a+b-c)]*f[15+ftoi(a-b+c)]*f[15+ftoi(-a+b+c)]/f[15+ftoi(a+b+c+1)]);
};

/*********************************************/

double threejs(double j1, double m1, double j2, double m2, double j3, double m3)

{
double answer,
     sum=0,
     tmp;
```

```
int k;

if (fabs(m1+m2+m3) <= 0.0001)
        {
        answer = pow(-1,ftoi(j1-j2-m3))*f_comb(j1,j2,j3)*sqrt(f[15+ftoi(j1+m1)]*
                 f[15+ftoi(j1-m1)]*f[15+ftoi(j2+m2)]*f[15+ftoi(j2-m2)]*
                 f[15+ftoi(j3+m3)]*
                 f[15+ftoi(j3-m3)]);
        for (k=0;k<=(j1+j2+j3);k++)
                 {
                 tmp=f[15+ftoi(j1+j2-j3-k)]*f[15+ftoi(j1-m1-k)]*f[15+ftoi(j2+m2-k)]*
                    f[15+ftoi(j3-j2+m1+k)]*f[15+ftoi(j3-j1-m2+k)]*f[15+k];
                 if (fabs(tmp) >= 0.0001)
                          sum+=pow(-1,k)/(tmp);
                 };

        return answer*sum;
        }
else
        return 0;
};

/*********************************************/

double Rot(double j, double mp, double m, double theta)

{
double tmp,
     sum=0.0,
     answer;

int k;

answer = sqrt(f[15+ftoi(j+m)]*f[15+ftoi(j-m)]*f[15+ftoi(j+mp)]*f[15+ftoi(j-mp)]);

for (k=0;k<=(fabs(m)+fabs(mp)+j);k++)
        {
        tmp = f[15+ftoi(j-m-k)]*f[15+ftoi(j-k-mp)]*f[15+ftoi(m+mp+k)]*f[15+k];

        if (fabs(tmp) >= 0.0001)
                 sum += pow(-1,ftoi(j-mp-k))*pow(cos(theta/2),2*k+m+mp)*
                          pow(sin(theta/2),2*j-2*k-m-mp)/tmp;
        };
```

```
return answer*sum;
};

/*********************************************/

double cg(double j1,double m1, double j2, double m2, double j3, double m3)

{
return pow(-1,ftoi(j1-j2+m3))*sqrt(2*j3+1)*threejs(j1,m1,j2,m2,j3,-m3);
};

/*********************************************/

double sixjs(double j1,double j2, double j3, double l1, double l2, double l3)

{
double tmp,
     sum=0,
     min,
     max;

int   k;

min = -j1-j2-j3;
if (min > -j1-l2-l3)
        min = -j1-l2-l3;
if (min > -l1-j2-l3)
        min = -l1-j2-l3;
if (min > -l1-l2-j3)
        min = -l1-l2-j3;

max = j1+j2+l1+l2;
if (max < j2+j3+l2+l3)
        max = j2+j3+l2+l3;
if (max < (j3+j1+l3+l1))
        max = j3+j1+l3+l1;

for(k=abs(ftoi(min));k<=ftoi(max);k++)
        {
        tmp = f[15+ftoi(k-j1-j2-j3)]*f[15+ftoi(k-j1-l2-l3)]*f[15+ftoi(k-l1-j2-l3)]*
            f[15+ftoi(k-l1-l2-j3)]*f[15+ftoi(j1+j2+l1+l2-k)]*
            f[15+ftoi(j2+j3+l2+l3-k)]*f[15+ftoi(j3+j1+l3+l1-k)];
        if (fabs(tmp) >= 0.0001)
                sum+=pow(-1,k)*f[15+k+1]/tmp;
        };
```

```
sum *= f_comb(j1,j2,j3)*f_comb(j1,l2,l3)*f_comb(l1,j2,l3)*f_comb(l1,l2,j3);
return sum;
};

/*********************************************/

double DipoleElement(double fa, double ja, double ma, double n,
                     double fb, double jb, double mb, double i)

{
return pow(-1,ftoi(1+ja+i+fa+fb-ma))*sqrt((2*fa+1)*(2*fb+1))*threejs(fa,-ma,1,n,fb,mb)*
    sixjs(ja,fa,i,fb,jb,1);
};

/*********************************************

double DipoleElement(double ja, double ma, double n,
                     double jb, double mb)

{
return pow(-1,ftoi(ja-ma))*threejs(ja,ma,jb,-mb,1,-n);
};

/*********************************************/

double TensorElement(double ja, double ma, double k, double q,
                     double jb, double mb)

{
return pow(-1,ftoi(ja-ma))*sqrt(2*k+1)*threejs(ja,ma,jb,-mb,k,-q);
};

/*********************************************/

double TensorElementC(double ja, double ma, double k, double q,
                      double jb, double mb)

{
return pow(-1,ftoi(jb-mb))*sqrt(2*k+1)*threejs(jb,mb,ja,-ma,k,-q);
};

/*********************************************/

void main()
```

```
{
FILE *data;

double m2pp=-2,
      f1,
      f1p,
      m1ppp,
      m1pp,
      mi2,
      mi0,
      f2,
      f2p,
      sum1=0,
      sum2=0,
      sum3=0,
      sum4=0,
      sum5=0;

int   K=0,
      k=0,
      qlab=0,
      n=1,
      np=1,
      x=1,
      xp=1;

for (k=-15;k<=15;k++)
          f[k+15] = factorial(k);

data=fopen("dpsmg.txt","w");

for(x=1;x>=-1;x-=2)
 for(np=1;np>=-1;np-=2)
  for(m2pp=0;ftoi(m2pp)<=2;m2pp++) {
   for(mi0=-2.5;ftoi(mi0-0.5)<=2;mi0+=1.0) {
    for(f1=1.5;ftoi(f1-0.5)<=3;f1+=1.0)
     if(ftoi(fabs(mi0-x)-0.5) <= ftoi(f1-0.5))
      for(f1p=1.5;ftoi(f1p-0.5)<=3;f1p+=1.0)
       if(ftoi(fabs(mi0-x)-0.5) <= ftoi(f1p-0.5)) {
        for(k=0;k<=ftoi(f1+f1p);k++)
         for(qlab=-k;qlab<=k;qlab++) {
           for(m1ppp=-f1;ftoi(m1ppp-0.5)<=ftoi(f1-0.5);m1ppp+=1.0)
            for(m1pp=-f1p;ftoi(m1pp-0.5)<=ftoi(f1p-0.5);m1pp+=1.0)
             if(ftoi(fabs(m1ppp-m1pp)) <= k)
```

```
            for(mi2=-2.5;ftoi(mi2-0.5)<=2;mi2+=1.0)
             if(ftoi(fabs(m1ppp-mi2-np))<=2)
              if(ftoi(fabs(m1pp-mi2-n))<=2) {
               for(f2=0.5;ftoi(f2-0.5)<=4;f2+=1.0)
                   if(ftoi(fabs(m1ppp-np)-0.5)<=ftoi(f2-0.5))
                    for(f2p=0.5;ftoi(f2p-0.5)<=4;f2p+=1.0)
                     if(ftoi(fabs(m1pp-n)-0.5)<=ftoi(f2p-0.5)) {
                      for(K=0;K<=4;K+=2)
                       if(abs(ftoi(m1pp-m1ppp-n+np))<=K)
                        sum5 += TensorElementC(2,m2pp,K,0,2,m2pp)*
                  TensorElement(2,m1pp-n-mi2,K,m1pp-m1ppp-    n+np,2,m1ppp-np-mi2)*
                  Rot(K,m1pp-m1ppp-n+np,0,PI/2.0);
                       sum4 += DipoleElement(f1p,1,m1pp,n,f2p,2,m1pp-n,2.5)*
                               DipoleElement(f1,1,m1ppp,np,f2,2,m1ppp-np,2.5)*
                               cg(2,m1pp-n-mi2,2.5,mi2,f2p,m1pp-n)*
                               cg(2,m1ppp-np-mi2,2.5,mi2,f2,m1ppp-np)*sum5;
                      sum5 = 0; };
                    sum3 += TensorElementC(f1,m1ppp,k,m1ppp-m1pp,f1p,m1pp)*
                        Rot(k,qlab,m1ppp-m1pp,PI/2)*sum4;
                    sum4 = 0; };
               sum2 += TensorElement(f1p,mi0-x,k,0,f1,mi0-x)*
                       Rot(k,0,qlab,PI/2)*pow(-1,ftoi(qlab))*sum3;
              sum3 = 0; };
             sum1 += DipoleElement(2.5,0,mi0,x,f1p,1,mi0-x,2.5)*
                  DipoleElement(2.5,0,mi0,x,f1,1,mi0-x,2.5)*sum2;
             sum2 = 0; };
               };*/
  fprintf(data,"\n %f %f %f",m2pp,mi0,sum1);
  fflush(data);
  };
 fprintf(data,"\nnp=%d n=%d xp=%d x=%d m2=%f sum=%f \n",np,n,x,x,m2pp,sum1);
 fflush(data);
 sum1=0.0;
 };

fclose(data);
};
```

Appendix 3 MCS Data Acquisition Program

The following program was written in Basic and compiled using Microsoft Quick Basic.

```
'program:  DATA_AQ.BAS
'date of last modification:  22-05-1998

DECLARE SUB set.bckgrnd (seg.bckgrnd%)
DECLARE SUB send.to.end (dwell%)
DECLARE SUB send.to.end.b (dwell%)
DECLARE SUB wave.gen (dwell%)
DECLARE SUB counter.set (num%)
DECLARE SUB count.b (num%, normalize!, max.num() AS LONG, old.num() AS INTEGER,
bin.width%)
DECLARE SUB count.a (num%, normalize!, max.num() AS LONG, old.num() AS INTEGER,
bin.width%)
DECLARE SUB count.m (num%, normalize!, max.num() AS LONG, old.num() AS INTEGER,
bin.width%)
DECLARE SUB get.mag (channel%, num&)
DECLARE SUB norm (normalize!, norm.num&)
DECLARE SUB display (normalize!, max.num() AS LONG, old.num() AS INTEGER, bin.width%)
DECLARE SUB rearrange (bin.num&, max.num() AS LONG)

DIM old.num(1 TO 600) AS INTEGER      'stores the vertical position of the data for display purposes
DIM max.num(1 TO 9) AS LONG           'keeps a record of the largest 9 numbers in the data

'address definitions and counter settings for the digital IO card
CONST cntr.cntrl = &H2A7              'address of clock control registers
CONST cntr.c1 = &H2A5                 'address of clock number 1
CONST cnt.cb1 = &H72
CONST cntr.cb1 = &H42
CONST wve.cb2 = &HB6
CONST clck.c2 = &H2A6                 'address of clock number 2
CONST ext.out = &H2A0                 'address of external output port #?
CONST int.out = &H2A2                 'address of internal output port #?
CONST int.in = &H2A2                  'address of internal input port #?
CONST clock = 25000

'determination of the code segments to be run according to specific function keys, or due to error trapping
KEY(1) ON
ON KEY(1) GOSUB stop.loop
KEY(2) ON
ON KEY(2) GOSUB stop.end
ON ERROR GOTO error.routine

'input the initialization data from the save file "data_aq.dat"
OPEN "data_aq.dat" FOR INPUT AS #1
INPUT #1, npass%, dwell%, mtr.period%, nchan%, file.name$
CLOSE #1
'npass%: total number of executions of the main loop
'dwell%:  default Divide by N
'mtr.period%:  number of stepper motor advances for one full revolution
```

```
'nchan%:  total number of MCS channels available
'file.name$:  string containing the location and name of the data file

'initialize the counters for a pulse train of zero length with frequency determined by dwell%
CALL wave.gen(dwell%)
CALL counter.set(0)

'rotate the polarizer until the optical switch is reached
CALL send.to.end(dwell%)

'initialize the graphics screen
SCREEN 2: CLS
LINE (0, 12)-(620, 195), , B                    'draws a box
LINE (0, 25)-(20, 25)                           'draws a reference line to indicate scaling
LOCATE 1, 5: PRINT "[F1=Stop][F2=Stop at End]"

'this segment of code calculates the total number of channels which will be viewed and determines the
'amount of binning which must take place to accommodate a screen width of 600 pixels.
chan% = 0
OPEN file.name$ FOR INPUT AS #1
DO
   INPUT #1, seg.chan%, seg.dwell%, seg.adv%, seg.mtr%, seg.bckgrnd%
   chan% = chan% + seg.chan%   'determines the total number of channels for the entire data file
LOOP UNTIL EOF(1)
CLOSE #1
bin.width% = INT(chan% / 600)                           'sets bin.width
least.bin% = chan% - bin.width% * 600                   'if the number of missed channels is less
IF least.bin% > 60 THEN bin.width% = bin.width% + 1     'than 10%, don't bother to increase the
                                                        'bin.width to accommodate.
FOR i = 1 TO 600                                        'initializes the vertical positions to zero
    old.num(i) = 0
    PSET (9 + i, 185)                                   'draws initial data
NEXT i
FOR i = 1 TO 9                                          'initializes max.num
    max.num(i) = i
NEXT i
normalize! = 1          'sets the normalization constant (ensures that the data is viewable)
pass% = 1               'sets the number of passes to be one

DO WHILE pass% <= npass%            'loop until the specified number of passes has occurred
    chan% = 0                       'start at the first channel

    LOCATE 3, 60: PRINT "# of Passes: "; pass%

    OUT ext.out, 1                  'send start pulse to mcs to start data acquisition
    OUT ext.out, 0

    OPEN file.name$ FOR INPUT AS #1

    DO                              'evaluate until the end of file is reached
        INPUT #1, seg.chan%, seg.dwell%, seg.adv%, seg.mtr%, seg.bckgrnd%
        'seg.chan%:  the current number of channels
        'seg.dwell%:  the current Divide by N
        'seg.adv%:  advances the MCS channels if TRUE (greater than zero)
```

```
        'seg.mtr%:  advances the motor if TRUE
        'seg.bckgrnd%:  electron gun off - TRUE; on - FALSE (zero)

        LOCATE 1, 35: PRINT "# of Channels:": LOCATE 1, 16: PRINT seg.chan%
        LOCATE 1, 60: PRINT "Background:"; seg.bckgrnd%

        CALL set.bckgrnd(seg.bckgrnd%)                  'turns the gun on or off
        CALL wave.gen(seg.dwell%)                       'sets the divide by N counter
        CALL counter.set(seg.chan%)                     'sets the length of the pulse train
        IF seg.adv% AND seg.mtr% THEN                   'both advance
            CALL count.b(seg.chan%, normalize!, max.num(), old.num(), bin.width%)
            chan% = chan% + seg.chan%
        ELSE
        IF seg.adv% AND seg.mtr% = 0 THEN               'MCS channels advance
            CALL count.a(seg.chan%, normalize!, max.num(), old.num(), bin.width%)
            chan% = chan% + seg.chan%
        ELSE
        IF seg.adv% = 0 AND seg.mtr% THEN               'motor advances
            CALL count.m(seg.chan%, normalize!, max.num(), old.num(), bin.width%)
        ELSE
            CALL send.to.end.b(seg.dwell%)              'if non of the above rotate until
        END IF                                          'the optical switch
        END IF
        END IF

    LOOP UNTIL EOF(1)
    CLOSE #1

    IF chan% < nchan% THEN                  'if the full number of MCS channels has not
        CALL wave.gen(2)                    'been used, quickly advance through them
        CALL count.a(nchan% - chan% + 15, normalize!, max.num(), old.num(), bin.width%)
    END IF

    pass% = pass% + 1
LOOP

END                             'end of main program

stop.loop:                      'immediately stops the program loop
    END
    RETURN

stop.end:
    pass% = npass% + 1          'prematurely sets the number of passes to be the maximum
    RETURN

error.routine:                  'on an error print the error code
    SCREEN 0: PRINT "Error"; ERR
    INPUT a
    END

'this sub-routine only advances the MCS channel
'num%:  the number of channels to advance
SUB count.a (num%, normalize!, max.num() AS LONG, old.num() AS INTEGER, bin.width%)
```

```
OUT cntr.cntrl, cnt.cb1                          'sets counter 1 to accept num%
OUT cntr.c1, num% - INT(num% / 256)              'formatting for num%
OUT cntr.c1, INT(num% / 256)

OUT int.out, &H44
OUT int.out, &H4C
OUT int.out, &H44
OUT int.out, &H54
OUT int.out, &H44
IF (INP(int.in) AND 2) = 2 THEN          'INP(int.in) AND 2 determines the state of the counter
    DO
        n = INP(int.in) AND 2
    LOOP UNTIL n = 0                     'waits for counter to start
    DO
        CALL display(normalize!, max.num(), old.num(), bin.width%)      'update viewing screen
        n = INP(int.in) AND 2
    LOOP UNTIL n = 2                     'waits for counter to finish
ELSE
    DO
        CALL display(normalize!, max.num(), old.num(), bin.width%)      'update viewing screen
        n = INP(int.in) AND 2
    LOOP UNTIL n = 2                     'waits for counter to finish, if it had already started
END IF

END SUB

'this sub-routine advances both the motor and the MCS concurrently
'num%:  the number of channels to advance
SUB count.b (num%, normalize!, max.num() AS LONG, old.num() AS INTEGER, bin.width%)

OUT cntr.cntrl, cnt.cb1
OUT cntr.c1, num% - INT(num% / 256)
OUT cntr.c1, INT(num% / 256)

OUT int.out, &H64
OUT int.out, &H6C
OUT int.out, &H64
OUT int.out, &H74
OUT int.out, &H64
IF (INP(int.in) AND 2) = 2 THEN
    DO
        n = INP(int.in) AND 2
    LOOP UNTIL n = 0                     'wait for counter to start
    DO
        CALL display(normalize!, max.num(), old.num(), bin.width%)
        n = INP(int.in) AND 2
    LOOP UNTIL n = 2                     'wait for counter to finish
ELSE
    DO
        CALL display(normalize!, max.num(), old.num(), bin.width%)
        n = INP(int.in) AND 2
    LOOP UNTIL n = 2
END IF
```

```
END SUB

'this sub-routine only advances the stepper motor
'num%:  the number of steps to advance
SUB count.m (num%, normalize!, max.num() AS LONG, old.num() AS INTEGER, bin.width%)

OUT cntr.cntrl, cnt.cb1
OUT cntr.c1, num% - INT(num% / 256)
OUT cntr.c1, INT(num% / 256)

OUT int.out, &H24
OUT int.out, &H2C
OUT int.out, &H24
OUT int.out, &H34
OUT int.out, &H24
IF (INP(int.in) AND 2) = 2 THEN
    DO
        n = INP(int.in) AND 2
    LOOP UNTIL n = 0                    'wait for counter to start
    DO
        CALL display(normalize!, max.num(), old.num(), bin.width%)
        n = INP(int.in) AND 2
    LOOP UNTIL n = 2                    'wait for counter to finish
ELSE
    DO
        CALL display(normalize!, max.num(), old.num(), bin.width%)
        n = INP(int.in) AND 2
    LOOP UNTIL n = 2
END IF

END SUB

'this sub-routine loads counter one with num% to set the length of the pulse train
SUB counter.set (num%)

num% = num% - 1

OUT cntr.cntrl, cnt.cb1                 'set counter 1 to  mode ?
OUT cntr.c1, num% - INT(num% / 256)
OUT cntr.c1, INT(num% / 256)

END SUB

'this sub-routine displays the data contained within the MCS
SUB display (normalize!, max.num() AS LONG, old.num() AS INTEGER, bin.width%)

num& = 0
channel% = 1

FOR i = 10 TO 609                       'step once through the entire display

   j = 0                                'j: bin width counter
   bin.num& = 0                         'bin.num&:  total counts per bin
```

```
    DO                                          'this loop bins the data according to bin.width%
        CALL get.mag(channel%, num&)
        bin.num& = bin.num& + num&
        channel% = channel% + 1
        j = j + 1
    LOOP UNTIL j >= bin.width%

    IF bin.num& > max.num(1) THEN               'if the number of counts in bin.num&
CALL rearrange(bin.num&, max.num())     'is greater than the ninth
                            highest count in max.num(), then
    END IF                                      'rearrange the list to include bin.num&

    bin.h% = CINT(bin.num& / normalize!)        'this segments converts bin.num& to
                                                'a position
    IF bin.h% <> old.num(i - 9) THEN            'on the screen.  An overall normalization factor
        IF 185 - old.num(i - 9) > 12 THEN       'is handled by normalize!
            PRESET (i, 185 - old.num(i - 9))
        END IF
        IF 185 - bin.h% > 12 THEN
            PSET (i, 185 - bin.h%)
        END IF
        old.num(i - 9) = bin.h%
    END IF
NEXT i

CALL norm(normalize!, max.num(1))               'recalculates the normalization factor wrt the ninth
                                                'highest number
END SUB

'this function retrieves the data from the MCS which is contained in channel% and places it in num&
SUB get.mag (channel%, num&) STATIC

DEF SEG = &HD000
num& = PEEK(4 * (channel% - 1) + 2) * 65536 + PEEK(4 * (channel% - 1) + 1) * 256& + PEEK(4 *
(channel% - 1))
DEF SEG

END SUB

'this function calculates the normalization factor according to the screen dimensions
SUB norm (normalize!, norm.num&)

IF (norm.num& / normalize!) >= 155 THEN
    normalize! = norm.num& / 80
    LOCATE 3, 3: PRINT 2 * norm.num&
ELSE
IF (norm.num& / normalize!) < 50 THEN
    normalize! = norm.num& / 80
    LOCATE 3, 3: PRINT 2 * norm.num&
END IF
END IF
IF normalize! < 1! THEN normalize! = 1

END SUB
```

```
'this function sorts the array max.num() and adds bin.num& into the appropriate cell.
'max.num() is sorted highest to lowest
SUB rearrange (bin.num&, max.num() AS LONG)

min.lim% = 1
max.lim% = 9
n% = 5

DO
    IF bin.num& >= max.num(n%) THEN
        min.lim% = n%
        stp% = INT((max.lim% - min.lim%) / 2)
        n% = n% + stp%
    ELSE
        max.lim% = n%
        stp% = INT((max.lim% - min.lim%) / 2)
        n% = n% - stp%
    END IF
LOOP UNTIL stp% = 0

IF bin.num& > max.num(9) THEN
    min.lim% = 9
ELSE
    IF bin.num& = max.num(min.lim%) OR bin.num& = max.num(min.lim% + 1) THEN
        min.lim% = 0
    END IF
END IF

FOR n% = 1 TO min.lim% - 1
    max.num(n%) = max.num(n% + 1)
NEXT n%
max.num(min.lim%) = bin.num&

END SUB

'rotates the polarizer until the photo-detector detects the start/end of the rotation
SUB send.to.end (dwell%)

OUT int.out, &H27                    'clck on/of = 1, mode1 = 1, mode2 = 0
OUT int.out, &H2F                    'toggle clock
OUT int.out, &H27
start! = TIMER
DO                                   'wait until at least 10
    finish! = TIMER                  'steps have been taken
LOOP UNTIL finish! - start! > dwell% * 15 / clock
OUT int.out, &H23                    'mode1 = 1

DO
    num = INP(int.in) AND 1
LOOP UNTIL num = 0                   'wait for clock on/off = 0

END SUB
```

```
'rotates the polarizer and advances the MCS until the photo-detector detects the start/end 'of the rotation
SUB send.to.end.b (dwell%)

OUT int.out, &H67                       'clck on/of = 1, mode1 = 1, mode2 = 0
OUT int.out, &H6F                       'toggle clock
OUT int.out, &H67
start! = TIMER
DO                                      'wait until at least 10
    finish! = TIMER                         'steps have been taken
LOOP UNTIL finish! - start! > dwell% * 15 / clock
OUT int.out, &H63                           'mode1 = 1

DO
    num = INP(int.in) AND 1
LOOP UNTIL num = 0                      'wait for clock on/off = 0

END SUB

'sets the background
SUB set.bckgrnd (seg.bckgrnd%)

OUT ext.out, 2 * seg.bckgrnd%

END SUB

'sets the frequency of the pulse train
SUB wave.gen (dwell%)

OUT cntr.cntrl, wve.cb2                 'set counter 2 to act as
OUT clck.c2, dwell% - INT(dwell% / 256)     'a wave-generator with
OUT clck.c2, INT(dwell% / 256)              'period .dwell.

END SUB
```

Appendix 4 PHA Data Acquisition Program

The following program was written in C, and compiled using Borland Turbo C V3.0. The program is split into two main sections. The first section describes the task of the Nucleus PHA, while the second section is a list of functions used to interface with the Nucleus PHA.

First section:

```
#include <stdio.h>
#include <dos.h>
#include <stdlib.h>

void init_pca(void);
void (*pcaptr)(void);
unsigned char get_byte(unsigned char f);
unsigned int get_2bytes(unsigned char f);
void get_bytes(unsigned char f, unsigned char *parameter);
void put_byte(unsigned char f, unsigned char parameter);
void put_3bcd(unsigned char f, unsigned int parameter);
void pca_func(unsigned char f);

unsigned int *pcasegptr = MK_FP(0, 0x3CA);
unsigned int *pcaoffsetptr = MK_FP(0, 0x3C8);
unsigned int pcaoffset,pcaseg;
unsigned int parmoffset, parmseg;
unsigned char *funptr;

#include "pca_int.c"
void main ()
{
unsigned char parameter,
             loop,
             done,
             half;

unsigned int parameter2;

init_pca();

pca_func(DISPINIT);                    /*display initialization*/

put_byte(MGRPNMBR, FULL);   /*prime pca for full memory group*/
pca_func(GROUP);                       /*change group*/
// pca_func(ERASEDAT);      /*erase data in memory group*/

pca_func(PHAMODE);          /*put pca into pha mode*/
put_3bcd(ACQPT, 60);        /*prime preset acquisition time to 1 minutes*/
pca_func(PHATMDS);          /*set preset time*/

pca_func(MCSMODE);          /*put pca into mcs mode*/
```

```
put_byte(MCSDWLNM, 28);                 /*prime mcs for external dwell time*/
pca_func(MCSTPDS);              /*set mcs to external*/

put_3bcd(MCSPSTP, 1);           /*prime mcs for one pass*/
pca_func(MCSTPDS);          /*set mcs for one pass*/

loop = TRUE;
while (loop)
  {
  for (half = 2; half < 4; half++)    /*loop to cover both polarizations*/
        {
        pca_func(ACQU);                         /*start acquisition*/
        while (!get_byte(ACQFLG));      /*wait for data acquisition to stop*/

        pca_func(PHAMODE);          /*switch to pha mode*/

        put_byte(MGRPNMBR, half);     /*prime pca for 'half' half o' memory*/
        pca_func(GROUP);            /*change memory group*/

        put_3bcd(ACQET, 0);             /*prime elapsed time for zero seconds*/
        pca_func(PHATMDS);              /*set elapsed time to zero*/

        pca_func(ACQU);                         /*start acquisition*/
        done = TRUE;
        while (done)
                {
                pca_func(SPUD);         /*update spectrum on the display*/
                pca_func(PARMUP);       /*updates parameters to the screen*/
                if (kbhit())
                        switch(getch()) {
                          case  0:
                            switch(getch()) {
                                case 59:                        /*F1: stop at end*/
                                  loop = FALSE;
                                  break;
                                case 72:            /*numberpad 8*/
                                  pca_func(CFSI);           /*increases full scale*/
                                  break;
                                case 80:            /*numberpad 2*/
                                  pca_func(CFSD);           /*decreases full scale*/
                                  break;
                                }
                            break;
                          case  93:
                          case 125:                             /*s and S: stop at once*/
                            exit(0);
                          };
                done = !get_byte(ACQFLG);
                }
        put_byte(MGRPNMBR, FULL);       /*prime pca for full memory group*/
        pca_func(GROUP);                /*change group*/

        pca_func(MCSMODE);          /*put pca into mcs mode*/
```

```
        put_3bcd(MCSPSTP, 1);    /*prime mcs for one pass*/
        pca_func(MCSTPDS);          /*set mcs for one pass*/
        }
  }
}
```

Second section: "pca_int.c"

```
/* parameter labels*/
#define MGRPNMBR  130          /*memory group number: one byte*/
#define MGRPDATA  133/*memory group data: two bytes*/
#define PHAFLAG        134     /*pha flag: one byte; '0FF' - selected, 0 - not selected*/
#define MCSFLAG         135    /*mcs flag: one byte; '0FF' - selected, 0 - not selected*/
#define ACQFLG          140    /*acquisition flag: one byte; 0 - aquiring,
                               1 - not aquiring & stopped by keyboard,
                               80 - not aquiring due to time out*/
#define ACQPT   141    /*acquisition preset time: 3 bytes packed BCD in seconds*/
                        #define ACQET 142      /*acquisition elapsed time: 3 bytes packed BCD in
                               seconds*/
#define MCSTCFLG       144     /*mcs time channel flag: 1 byte; 0 - time display mode,
                               '0FF' - channel display mode*/
#define MCSDWLNM 146           /*mcs dwell number: 1 byte; 28 - external dwell time,
                               0-27 - 10 microsecond to 60 second range*/
#define MCSPSTP        147     /*mcs preset passes: 3 byte packed BCD*/

/* function labesl*/
#define DISPINIT       2       /*display initialization*/
#define PARMUP         3       /*updates all the parameters to the screen*/
#define SPUD           4       /*spectrum update*/
#define ACQU           5       /*start or stop the acquisition*/
#define ERASEDAT  6    /*erase all data in the current memory group*/
#define GROUP  7       /*selects memory group according to MGRPNMBR*/
#define PHAMODE        19      /*selects pha data acquisition mode*/
#define MCSMODE        20      /*selects mcs data acquisition mode*/
#define PHATMDS        25      /*displays preset time, elasped time, & time remaining;
                               must be run to set preset time*/
#define MCSTPDS        26      /*displays current dwell time, preset # of passes,
                               passes elapsed, and passes remaining; must be run
                               to set preset time or preset # of passes*/
#define CFSI           30      /*full scale counts increase*/
#define CFSD           31      /*full scale counts decrease*/

/*other definitions*/
#define FULL     1
#define HALF1    2
#define HALF2    3
#define TRUE     1
#define FALSE    0

/*****************************************************************/
unsigned char get_byte(f)
```

```
unsigned char f;
{
unsigned char *paramptr;

*funptr = f;

(*pcaptr)();

paramptr = *(unsigned char **)(funptr + 1);
return *paramptr;
}

/*****************************************************************/
void put_byte(f, parameter)

unsigned char f, parameter;
{
unsigned char *paramptr;

*funptr = f;

(*pcaptr)();

paramptr = *(unsigned char **)(funptr + 1);
*paramptr = parameter;
}

/*****************************************************************/
void put_3bcd(f, parameter)

unsigned char f;
unsigned int parameter;
{
unsigned char *paramptr;
unsigned char bcd[3];
int i;
div_t d;

for (i = 0; i < 3; i++)          /*changes parameter into 3 bytes of*/
        {                       /*BCD format, LSByte in bcd[0]*/
        d = div(parameter,100);
        bcd[i] = d.rem;
        parameter = d.quot;
        }

*funptr = f;

(*pcaptr)();

paramptr = *(unsigned char **)(funptr + 1);
for (i = 0; i < 3; i++)
        *(paramptr+i) = bcd[i];
}
```

```
/*****************************************************************/
void pca_func(f)

unsigned char f;
{
unsigned char *paramptr;

*funptr = f;

(*pcaptr)();
}

/*****************************************************************/
unsigned int get_2bytes(f)

unsigned char f;
{
unsigned int *paramptr;

*funptr = f;

(*pcaptr)();

paramptr = *(unsigned int **)(funptr + 1);
return *paramptr;
}

/*****************************************************************/
void get_bytes(f, parameter)

unsigned char f;
unsigned char *parameter;
{
*funptr = f;
(*pcaptr)();
parameter = *(unsigned char **)(funptr + 1);
}

/*****************************************************************/
void init_pca()
{
pcaoffset = *pcaoffsetptr;
pcaseg = *pcasegptr;

pcaptr = MK_FP(pcaseg,pcaoffset);
funptr = MK_FP(pcaseg,(pcaoffset + 3));
}
```